CHARACTERIZATION OF CAM FEMOROACETABULAR IMPINGEMENT USING SUBJECT-SPECIFIC BIOMECHANICS AND POPULATION-BASED MORPHOLOGICAL MEASUREMENTS

by

Penny Renee Atkins

A dissertation submitted to the faculty of
The University of Utah
in partial fulfillment of the requirements for the degree of

Doctor of Philosophy

Department of Bioengineering

The University of Utah

August 2018

The University of Utah Graduate School

STATEMENT OF DISSERTATION APPROVAL

The dissertation of **Penny Renee Atkins**

has been approved by the following supervisory committee members:

		Date Approved
Andrew E. Anderson	, Chair	**May 25, 2018**
Jeffrey A. Weiss	, Member	**May 25, 2018**
Robert T. Bowles	, Member	**May 25, 2018**
Ross T. Whitaker	, Member	**May 25, 2018**
Christopher L. Peters	, Member	**May 23, 2018**
Stephen K. Aoki	, Member	**May 25, 2018**

and by **David W. Grainger** , Chair

of the Department of **Bioengineering**

and by David B. Kieda, Dean of The Graduate School.

ABSTRACT

Cam-type femoroacetabular impingement syndrome (FAIS) is a recently described pathology of the hip, characterized by reduced sphericity of the femoral head and pain during high range-of-motion activities. While cam FAIS is thought to be a major etiologic factor for the development of hip osteoarthritis, the natural history of cam FAIS is unknown. The over-arching objective of this dissertation was to address this knowledge gap by quantifying the morphological and biomechanical characteristics of cam FAIS.

The aspherical femoral head in cam FAIS patients is thought to alter hip articulation patterns. However, the conclusions from studies evaluating hip kinematics in cam FAIS patients have been inconsistent. Unfortunately, skin marker motion capture is subject to substantial errors of up to 20° in rotation due to soft tissue artifact, and thus is likely not sufficient to study differences in hip motion between cam FAIS patients and control subjects. To this end, dual fluoroscopy has been used to quantify in-vivo hip kinematics during activities of daily living to within 1 mm and 1° in patients with cam FAIS.

Measurements of morphology from radiographs are used to quantify femoral shape for diagnosis and to evaluate the sufficiency of surgical correction. However, there is little agreement as to which radiographic view provides the best visualization of the asphericity of the femoral head. Using statistical shape modeling, the specific shape variability of cam FAIS has been defined and used to evaluate various radiographic views on their ability to capture cam morphology. Importantly, insufficient resection is the most common reason

for revision arthroscopy, indicating that further research on this topic is necessary. As such, cortical bone thickness was incorporated into statistical shape models to assess differences in cortical morphology that should be considered when investigating femoral resection and to evaluate whether cortical thickness could be used to guide the depth of surgical resection.

Together, this work provided comprehensive measurements of hip morphometrics and biomechanics in patients with cam FAIS that improved our understanding of the role of morphology and movement patterns in FAIS hip joint degeneration.

TABLE OF CONTENTS

ABSTRACT iii

LIST OF TABLES vii

ACKNOWLEDGMENTS ix

Chapters

1. INTRODUCTION AND BACKGROUND 1

Motivation 1
Basic Hip Anatomy and Physiology 2
Pathology and Osteoarthritis 4
Hip Joint Function 9
Kinematic Analysis of FAIS 9
Analysis of Morphology 19
Research Goals 25
Overall Significance 26
Summary of Chapters 26
References 29

2. ALTERED PELVIC AND HIP JOINT KINEMATICS IN PATIENTS WITH CAM FEMOROACETABULAR IMPINGEMENT: A DUAL FLUOROSCOPY STUDY 46

Abstract 46
Introduction 48
Participants and Methods 50
Results 54
Discussion 62
Acknowledgments 65
References 66

3. HOW WELL CAN 2D RADIOGRAPHIC MEASUREMENTS OF CAM FEMOROACETABULAR IMPINGEMENT DESCRIBE THE 3D SHAPE OF THE PROXIMAL FEMUR? 69

Abstract 69
Introduction 71
Participants and Methods 73
Results 78

Discussion ... 84
Acknowledgments ... 88
References ... 89

4. QUANTITATIVE COMPARISON OF CORTICAL BONE THICKNESS USING CORRESPONDENCE-BASED SHAPE MODELING IN PATIENTS WITH CAM FEMOROACETABULAR IMPINGEMENT ... 92

Abstract ... 93
Introduction ... 93
Methods ... 94
Results ... 96
Discussion ... 98
Authors' Contributions ... 102
Acknowledgments ... 102
References ... 102

5. DOES REMOVAL OF SUBCHONDRAL CORTICAL BONE PROVIDE SUFFICIENT RESECTION DEPTH FOR TREATMENT OF CAM FEMOROACETABULAR IMPINGEMENT? ... 104

Abstract ... 105
Introduction ... 106
Patients and Methods ... 107
Results ... 110
Discussion ... 111
Acknowledgments ... 113
References ... 113

6. IMPACT, ONGOING RESEARCH, FUTURE DIRECTIONS ... 115

Impact ... 115
Ongoing Research – Finite Element and Musculoskeletal Models ... 119
Ongoing Research – Magnetic Resonance Imaging and Dual-Fluoroscopy ... 127
Ongoing Research – Statistical Shape Modeling ... 129
Future Directions ... 131
References ... 135

LIST OF TABLES

Tables

2.1 Participants for each activity, listed by sex... 52

2.2 Correlation between joint angle range of motion and pelvic rotation range of motion 57

2.3 Hip joint angles during standing and the maximum range of motion for the internal and external rotational pivot 58

2.4 Percent of gait cycle that the pelvic position was significantly different than during stance... 60

3.1 Femur positioning for the digitally reconstructed radiographs representing eight plain film views... 77

3.2 Alpha angle and head-neck offset measurements of control subjects and cam femoroacetabular impingement (FAI) patients, as measured from digitally reconstructed radiographs (DRRs) representing eight plain film views 79

3.3 Spearman correlation coefficients between the alpha angle or head-neck offset measurements of each radiographic view to three-dimensional shape scores from statistical shape modeling 83

3.4 Partial least squares regression model coefficients and variable influence on projection values for the optimized model predicting the shape score from statistical shape modeling relative to the entire proximal femur and the region specific to the cam lesion... 85

4.1 Demographics for groups and subgroups of the population represented as median [interquartile range] 97

4.2 Median and interquartile range (IQR) of subject specific maximum, median, and mean regional and medial proximal femur thickness for all groups and subgroups 100

4.3 Median and interquartile range (IQR) of regional and overall thickness for mean shapes for all groups and subgroups.. 100

5.1 Summary of subject cohort demographics presented as median (range).................. 108

6.1. Boundary and loading conditions used to assess the sensitivity of chondrolabral stress and strain to various input data 125

ACKNOWLEDGMENTS

I would like to express explicit gratitude to my advisor, Dr. Andrew Anderson, and to all others who have provided guidance and mentorship through this process: Dr. Jeff Weiss, Dr. Ross Whitaker, Dr. Bo Foreman, Dr. Robert Bowles, Dr. Stephen Aoki, Dr. Christopher Peters, and Dr. Niccolo Fiorentino. I also want to thank the individuals who have taught me so much over the years: Dr. Shireen Elhabian, Praful Agrawal, Dr. Steve Maas, Sumedha Singla, Koren Roach, Dr. Ashley Kapron, Dr. Michael Harris, Dr. Christine Abraham, Dr. Keisuke Uemura, Dr. Matthijs Jacxsens, Klevis Aliaj, Alex Drew, Dr. Heath Henninger, and Dr. Iain Elliott. Additionally, I am extremely grateful for all of the undergraduates who have helped process endless hours of data: Mikey Kutschke, Justine Goebel, Trevor Hafer, Elliott Hurd, Tyler Skinner, Sara Fauver, Sam Colby, Joe Hartle, YoungJae Shin, and Lindsay Schuring.

I would also like to acknowledge financial support from AMTI Force and Motion, the Department of Orthopaedics Obyn Memorial Endowed Scholarship, and Louis S. Peery Discovery Program in Musculoskeletal Restoration, with special thanks to LeAnn Chandler and Art Swindle for all of their hard work and dedication to supporting student researchers.

Lastly, to all my friends and family, thank you for your support and guidance.

CHAPTER 1

INTRODUCTION AND BACKGROUND

Motivation

Cam-type femoroacetabular impingement syndrome (FAIS) is a recently described pathology of the hip, characterized by an abnormally shaped, aspherical femoral head, reduced range of motion, and groin pain.[1; 2] Mounting evidence collected over the last two decades suggests that cam morphology is a major etiologic factor for the development of hip osteoarthritis (OA), especially among young, active adults.[1; 3] As a recently recognized condition, the natural history of cam FAIS is still largely unknown. However, research indicates that both genetic and activity-based factors are involved in the progression of the disease.[4; 5] The number of patients treated for cam FAIS has been steadily increasing in recent years.[6-8] Accordingly, clinicians and healthcare systems are concerned about the rapid rise in a previously unrecognized condition, the ambiguity of the diagnostic criteria, and the costs and uncertainties of treatment.[2] The over-arching objective of this dissertation was to narrow this knowledge gap by quantifying the morphological and biomechanical characteristics of cam FAIS.

Basic Hip Anatomy and Physiology

The hip joint connects the torso and the lower limbs and acts as the interface between the proximal femur and the acetabulum. The femoral head is the proximal epiphysis of the femur which extends superomedially from the femoral shaft via the femoral neck and acts as the ball of the hip joint. The three pelvic bones, the ilium, ischium, and pubis come together to form the acetabulum, or socket, of the hip joint. While it is classically-defined as a ball and socket joint that is restricted to three rotational degrees of freedom, the hip joint is not perfectly congruent or spherical, and thus, also experiences translational motion.[9] While the cortical bone of the proximal femur and hemi-pelvis is generally thin, thicker and denser cortical bone can be found along the diaphysis of the femoral shaft to resist bending moments created by the offset between the femoral head center and axis along the shaft of the femur.

As with all articulating joints, a layer of articular, or hyaline, cartilage covers the subchondral bone of both the femoral head and the acetabulum, providing the hip with low friction articulation.[10] Additionally, the cartilage facilitates the transmission of loads across the two articular surfaces.[10] Hyaline cartilage is composed predominantly of water, extracellular matrix of type II collagen, and proteoglycans.[10; 11] The composition and organization of the cartilage varies through the thickness with three general zones.[10] The deep zone along the subchondral bone has the highest proteoglycan content with perpendicularly aligned collagen fibers, the middle zone serves as a transition between the deep and superficial zones and has low chondrocyte content and obliquely aligned collagen fibrils, and finally, the superficial zone is primarily flattened chondrocytes and collagen fibers aligned with the articulating surface.[10] As cartilage degenerates and OA begins to manifest, collagen organization is disturbed, proteoglycan content is reduced, and the matrix to becomes more permeable to water.[11]

The fibro-cartilaginous labrum runs the periphery of the acetabulum and is joined with the transverse ligament inferiorly to surround the femoral head (Fig. 1.1).[12] The labrum provides stability to reduce subluxation of the joint and to prevent dislocation,[13-15] and may offer a seal to maintain synovial fluid within the joint.[16-19] The labrum consists of

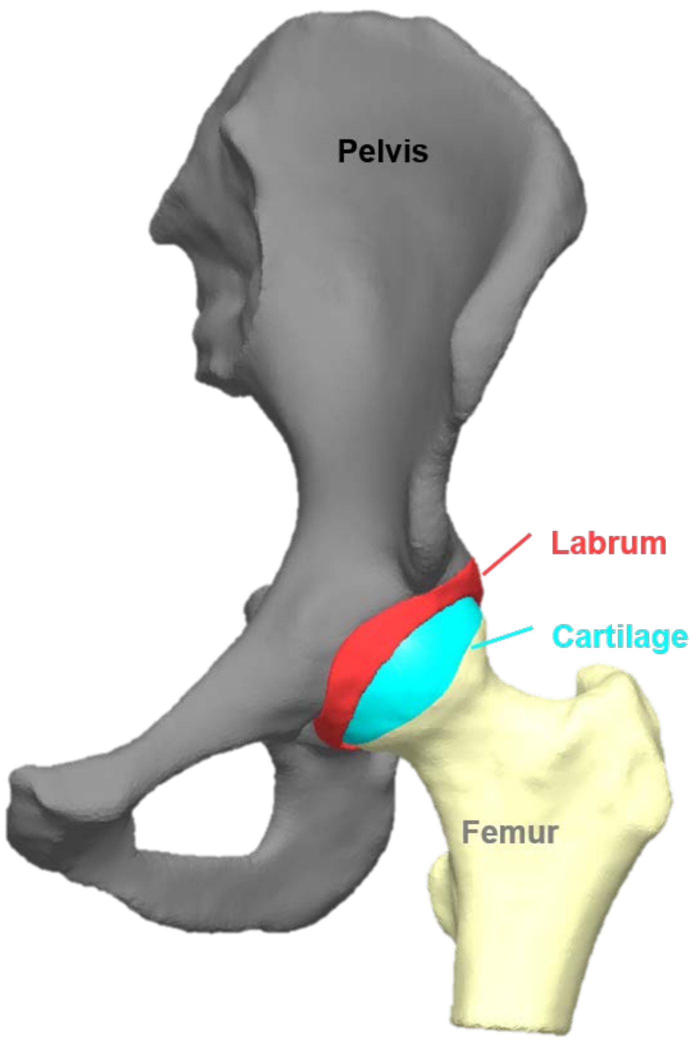

Figure 1.1. The hip joint includes the proximal femur, femoral cartilage, acetabulum of the hemi-pelvis, acetabular cartilage, and labrum.

three distinct layers; the articular surface is a meshwork of thin fibrils, beneath this, a layer of lamella-like collagen fibrils, and finally circumferential Type 1 collagen fibers.[20] The three ligaments of the hip capsule, including the iliofemoral, ischiofemoral, and pubofemoral ligaments, span between the femoral neck and pelvis to provide additional joint stability, limiting anterior translation and external rotation.[21; 22] There are two additional ligaments in the proximity of the hip joint, the zona orbicularis that encircles the femoral neck, and the ligamentum teres which connects the femoral fovea and the acetabular fossa. The ligamentum teres also serves to supply blood to the proximal femoral head during skeletal maturity, when the growth plate has not yet fused. Although its function in the adult hip is unclear, it may serve as a secondary stabilizer to contain the femoral head within the socket, which is evident by the finding that injuries to the ligament teres seem to occur concurrently with cartilage damage.[23]

Pathology and Osteoarthritis

While the nonpathological hip can provide smooth articulation for several decades, degeneration of the cartilage and acetabular labrum can cause significant pain, and mechanical symptoms, such as giving way, locking, or clicking. Left untreated, damage to cartilage and labrum may result in end-stage OA.[2; 24; 25] Radiographic images are usually evaluated for the presence of osteophytes, narrowing of the joint space, and altered shape of the articulating surfaces in the diagnosis of end-stage hip OA using the Kellgren Lawrence (KL) grading system.[26] Here, grades of 0, 1, or 2 signify little evidence of OA and grades of 3 or 4 indicate moderate to severe arthritis.[26] Once diagnosed with end-stage OA, the only proven treatment option for patients is total hip arthroplasty (THA). The number of THA procedures performed each year continues to increase, especially among younger individuals (45-64 years of age) where THA procedures more than doubled between 2000 and 2010.[27] Given their young age, many of these patients can anticipate outliving their index THA prosthesis, necessitating a costly revision procedure.[28] For this reason, there is an immediate need to develop a more in-depth understanding of the etiological factors for the development of hip OA among younger adults. Ideally, the native hip joint would be repaired and preserved as long as possible to delay or prevent the need for THA.

While many cases of hip OA were once thought to be idiopathic, there is mounting evidence that most cases of this disease can be attributed to structural hip deformities and abnormal biomechanics that result from such morphologic irregularities.[1; 29-32] The relationship between abnormal morphology and end-stage OA was recognized more than three decades ago in a study that identified 90% of hips with end-stage OA had evidence of some deformity of the femur or pelvis, 40% of which presented with loss of the normal contour over the femoral head-neck junction.[30] Since then, this pathomorphology of the femur has been identified in as many as 80% of patients with end-stage OA.[33] The asphericity of the femoral head-neck junction was first termed as a pistol-grip deformity, but is now more commonly referred to as cam morphology (Fig. 1.2).[30; 34] Compared to other hip pathomorphologies, cam deformities have been observed to result in more rapid joint degeneration, including separation of tissue at the cartilage and labrum (i.e., chondrolabral) boundary.[29] As such, the focus of this dissertation was the study of cam FAIS.

A diagnosis of cam FAIS requires the presence of both deformities and symptoms,

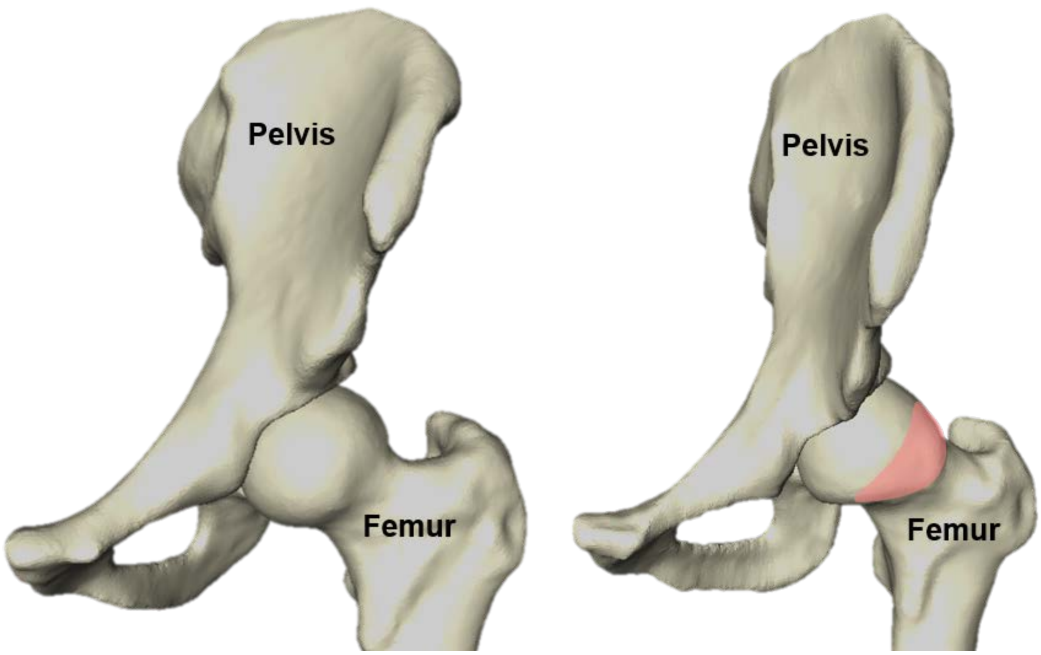

Figure 1.2. Normal proximal femur and pelvic anatomy (left) and altered anatomy over the femoral head-neck junction in cam femoroacetabular impingement syndrome is highlighted in red (right).

including motion- or position-related hip or groin pain. Most often, pain can be reproduced using specific clinical examinations that incorporate flexion, adduction, and internal rotation.[2; 35] Treatment for cam FAIS often begins with conservative methods, including activity modification and/or nonsteroidal anti-inflammatory medications. If conservative treatments fail, then hip preserving surgery is often recommended. Open surgical hip dislocation and anthroscopic osteochondroplasty are often used to resect the offending cam lesion.[36-39] While the open surgical technique has been preferred due to the improved visualization of and access to the joint, the use of arthroscopic techniques offer a reduced recovery period with fewer complications.[40-43] Both techniques have proven to be effective at improving patient function in the short-term, but it is still unknown whether hip preserving surgery alters the course of joint degeneration in cam FAIS patients.[36; 44; 45]

The natural history of cam FAIS is not completely understood, but it is widely-believed that both genetic and functional factors are responsible for tissue damage.[5; 45-48] While specific genes have been associated with osteoarthritis, and even abnormal hip morphology, the relationship between genetics and FAIS has yet to be fully clarified.[5; 49; 50] Nevertheless, it has been demonstrated that siblings of patients with a cam deformity are 2.8 times more likely to have similar cam morphology than the general population.[48] Relative to functional factors, participants of high-intensity activities, especially during skeletal maturation, are more likely to have FAIS morphology, as has been shown in numerous morphological studies of athletes.[47; 51-55] From these observations, it has been hypothesized and observed that the morphology of cam FAIS likely develops gradually prior to closure of the femoral head physis, or growth plate, dependent on both genetic factors and activity participation.[46; 56]

The aspheric morphology of cam FAIS is thought to cause deleterious stresses and strains on the chondrolabral boundary, resulting in cartilage delamination and labral tears.[1; 31] During dynamic movements, the rotation of the aspherical femoral head within the acetabulum results in increased shear stress on the peripheral cartilage and chondrolabral boundary which leads to abrasions and delamination from the underlying bone and labrum (Fig. 1.3).[1; 57; 58] In addition to cartilage fibrillation and tearing, FAIS patients often present with increased synovial inflammation and paralabral cysts.[59; 60] Further, the increased stress on the bone may result in the formation of subchondral cysts or bone marrow edemas.[61-63]

Cartilage is avascular and aneural, but as a proprioceptive tissue, the labrum contains free nerve endings.[10; 15] Thus, damage to the labrum is the most likely source of

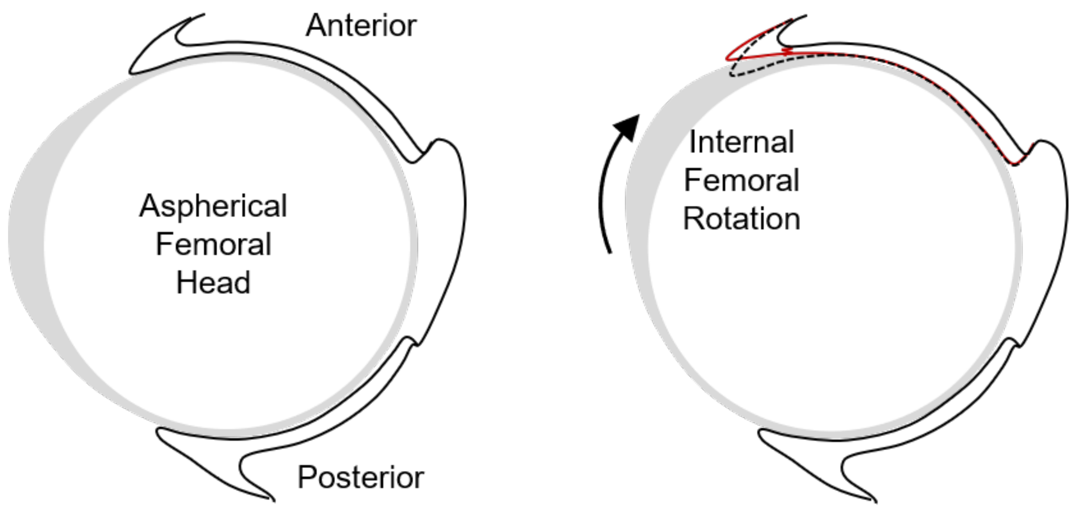

Figure 1.3. The aspherical femoral head of cam FAIS (left) results in increased labral translation and strain over the chondrolabral junction during rotation (right).

hip pain in patients with cam FAIS.[15; 64-66] Pain is often reported in localized regions of the anterior groin, lateral trochanter, and posterior buttock.[35] The fact that the hip is located so deep within the soft tissue of the body may explain the lack of specificity in the location of pain. In particular, inflammation of the labrum, synovium, and capsule could refer pain in several anatomic directions. In addition, muscle wasting or over-use resulting from abnormal hip morphology could cause compensatory changes in hip biomechanics, which in turn could cause muscular pain.[67] For this reason, diagnostic, anesthetic injections into the joint capsule are often used to identify whether the source of the pain is intra-articular in nature, such as that caused by labral tears or cartilage delaminations.[68-70]

Hip Joint Function

The uninhibited range of motion of the hip is relatively high with more than 150° of flexion-extension, 80° of abduction-adduction, and 90° of internal-external rotation.[71] The aspherical femoral head characteristic of cam morphology is thought to limit this inherent range of motion due to abnormal abutment between the femoral head and the acetabulum or labrum.[72-75] A combination of aspherical femoral morphology and motion adaptations are believed to result in altered hip biomechanics which may begin the process of degeneration and lead to early onset OA.[31; 74; 76-78]

Kinematic Analysis of FAIS

While the concept of reduced range of motion due to cam morphology is generally accepted, findings from numerous motion analysis studies employing a variety of techniques have not found consistent, conclusive evidence that cam FAIS is characterized by abnormal motion patterns.[2; 24; 72-74; 79-84] Skin marker motion analysis and other noninvasive methods of capturing whole body kinematics have been the most widely used methods.[73; 79; 81; 82; 84-86] These methods include data collection of active or passive motions in a variety of environments and data processing that can be done efficiently, sometimes even in real-time to provide biofeedback for movement training.[86-88] Since these methods are capturing the external motion of the body, the specific motion of the underlying bone may not be accurately measured. Previous studies have evaluated the effect of soft-tissue artifact by comparing kinematics resultant of tracking the surface of the skin to those representing in-vivo bone motion and have found errors in all three planes of motion and of up to 20° in magnitude.[89-92] With errors of this magnitude, it is likely that subtle variations in motion resultant of the anatomical variation may be masked by the errors inherent to soft tissue artifact. Nevertheless, some previous studies using skin-based motion analysis have still been able to detect reduced peak joint angles and reduced range of motion in patients with cam FAIS.[79-82; 93]

Another source of error in quantifying motion with skin marker motion capture is a result of the deep location of the hip joint center within the body, making it difficult to identify from bony prominences alone.[89; 94-97] Previous studies have used both predictive and functional methods to determine the hip joint center.[94; 95; 98] Predictive methods use bony landmarks and established regression equations to identify the location of the hip joint center,[98-100] while functional methods use the data collected during a functional activity that incorporates rotational motion in all three planes to determine the center of rotation of the thigh segment.[101; 102] It is generally accepted that functional methods more accurately identify the center of hip rotation, but both methods are prone to errors associated with anatomical bone morphological variation and motion of the skin relative to the bone.[89; 95; 96] For example, studies have demonstrated that approximating the hip joint center of rotation from skin markers leads to errors on the order of 2 cm, which is approximately the radius of the femoral head.[89; 94]

Often, idealized morphology, including spherical and concentric geometry for the hip, is used calculate hip kinematics. While the use of idealized anatomy removes the need to image subjects to define hip morphology, it is well-known that even the anatomically normal hip is not perfectly spherical or concentric.[9; 103; 104] Further, use of spherical geometry for the hip precludes the study of conditions known to affect the shape of the femur and pelvis, including FAIS, Legg-Calve-Perthes, or acetabular dysplasia.[9; 103-107]

Moreover, assuming the hip to be spherical and concentric prohibits calculation of hip joint translations, which may play an important role in causing tissue damage.[1; 31] To this end many studies have used ellipsoidal or conchoidal approximations to represent pathological hip anatomy associated with these disease patterns.[108-112] While these aspherical approximations provide generalized understanding of the effect of morphology on motion and mechanics, they lack localized incongruencies of the joint that may be a stronger driver of altered motion joint loading patterns.[113; 114]

Computer simulations have been widely used to evaluate the effect of hip anatomy on passive range of motion.[72; 74; 115; 116] These simulations incorporate subject-specific anatomy from three-dimensional (3D) imaging to evaluate the isolated effect of anatomy on range of motion.[115] While these studies often do not represent subject-specific motion patterns, they provide crucial insight on range of motion limitations that would result due to direct impingement between the femur and the acetabulum. Computer simulations do, however, employ a number of important assumptions which must be considered. First, soft tissues are ignored, such that the effect of both the cartilage and labrum are ignored. The effect of the labrum is likely crucial to understanding dynamic impingement, as the femur makes contact with the labrum and not the acetabular rim, even during high range of motion clinical exams.[117] This abutment with the labrum is an important consideration, as the increased strain on the chondrolabral boundary may be an initiator to damage of both cartilage and labrum.[1; 39; 118] Secondly, the center of rotation of the joint is considered to remain constant, ignoring translations within the joint. Errors in identifying the center of rotation of the femur and pelvis would then also propagate errors in measured motion patterns. Finally, simulations often incorporate rotations from only one plane of motion at a time, while motions of daily living often combine all six degrees-of-freedom of the hip joint simultaneously.[90; 117] Importantly though, these simulations provide evidence of possible limitations in range of motion due to cam morphology and may provide preoperative guidance in defining the region and depth of femoral resection necessary to improve function.[119; 120185; 186]

Another method used to incorporate subject specific morphology has been to use cadavers to evaluate the passive motion of the hip.[115; 121-123] Importantly, cadaveric models often preserve some of the soft tissues within and around the hip joint allowing for explicit evaluation of the role each of these tissues has in range of motion.[58; 121] However, not all soft tissues and musculature can be preserved while still providing visualization of the hip joint and the motions applied to the cadaveric joint may not accurately represent passive motions in live subjects. While data from cadaveric models can be used to improve computer simulations and to study relationships between shape and motion, these data likely do not represent in-vivo joint motion.

Imaging of Joint Health

Volumetric and two-dimensional (2D) projection imaging are often used to visualize the health of the joint.[69; 118; 124-126] Radiographic plain films obtain a snapshot of hip joint shape clinically, with various projections providing different views of the femoral head-neck junction, acetabulum, and overall congruency of the joint.[104; 125; 127-129] Importantly, plain films can be acquired during a clinical appointment and are typically available at the time of initial consultation. However, plain films do not visualize soft tissue structures, and thus, only when cartilage has become grossly thinned does it become apparent that the joint has suffered damage.[130] This is problematic, as full thickness delaminations to cartilage are relatively common among cam FAIS patients.[31; 131]

Magnetic resonance (MR) imaging of the hip is often acquired prior to surgical intervention to better visualize the 3D morphology of the hip. MRI uses the polarization of water molecules to determine pixel or voxel intensity values in the resultant image. Various sequences use different values and ratios of repetition time (TR) and echo time (TE) to preferentially excite water molecules in tissues. T1-weighted images use short TR and TE to measure spin-lattice relaxation and provide imaging of the overall anatomy. T2-weighted images use long TR and TE to measure spin-spin relaxation and provide imaging of abnormal fluid or inflammation. More recently, quantitative MRI (qMRI) has been used to quantify cartilage with T1ρ and T2 mapped images. Here, T1ρ mapping provides a measure of glycosaminoglycan (GAG) and proteoglycan content and T2 mapping provides a measure of water content, which indirectly represents collagen content and orientation.[61; 132-134] Since collagen and proteoglycan content are diminished in arthritic cartilage, even before the cartilage undergoes gross thinning, these images provide an early detection of joint degeneration.[132]

MRI was originally used for the visualization of soft-tissues and bony contours, but more recently, with the introduction of dual-echo or ultrashort-TE imaging, has been used to accurately visualize cortical bone.[135] MR images are reconstructed from field gradient data in the frequency domain. Longer acquisition scans are often necessary to obtain enough magnetic field gradient data in the frequency domain to produce high resolution images without wrapping or aliasing issues. Due to the reconstruction process of these images, a series of 2D images slices, which can be each be reconstructed twodimensionally, often need shorter scan times than 3D image sequences which require more frequency data for reconstruction. However, more recently, 3D MR imaging sequences with relatively low scan times have been used for musculoskeletal imaging.[105; 136]

Computed tomography (CT) imaging is a radiation-based imaging modality that uses a rotating x-ray tube and detectors to generate a 3D image volume. The use of a radiation-based modality results in clear delineation of bone and other calcified tissues, but can also be used to delineate separate muscle bellies and some other soft-tissues. CT imaging can provide high-resolution images very quickly, taking only a few seconds, and thus motion artifact is typically not a problem with this imaging modality.

Most MR or CT images are acquired along an imaging plane, however radial imaging, acquired about the femoral neck axis or the axis perpendicular to the plane of the acetabular rim, has recently become more prevalent.[137-139] Slices of radial volumetric images are often used to define the shape of the femoral head and to assess the ability of radiographic views to capture the morphology of the cam lesion.[138; 140; 141] Similar to standard, planar images, radial images can also be used to assess regions of damage to the cartilage and labrum.[131; 138; 139; 142; 143] However, visualization of cartilage and labral damage may be difficult without the use of a contrast agent.[60; 131] For this reason, MR or CT arthrograms are often used as diagnostic tools when labral tears are suspected. For MR, saline can be used as contrast agent, while for CT, radiopaque liquids are needed.[144; 145] The use of a contrast agent provides improved visualization of labral tears and cartilage delamination, but still may not provide accurate visualization of the thickness of cartilage, as the two cartilage layers are often in contact, and thus may not be clearly separated. It is for this reason that traction is recommended during the acquisition of CT or MR images.[145-

[147] For CT, traction only needs to be applied for a few seconds, however, for MR, imaging sequences can require several minutes. The application of traction in MR is therefore less practical as the joint may relax over time resulting in motion artifact. Importantly, longer scans while under traction may be discomforting, especially for patients with hip pathology.

While static imaging methods have been used for decades, several dynamic methods have recently been identified which allow for the quantification of in-vivo bone motion relative to the subject's underlying joint morphology. These methods have included the use of dynamic ultrasound, CT, or MRI to capture specific positions of interest which are thought to represent positions of impingement.[148-150]

Dual fluoroscopy (DF) is another dynamic imaging technique where two pairs of fluoroscopes, each consisting of an x-ray emitter and an image intensifier, are arranged to share a combined field of view.[151-154] In a clinical setting, the emitter is offset a fixed distance from the image intensifier by a metal c-arm-shaped connection. However, in a research setting, each emitter and image intensifier is mounted separately on a movable cart to provide flexibility in arrangement of the DF system such that the subject can perform activities within the combined field of view of the DF system. Digitally reconstructed radiographs (DRRs) of each bone from CT are then aligned with the two fluoroscope images to calculate the in-vivo bone position for each image frame. These data can then be used to visualize arthrokinematics and calculate joint angles and translations.[117]

DF has been applied to a variety of joints, including the ankle, knee, hip, and shoulder.[151-155] However, the hip provides unique imaging challenges as the hip joint is surrounded by large muscle groups and panniculus, resulting in high levels of scatter and poor signal-to-noise ratio images. DF of the hip has been validated to capture dynamic, in-vivo bone motion to sub-millimeter and sub-degree accuracy.[151] DF has since been used to capture in-vivo motion of the femur and pelvis during the impingement exam for both control subjects and cam FAIS patients,[117; 156] and more recently, during weight-bearing activities for control subjects.[89; 90; 94; 157; 158]

Joint Loading and Biomechanics

Full-thickness chondral lesions and extensive labral tears observed in patients with cam FAIS are likely a result of altered joint biomechanics and increased cartilage stresses which hasten joint degeneration and lead to early onset OA.[1; 31; 32; 39; 77; 126] Measurement of in-vivo joint mechanics is not feasible, but finite element (FE) analysis of cartilage and labral stresses and strains can provide data to better-understand the role of altered mechanics in joint degeneration.[75; 109; 159-165] Mappings of stress and strain measures of the cartilage and labrum can be used to identify regions of the cartilage or labrum that experience increased loading and are likely to experience early degeneration.[160; 166; 167] As part of preoperative planning, FE analysis results can also be used to identify bony protrusions that increase chondrolabral stresses and strains and then to evaluate resultant stresses and strains after a simulated resection.[120; 168] By verifying that surgical intervention will reduce peak stresses and strains within the joint prior to surgery, the risk for revision surgery and early onset of OA may be largely diminished.

As is true with all computational models, a model is only valuable if it is properly validated.[169] The validation of FE models of the hip joint has been reported relative to cartilage contact stresses measured ex-vivo under specified loading conditions.[75; 159; 170] In addition to validating a specific model, validation data can be used to assess the sensitivity of a model to various defining attributes, such as geometry or material properties.[75; 171] By understanding the sensitivity of FE models to these parameters, informed decisions can be made as to whether a model can be simplified without losing validity. Notably, there are large computational benefits that can be gained when answering the question at hand does not require a subject-specific level of detail.

Since the collection and processing of volumetric images required to generate FE models of subject-specific anatomy is extremely time- and labor-intensive, investigators have used spherical anatomy to depict the anatomy of the femur and acetabulum.[109; 110; 112; 165] Depending on the purpose of the model, the assumption of idealized anatomy may be valid, but this may be an over-simplification when attempting to study hips with abnormal anatomy. Specifically, the irregular shape of the joint and localized incongruencies may play a major role in the magnitude of stress and strain on the tissue, which is important for identifying potential mechanisms of tissue damage.

Most FE models of the hip joint include, at a minimum, meshes representing the articular cartilage of the femoral head and acetabulum. If bones are included in the model, the cartilage is either assigned rigid contact with the bone, or tied contact if bones are allowed to deform. Beyond the structures of the bones and cartilage, the labrum is often also included, but the ligaments of the hip capsule are not when modeling nontraumatic activities. The labrum has been shown to play a role in load transfer and stability of the hip, especially in patients with reduced joint coverage.[162] Even in hips with adequate coverage, the labrum still provides a boundary for the peripheral edge of the cartilage which alters predicted values of first principal strain and maximum shear stress.[75; 165]

Beyond the decision of what geometries should be included, the determination of material properties is a crucial step in the development of an FE model. The material properties of bone have varied between localized material properties from subject-specific imaging to fully rigid representations.[164; 165; 172; 173] When bones are represented to be deformable, often only the cortex is included since the contribution of the trabecular bone to cartilage contact stresses is minimal.[171] Since cartilage shear stress and strain are often the measure of interest in these models, the material properties of cartilage have been a higher priority of investigation. In recent models, cartilage has been represented as either an isotropic, linear elastic material,[109; 112] a nearly incompressible hyperelastic material,[159; 160] or as a continuous fiber distribution material with a neo-Hookean ground matrix.[161; 164; 165; 173] Experimental data of bovine labrum have been used to define the material properties of the labrum as a transversely isotropic hyperelastic material with a fiber family embedded in a neo-Hookean ground matrix.[161; 164; 165; 173-175]

After determining the geometries and material properties, boundary and loading conditions must be applied to the model to represent the position and loading of interest. Kinematics and joint reaction forces obtained from individuals with instrumented hip prostheses have been used to define boundary and loading conditions of many hip joint models.[176] While these data, published by Bergmann et al., provide in-vivo kinematic and loading data, the THA patients monitored during their study may have altered gait patterns due to surgical recovery or the presence of osteoarthritis that may not accurately represent the kinematics of younger, nonarthritic subjects.[176] It is unclear if such generalized models are appropriate for the study of cam FAIS, given that cam FAIS is defined as a condition for which both hip anatomy and joint articulation are altered. As such, patient-specific boundary and loading conditions may be necessary inputs to ensure accurate predictions of hip contact mechanics. Accordingly, subject-specific kinematics and kinetics can be obtained from motion capture data collection or 3D imaging in high-range of motion positions of interest to drive FE models of the hip.[164; 177; 178]

Ultimately, the accuracy of the model inputs will dictate the accuracy of model outputs. In certain scenarios, it may be reasonable to assume generic anatomy, loads, and kinematics. However, the importance of each parameter cannot be ascertained unless the investigator employs sensitivity studies to demonstrate how key model outputs, such as contact or shear stress, change as a result of altering model inputs. In support of future FE analysis, kinematics and kinetics calculated from musculoskeletal models from both skin markers and DF will be used to drive subject-specific FE models and to define the sensitivity of FE models of the hip to various boundary and loading conditions. The results from these sensitivity studies may illuminate aspects of the modeling protocol that could be streamlined to improve efficiency in the processing pipeline and increase the feasibility of analyzing a larger cohort of subjects.

Analysis of Morphology

The morphology of the femur is one of the major indications for a diagnosis of cam FAIS, yet how these morphological variants relate to long-term joint health is not well understood. The morphology of the femoral head-neck junction in cam FAIS is generally visualized and measured using radiographs and 3D imaging techniques, such as CT or MRI.[124; 126; 140] From these images, both angular and distance based measurements have been used to quantify femoral head asphericity. Specifically, the alpha angle is an angular measurement between the femoral neck axis and the point at which the femoral head loses sphericity,[179] whereas head-neck offset is defined as the distance between parallel lines along the femoral neck axis representing the lowest point on the femoral neck and the outermost point of the femoral head (Fig. 1.4). Beyond 2D analysis of cam morphology, 3D surface-based measurements, such as maximum deviation from a sphere, have been utilized to define the severity of the cam lesion.[104]

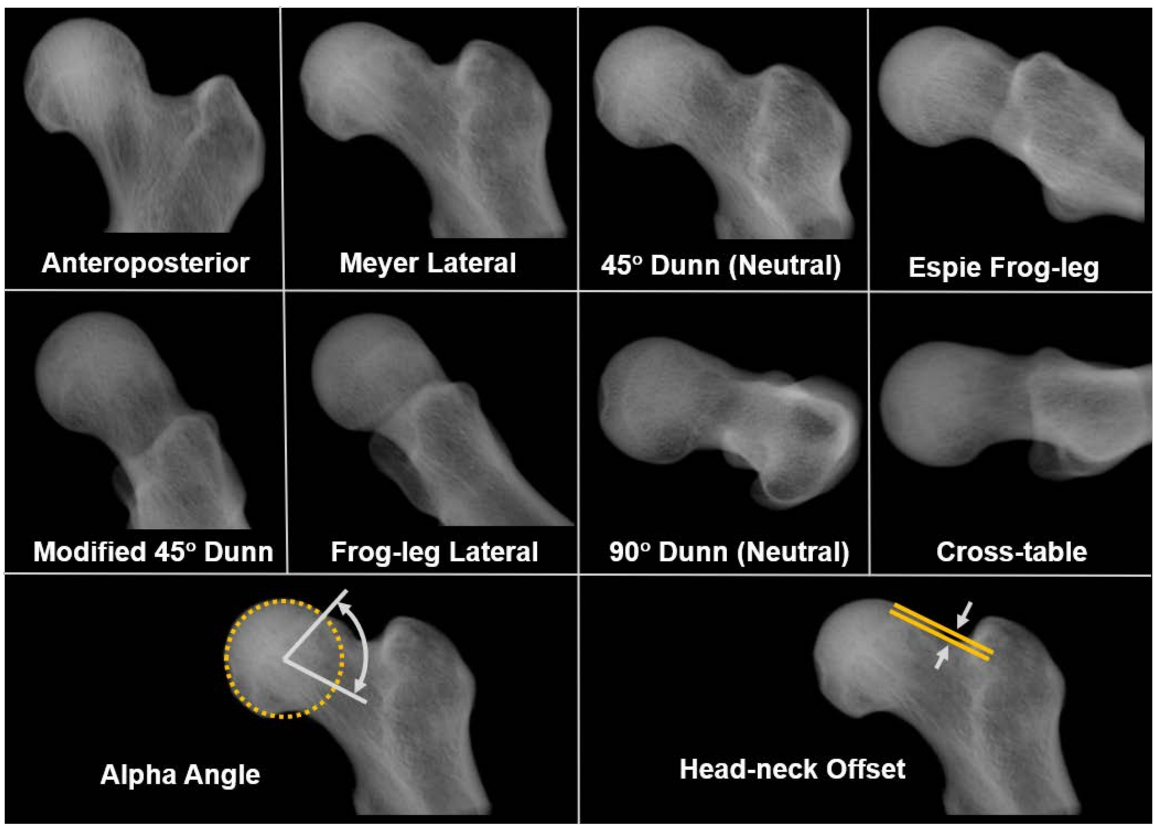

Figure 1.4. Radiographic projections and measurements commonly used in the diagnosis of cam femoroacetabular impingement syndrome.

Diagnosis

Clinically, morphologic measurements are most commonly obtained from radiographs during the initial clinical consult to classify femoral morphology as being pathologic or normal.[179] Upon the original recognition of cam morphology, alpha angle and head-neck offset measurements greater than 50° and 10 mm, respectively, indicated cam morphology.[128; 180; 181] However, these cutoff values have been questioned due to the overwhelming presence of cam morphology in asymptomatic individuals.[182] Agricola et al. found that from an anteroposterior radiograph, alpha angles greater than 60° indicated the presence of cam morphology, while alpha angles greater than 78° indicated progression to end-stage OA within five to 20 years.[183] These results indicate a strong relationship between abnormal morphology and OA progression, but not for subtle morphological differences. A difference in femoral anatomy, especially with regards to femoral head asphericity, has been identified between sexes, where females naturally have more head-neck offset than males.[184] Another important observation has been the variability in normal measures of morphology based on alpha angles or head-neck offset values among imaging projections and modalities.[104; 129; 137; 185-187]

A variety of radiographic views have been identified to provide unique views of the cam lesion.[138; 188] While each view provides a unique projection of the femoral head, several studies have aimed to identify which view provides the optimal view of the femoral head to diagnose cam FAIS. Views that produce the highest alpha angle or the alpha angle most similar to those from radial slices of 3D images are often preferred as they are thought to best capture morphology.[137; 141; 189] However, a previous study evaluating 3D femoral head shape relative to radiographic measurements indicated that larger alpha angle measurements do not necessarily correlate to the best predictors of 3D shape.[78; 104]

While there is little agreement between clinicians on the specific view of choice, most agree that a lateral view of the femur provides the best visualization of the morphology of the femoral head-neck junction.[2; 129] However, the overall morphology of cam FAIS may not be accurately represented on a two-dimensional radiograph. This idea is in agreement with a previous study, which indicated that measurements of increased alpha angle and reduced head neck offset do not correlate well with increased femoral head asphericity.[104] However, the basis of asphericity measurements lies in the assumption that femoral head morphology should be spherical, which is not the case, even among normal hips.[9; 104] A more objective method to assess the ability of radiographic projections to capture 3D shape variation is needed to provide consistency in patient diagnosis.

More than 35% of asymptomatic young adults have radiographic evidence of cam FAI.[182] Radiographic prevalence of cam morphology is even higher in athletes, with 60-75% of asymptomatic athletes having radiographic findings consistent with cam morphology without obvious joint space narrowing indicative of OA.[54; 190] From the image-based analysis of cam morphology, the prevalence of cam morphology is common in asymptomatic individuals, especially athletes.[46; 51; 53-55; 190-192] These factors indicate that using current measurement techniques, we may not properly identify the morphological features unique to symptomatic hips with cam FAI.[53; 54] However, a recent study found that even in the absence of pain, cartilage degeneration was found in subjects with cam morphology, which could indicate that femoral head asphericity may initiate the degeneration associated with OA.[193] However, if we do not fully understand the 3D morphological signature of cam FAI, asymptomatic morphology may be treated with unnecessary surgery.[194] Thus, it has recently been recognized that cam morphology alone should not be interpreted as a diagnosis of cam FAIS.[2; 24]

To identify morphological differences of the femur associated with this disease, 2D and 3D statistical shape modeling (SSM) techniques have been applied to radiographs or volumetric images of the hip.[78; 195-201] Radiographic based studies were initially used to identify altered anatomy of the proximal femur, including regions of the head-neck junction, in patients with OA.[195-199] While this observation provides further evidence of the relationship between altered morphology and OA, it is still unclear whether there are specific morphological traits of FAIS patients that lead to pain and tissue degradation long before the onset of OA. The shape variations specific to cam FAIS may be subtler than those associated with OA, such that radiographic shape analysis may not accurately identify abnormal morphology of cam FAIS. For this reason, SSM of 3D image-based surface representations has been applied to quantifying femoral morphology in patients and asymptomatic control subjects.[78; 200; 201]

Treatment

After diagnosis, cam FAIS is often treated first with conservative methods, including activity modification, anti-inflammatory medications, or an injection of steroid and long-acting anesthetic into the joint. In addition to serving as a possible method of treatment, intra-articular injections have also been shown to be a helpful diagnostic tool in identifying the pain as intra-articular.[68-70] After failed conservative treatment, FAIS is often treated surgically with the aim of creating normal morphology so as to improve biomechanics and slow or halt further degeneration to the cartilage and acetabular labrum.

Insufficient surgical resection may result in residual impingement and require revision femoroplasty,[202] while too aggressive of a resection may result in iatrogenic femoral neck fracture.[203] Although only a few iatrogenic fractures have been documented, insufficient resection is noted as the leading cause for revision femoroplasty.[202-204]

In response to the risk of iatrogenic femoral neck fracture, studies have evaluated postoperative strength of the resected femur using both in-vitro and in-silico techniques.[205-208] Importantly though, these studies have used generalized femoral anatomy without evidence of a cam lesion, which may not accurately represent the effect of femoral resection in cam FAIS patients. In addition to the inherent differences in morphology, increased cortical bone density over the region of impingement would likely increase the strength of the femoral neck.[209; 210] For these reasons, it is important to consider subject-specific anatomy, including the density and thickness of the cortical bone layer, in the analysis of the effect of resection on femoral strength.

Preoperative computer simulations can be used to identify the region of the femur that should be resected to provide the patient with impingement-free range of motion.[185; 186] However, intra-operative imaging provides real-time analysis of whether a resection has sufficiently removed the regions of bone responsible for impingement.[139] Fluoroscopic projections of bony anatomy provide a 2D image of the resultant shape of the femoral neck, while intra-operative arthroscope images can be used to assess dynamic motion between the femoral head and the labrum. Given these tools, residual impingement continues to be the leading cause of revision hip arthroscopy, therefore it is necessary to define surgical guidelines for consistent and sufficient bony resection.[191; 193]

Research Goals

This dissertation is comprised of two major objectives. First, motion capture, DF and computer models were used to investigate the pathomechanics of the hip with cam FAIS. Second, SSM was applied to gain a deeper understanding of the pathomorphology of cam FAIS and the implications to diagnosis and treatment.

Hip pathomechanics in cam FAIS patients are important to our understanding of altered motion patterns and joint loading that may initiate joint degeneration in these otherwise healthy individuals.[32] Herein, hip kinematics were quantified using DF and skin marker motion capture to capture in-vivo joint motion of the hip and whole-body kinematics, respectively. During kinematic data capture, ground reaction forces were collected from an instrumented treadmill to provide the ability to calculate muscle and joint reaction forces using musculoskeletal models. Finally, the kinematic and joint reaction force data provide boundary and loading conditions for finite element analysis of subject-specific hip biomechanics.

While cam FAIS has been described relative to specific pathomorphology, the guidelines used for diagnosis and surgical resection may not be specific, as a large population of asymptomatic individuals have cam morphology.[182] Statistical shape modeling (SSM) provides an objective method to quantify anatomical variation of anatomy, specifically of the proximal femur for the quantification of cam morphology. The shape statistics from SSM were used to evaluate commonly used radiographic measurements to determine the validity of currently used clinical measures, while the analysis of cortical bone thickness quantified differences in morphology and provided the data necessary to establish surgical resection guidelines.

Overall Significance

In general, our understanding of the natural history of cam FAIS and the etiological factors that may lead to early degeneration and the eventual onset of OA is insufficient. Over the past decade, there has been a substantial increase in the number of young adults treated for morphological hip diseases, including FAIS.[6; 7; 211] The prevalence of altered femoral head morphology in both young, active individuals and patients with end-stage OA is concerning as it presents a potentially grim future for the otherwise healthy person with cam morphology. The use of in-vivo kinematics of cam FAIS towards understanding subtle differences in motion patterns and to evaluate subject-specific hip contact mechanics may provide necessary insight to understand the role of cam morphology in hip joint degeneration prior to the onset of OA.

The relationship between population-based shape metrics of cam FAIS and radiographic diagnosis and treatment strategies provide clinically relevant and objective data on femoral morphology in cam FAIS. By quantifying the morphology, kinematics, and mechanics of cam FAIS, we begin to address the role of morphology and function in hip degeneration. Collectively, this research has provided crucial insight on metrics of morphology and biomechanics relevant to cam FAIS.

Summary of Chapters

The first chapter of this dissertation provides the foundation for this research, including an introduction to the anatomy, pathology, measures of shape and function, and motivation for the specific goals of this research. While it may not discuss all studies relevant to hip biomechanics, it does provide the necessary background to review the research herein.

While many studies have indicated that abnormal articulation may be the cause of tissue degeneration associated with cam FAIS, conclusions about altered motion patterns have yet to be fully defined.[2] For this reason, DF imaging was used to measure in-vivo bone motion of the hip for control subjects and cam FAIS patients. Previously, the in-vivo kinematic data for control subjects has been combined with whole body skin marker motion data to define the accuracy of methods used to estimate the location of the hip joint center, to determine the errors associated with soft-tissue artifact, and to understand the relationship between bony morphology and motion patterns.[89; 90; 94; 157; 158] The comparison between hip and pelvic kinematics of cam FAIS patients relative to control subjects is included in Chapter 2, which is in preparation for submission to *Clinical Orthopaedics and Related Research*.

Towards the quantification of cam morphology, SSM has been used to identify the specific 3D shape of the proximal femur in these patients.[78] Cam FAIS is often diagnosed based on a culmination of hip pain, reduced range of motion, and morphological measurements from radiographs. Importantly, a large number of asymptomatic individuals have cam morphology. For this reason, shape statistics from SSM were used as a reference for the evaluation of common clinical radiographic projections for their ability to visualize the cam lesion and diagnose cam FAIS. By identifying the radiographic projections that provide the best representation of 3D cam morphology, we can provide clinicians with improved recommendations for using radiographs in the diagnosis of cam FAIS. Chapter 3 is under peer review in *Clinical Orthopaedics and Related Research*.

In addition to radiographic measurements of morphology, a diagnosis of FAIS requires symptoms, specifically the presence of pain and positive clinical exams. The pain of cam FAIS is thought to originate as a result of impingement between the aspherical femoral head and the acetabular rim and labrum. Importantly, this impingement may result in increased stress over the region of cam morphology, which in turn would lead to bone remodeling and increased cortical thickness. To investigate this hypothesis, the inner and outer layers of the proximal femoral cortical bone were segmented and reconstructed to provide cortical thickness data relative to the surface of the outer cortex. These data were input into a statistical shape model of the proximal femur to investigate differences in cortical thickness between the two groups. Chapter 4 has been published in the *Journal of Orthopaedic Research*.[212]

The cortical thickness data from Chapter 5 was then used to simulate a surgical resection of cam FAIS using the thickness of the cortex as a guide for resection depth. After the simulated resection, SSM was used to evaluate the shape of the proximal femur in cam FAIS patients after the simulated resection relative to control subjects. With the risks of residual impingement, the use of an inherent surgical guide of proper resection depth may improve patient outcomes and reduce the rate of reoperation. Chapter 5 has been published in *Clinical Orthopaedics and Related Research*.[213]

Finally, Chapter 6 reviews the main objectives of this collection of research and discusses the ongoing research towards understanding the pathomechanics and pathomorphology of cam FAIS. Future research concepts and goals are presented which aim improve the impact of future work by streamlining the data collection and processing pipelines.

References

1. Ganz R, Parvizi J, Beck M, et al. 2003. Femoroacetabular impingement: A cause for osteoarthritis of the hip. Clin Orthop Relat Res:112-120.

2. Griffin DR, Dickenson EJ, O'Donnell J, et al. 2016. The Warwick Agreement on femoroacetabular impingement syndrome (FAI syndrome): An international consensus statement. Br J Sports Med 50:1169-1176.

3. Tanzer M, Noiseux N. 2004. Osseous abnormalities and early osteoarthritis: The role of hip impingement. Clin Orthop Relat Res:170-177.

4. Kuhns BD, Weber AE, Levy DM, et al. 2015. The natural history of femoroacetabular impingement. Front Surg 2:58.

5. Packer JD, Safran MR. 2015. The etiology of primary femoroacetabular impingement: Genetics or acquired deformity? J Hip Preserv Surg 2:249-257.

6. Montgomery SR, Ngo SS, Hobson T, et al. 2013. Trends and demographics in hip arthroscopy in the United States. Arthroscopy 29:661-665.

7. Colvin AC, Harrast J, Harner C. 2012. Trends in hip arthroscopy. J Bone Joint Surg Am 94:e23.

8. Bonazza NA, Homcha B, Liu G, et al. 2018. Surgical trends in arthroscopic hip surgery using a large national database. Arthroscopy.

9. Menschik F. 1997. The hip joint as a conchoid shape. J Biomech 30:971-973.

10. Fox AJS, Bedi A, Rodeo SA. 2009. The basic science of articular cartilage: Structure, composition, and function. Sports Health 1:461-468.

11. Buckwalter JA, Mankin HJ. 1998. Articular cartilage: Degeneration and osteoarthritis, repair, regeneration, and transplantation. Instr Course Lect 47:487-504.

12. Jesse MK, Petersen B, Strickland C, et al. 2013. Normal anatomy and imaging of the hip: Emphasis on impingement assessment. Semin Musculoskelet Radiol 17:229-247.

13. Bonner TF, Colbrunn RW, Bottros JJ, et al. 2015. The contribution of the acetabular labrum to hip joint stability: A quantitative analysis using a dynamic three-dimensional robot model. J Biomech Eng 137:061012.

14. Lertwanich P, Plakseychuk A, Kramer S, et al. 2016. Biomechanical evaluation contribution of the acetabular labrum to hip stability. Knee Surg Sports Traumatol Arthrosc 24:2338-2345.

15. Grant AD, Sala DA, Davidovitch RI. 2012. The labrum: Structure, function, and injury with femoro-acetabular impingement. J Child Orthop 6:357-372.

16. Nepple JJ, Philippon MJ, Campbell KJ, et al. 2014. The hip fluid seal--part II: The effect of an acetabular labral tear, repair, resection, and reconstruction on hip stability to distraction. Knee Surg Sports Traumatol Arthrosc 22:730-736.

17. Philippon MJ, Nepple JJ, Campbell KJ, et al. 2014. The hip fluid seal--part I: The effect of an acetabular labral tear, repair, resection, and reconstruction on hip fluid pressurization. Knee Surg Sports Traumatol Arthrosc 22:722-729.

18. Bsat S, Frei H, Beaule PE. 2016. The acetabular labrum: A review of its function. Bone Joint J 98-b:730-735.

19. Dwyer MK, Jones HL, Hogan MG, et al. 2014. The acetabular labrum regulates fluid circulation of the hip joint during functional activities. Am J Sports Med 42:812-819.

20. Petersen W, Petersen F, Tillmann B. 2003. Structure and vascularization of the acetabular labrum with regard to the pathogenesis and healing of labral lesions. Arch Orthop Trauma Surg 123:283-288.

21. Cooper HJ, Walters BL, Rodriguez JA. 2015. Anatomy of the hip capsule and pericapsular structures: A cadaveric study. Clin Anat 28:665-671.

22. Nepple JJ, Smith MV. 2015. Biomechanics of the hip capsule and capsule management strategies in hip arthroscopy. Sports Med Arthrosc Rev 23:164-168.

23. Kaya M, Suziki T, Minowa T, et al. 2014. Ligamentum teres injury is associated with the articular damage pattern in patients with femoroacetabular impingement. Arthroscopy 30:1582-1587.

24. Freke MD, Kemp J, Svege I, et al. 2016. Physical impairments in symptomatic femoroacetabular impingement: A systematic review of the evidence. Br J Sports Med 50:1180.

25. Diamond LE, Dobson FL, Bennell KL, et al. 2015. Physical impairments and activity limitations in people with femoroacetabular impingement: A systematic review. Br J Sports Med 49:230-242.

26. Kellgren JH, Lawrence JS. 1957. Radiological assessment of osteo-arthrosis. Ann Rheum Dis 16:494-502.

27. National Center for Health Statistics. 2017. Health, United States, 2016: With chartbook on long-term trends in health. Hyattsville (MD): National Center for Health Statistics (US).

28. Rajaee SS, Campbell JC, Mirocha J, et al. 2018. Increasing burden of total hip arthroplasty revisions in patients between 45 and 64 years of age. J Bone Joint Surg Am 100:449-458.

29. Ganz R, Leunig M, Leunig-Ganz K, et al. 2008. The etiology of osteoarthritis of the hip: An integrated mechanical concept. Clin Orthop Relat Res 466:264-272.

30. Harris WH. 1986. Etiology of osteoarthritis of the hip. Clin Orthop Relat Res:20-33.

31. Beck M, Kalhor M, Leunig M, et al. 2005. Hip morphology influences the pattern of damage to the acetabular cartilage: Femoroacetabular impingement as a cause of early osteoarthritis of the hip. J Bone Joint Surg Br 87:1012-1018.

32. Matheney T, Sandell L, Foucher K, et al. 2013. Motion analysis, cartilage mechanics, and biology in femoroacetabular impingement: Current understanding and areas of future research. J Am Acad Orthop Surg 21 Suppl 1:S27-32.

33. Barros HJ, Camanho GL, Bernabe AC, et al. 2010. Femoral head-neck junction deformity is related to osteoarthritis of the hip. Clin Orthop Relat Res 468:1920-1925.

34. Ito K, Minka MA, 2nd, Leunig M, et al. 2001. Femoroacetabular impingement and the cam-effect. A MRI-based quantitative anatomical study of the femoral head-neck offset. J Bone Joint Surg Br 83:171-176.

35. Philippon MJ, Maxwell RB, Johnston TL, et al. 2007. Clinical presentation of femoroacetabular impingement. Knee Surg Sports Traumatol Arthrosc 15:1041-1047.

36. MacFarlane RJ, Konan S, El-Huseinny M, et al. 2014. A review of outcomes of the surgical management of femoroacetabular impingement. Ann R Coll Surg Engl 96:331-338.

37. McCarthy JC, Lee J. 2005. Hip arthroscopy: Indications and technical pearls. Clin Orthop Relat Res 441:180-187.

38. Wall PD, Fernandez M, Griffin DR, et al. 2013. Nonoperative treatment for femoroacetabular impingement: A systematic review of the literature. PM R 5:418-426.

39. Wang WG, Yue DB, Zhang NF, et al. 2011. Clinical diagnosis and arthroscopic treatment of acetabular labral tears. Orthop Surg 3:28-34.

40. Alvarez DR, Mardones RM. 2010. Efficacy of osseous abnormalities correction with arthroscopic surgery in femoroacetabular impingement. Cartilage 1:233-237.

41. Aoki SK, Beckmann JT, Wylie JD. 2016. Arthroscopic femoral osteochondroplasty for cam-type femoroacetabular impingement: The trough technique. Arthrosc Tech 5:e743-e749.

42. Harris JD, McCormick FM, Abrams GD, et al. 2013. Complications and reoperations during and after hip arthroscopy: A systematic review of 92 studies and more than 6,000 patients. Arthroscopy 29:589-595.

43. Weiland DE, Philippon MJ. 2005. Arthroscopic technique of femoroacetabular impingement. Oper Tech Orthop 15:256-260.

44. Lynch TS, Terry MA, Bedi A, et al. 2013. Hip arthroscopic surgery: Patient evaluation, current indications, and outcomes. Am J Sports Med 41:1174-1189.

45. Werner BC, Gaudiani MA, Ranawat AS. 2016. The etiology and arthroscopic surgical management of cam lesions. Clin Sports Med 35:391-404.

46. Agricola R, Heijboer MP, Ginai AZ, et al. 2014. A cam deformity is gradually acquired during skeletal maturation in adolescent and young male soccer players: A prospective study with minimum 2-year follow-up. Am J Sports Med 42:798-806.

47. Murray RO, Duncan C. 1971. Athletic activity in adolescence as an etiological factor in degenerative hip disease. J Bone Joint Surg Br 53:406-419.

48. Pollard TC, Villar RN, Norton MR, et al. 2010. Genetic influences in the aetiology of femoroacetabular impingement: A sibling study. J Bone Joint Surg Br 92:209-216.

49. Hoaglund FT. 2013. Primary osteoarthritis of the hip: A genetic disease caused by european genetic variants. J Bone Joint Surg Am 95:463-468.

50. Sandell LJ. 2012. Etiology of osteoarthritis: Genetics and synovial joint development. Nat Rev Rheumatol 8:77-89.

51. Nepple JJ, Vigdorchik JM, Clohisy JC. 2015. What is the association between sports participation and the development of proximal femoral cam deformity? A systematic review and meta-analysis. Am J Sports Med 43:2833-2840.

52. Siebenrock KA, Ferner F, Noble PC, et al. 2011. The cam-type deformity of the proximal femur arises in childhood in response to vigorous sporting activity. Clin Orthop Relat Res 469:3229-3240.

53. Anderson LA, Anderson MB, Kapron A, et al. 2016. The 2015 Frank Stinchfield award: Radiographic abnormalities common in senior athletes with well-functioning hips but not associated with osteoarthritis. Clin Orthop Relat Res 474:342-352.

54. Kapron AL, Anderson AE, Aoki SK, et al. 2011. Radiographic prevalence of femoroacetabular impingement in collegiate football players: AAOS exhibit selection. J Bone Joint Surg Am 93:e111(111-110).

55. Lerebours F, Robertson W, Neri B, et al. 2016. Prevalence of cam-type morphology in elite ice hockey players. Am J Sports Med 44:1024-1030.

56. Roels P, Agricola R, Oei EH, et al. 2014. Mechanical factors explain development of cam-type deformity. Osteoarthritis Cartilage 22:2074-2082.

57. Kumar D, Wyatt CR, Lee S, et al. 2013. Association of cartilage defects, and other MRI findings with pain and function in individuals with mild-moderate radiographic hip osteoarthritis and controls. Osteoarthritis Cartilage 21:1685-1692.

58. Ollivier M, Le Corroller T, Parratte S, et al. 2017. Mechanical strains passing through the acetabular labrum modify its shape during hip motion: An anatomical study. Knee Surg Sports Traumatol Arthrosc 25:1967-1974.

59. Abrams GD, Luria A, Sampson J, et al. 2017. Decreased synovial inflammation in atraumatic hip microinstability compared with femoroacetabular impingement. Arthroscopy 33:553-558.

60. Kassarjian A, Yoon LS, Belzile E, et al. 2005. Triad of MR arthrographic findings in patients with cam-type femoroacetabular impingement. Radiology 236:588-592.

61. Riley GM, McWalter EJ, Stevens KJ, et al. 2015. MRI of the hip for the evaluation of femoroacetabular impingement; past, present, and future. J Magn Reson Imaging 41:558-572.

62. Krych AJ, King AH, Berardelli RL, et al. 2016. Is subchondral acetabular edema or cystic change on MRI a contraindication for hip arthroscopy in patients with femoroacetabular impingement? Am J Sports Med 44:454-459.

63. Roemer FW, Hunter DJ, Winterstein A, et al. 2011. Hip osteoarthritis MRI scoring system (HOAMS): Reliability and associations with radiographic and clinical findings. Osteoarthritis Cartilage 19:946-962.

64. Kim YT, Azuma H. 1995. The nerve endings of the acetabular labrum. Clin Orthop Relat Res:176-181.

65. Alzaharani A, Bali K, Gudena R, et al. 2014. The innervation of the human acetabular labrum and hip joint: An anatomic study. BMC Musculoskelet Disord 15:41.

66. Haversath M, Hanke J, Landgraeber S, et al. 2013. The distribution of nociceptive innervation in the painful hip: A histological investigation. Bone Joint J 95-b:770-776.

67. Bedi A, Dolan M, Leunig M, et al. 2011. Static and dynamic mechanical causes of hip pain. Arthroscopy 27:235-251.

68. Kivlan BR, Martin RL, Sekiya JK. 2011. Response to diagnostic injection in patients with femoroacetabular impingement, labral tears, chondral lesions, and extra-articular pathology. Arthroscopy 27:619-627.

69. Byrd JW, Jones KS. 2004. Diagnostic accuracy of clinical assessment, magnetic resonance imaging, magnetic resonance arthrography, and intra-articular injection in hip arthroscopy patients. Am J Sports Med 32:1668-1674.

70. Pateder DB, Hungerford MW. 2007. Use of fluoroscopically guided intra-articular hip injection in differentiating the pain source in concomitant hip and lumbar spine arthritis. Am J Orthop (Belle Mead NJ) 36:591-593.

71. Tannast M, Kubiak-Langer M, Langlotz F, et al. 2007. Noninvasive three-dimensional assessment of femoroacetabular impingement. J Orthop Res 25:122-131.

72. Audenaert E, Van Houcke J, Maes B, et al. 2012. Range of motion in femoroacetabular impingement. Acta Orthop Belg 78:327-332.

73. Bagwell JJ, Snibbe J, Gerhardt M, et al. 2016. Hip kinematics and kinetics in persons with and without cam femoroacetabular impingement during a deep squat task. Clin Biomech (Bristol, Avon) 31:87-92.

74. Kubiak-Langer M, Tannast M, Murphy SB, et al. 2007. Range of motion in anterior femoroacetabular impingement. Clin Orthop Relat Res 458:117-124.

75. Henak CR, Kapron AL, Anderson AE, et al. 2014. Specimen-specific predictions of contact stress under physiological loading in the human hip: Validation and sensitivity studies. Biomech Model Mechanobiol 13:387-400.

76. Guilak F. 2011. Biomechanical factors in osteoarthritis. Best Pract Res Clin Rheumatol 25:815-823.

77. Buckwalter JA, Anderson DD, Brown TD, et al. 2013. The roles of mechanical stresses in the pathogenesis of osteoarthritis: Implications for treatment of joint injuries. Cartilage 4:286-294.

78. Harris MD, Datar M, Whitaker RT, et al. 2013. Statistical shape modeling of cam femoroacetabular impingement. J Orthop Res 31:1620-1626.

79. Diamond LE, Wrigley TV, Bennell KL, et al. 2016. Hip joint biomechanics during gait in people with and without symptomatic femoroacetabular impingement. Gait Posture 43:198-203.

80. Hetsroni I, Funk S, Ben-Sira D, et al. 2015. Femoroacetabular impingement syndrome is associated with alterations in hindfoot mechanics: A three-dimensional gait analysis study. Clin Biomech (Bristol, Avon) 30:1189-1193.

81. Hunt MA, Guenther JR, Gilbart MK. 2013. Kinematic and kinetic differences during walking in patients with and without symptomatic femoroacetabular impingement. Clin Biomech (Bristol, Avon) 28:519-523.

82. Kennedy MJ, Lamontagne M, Beaule PE. 2009. Femoroacetabular impingement alters hip and pelvic biomechanics during gait walking biomechanics of FAI. Gait Posture 30:41-44.

83. Turley GA, Williams MA, Wellings RM, et al. 2013. Evaluation of range of motion restriction within the hip joint. Med Biol Eng Comput 51:467-477.

84. Van Houcke J, Pattyn C, Vanden Bossche L, et al. 2014. The pelvifemoral rhythm in cam-type femoroacetabular impingement. Clin Biomech (Bristol, Avon) 29:63-67.

85. Farkas GJ, Cvetanovich GL, Rajan KB, et al. 2015. Impact of femoroacetabular impingement morphology on gait assessment in symptomatic patients. Sports Health 7:429-436.

86. Lahner M, Musshoff D, von Schulze Pellengahr C, et al. 2015. Is the kinect system suitable for evaluation of the hip joint range of motion and as a screening tool for femoroacetabular impingement (FAI)? Technol Health Care 23:75-81.

87. Howell AM, Kobayashi T, Hayes HA, et al. 2013. Kinetic gait analysis using a low-cost insole. IEEE Trans Biomed Eng 60:3284-3290.

88. Zeni J, Jr., Abujaber S, Flowers P, et al. 2013. Biofeedback to promote movement symmetry after total knee arthroplasty: A feasibility study. J Orthop Sports Phys Ther 43:715-726.

89. Fiorentino NM, Atkins PR, Kutschke MJ, et al. 2016. In-vivo quantification of dynamic hip joint center errors and soft tissue artifact. Gait Posture 50:246-251.

90. Fiorentino NM, Atkins PR, Kutschke MJ, et al. 2017. Soft tissue artifact causes significant errors in the calculation of joint angles and range of motion at the hip. Gait Posture 55:184-190.

91. Hara R, Sangeux M, Baker R, et al. 2014. Quantification of pelvic soft tissue artifact in multiple static positions. Gait Posture 39:712-717.

92. Rouhandeh A, Joslin C, Zhen Q, et al. 2014. Non-invasive assessment of soft-tissue artefacts in hip joint kinematics using motion capture data and ultrasound depth measurements. Conf Proc IEEE Eng Med Biol Soc 2014:4342-4345.

93. Rylander JH, Shu B, Andriacchi TP, et al. 2011. Preoperative and postoperative sagittal plane hip kinematics in patients with femoroacetabular impingement during level walking. Am J Sports Med 39 Suppl:36s-42s.

94. Fiorentino NM, Kutschke MJ, Atkins PR, et al. 2016. Accuracy of functional and predictive methods to calculate the hip joint center in young non-pathologic asymptomatic adults with dual fluoroscopy as a reference standard. Ann Biomed Eng 44:2168-2180.

95. Piazza SJ, Okita N, Cavanagh PR. 2001. Accuracy of the functional method of hip joint center location: Effects of limited motion and varied implementation. J Biomech 34:967-973.

96. Sangeux M, Pillet H, Skalli W. 2014. Which method of hip joint centre localisation should be used in gait analysis? Gait Posture 40:20-25.

97. Stagni R, Leardini A, Cappozzo A, et al. 2000. Effects of hip joint centre mislocation on gait analysis results. J Biomech 33:1479-1487.

98. Bell AL, Pedersen DR, Brand RA. 1990. A comparison of the accuracy of several hip center location prediction methods. J Biomech 23:617-621.

99. Harrington ME, Zavatsky AB, Lawson SE, et al. 2007. Prediction of the hip joint centre in adults, children, and patients with cerebral palsy based on magnetic resonance imaging. J Biomech 40:595-602.

100. Davis III RB, Ounpuu S, Tyburski D, et al. 1991. A gait analysis data collection and reduction technique. Hum Mov Sci 10:575-587.

101. Ehrig RM, Heller MO, Kratzenstein S, et al. 2011. The score residual: A quality index to assess the accuracy of joint estimations. J Biomech 44:1400-1404.

102. Schwartz MH, Rozumalski A. 2005. A new method for estimating joint parameters from motion data. J Biomech 38:107-116.

103. Cerveri P, Manzotti A, Baroni G. 2014. Patient-specific acetabular shape modelling: Comparison among sphere, ellipsoid and conchoid parameterisations. Comput Methods Biomech Biomed Engin 17:560-567.

104. Harris MD, Kapron AL, Peters CL, et al. 2014. Correlations between the alpha angle and femoral head asphericity: Implications and recommendations for the diagnosis of cam femoroacetabular impingement. Eur J Radiol 83:788-796.

105. Standefer KD, Dempsey M, Jo C, et al. 2017. 3D MRI quantification of femoral head deformity in legg-calve-perthes disease. J Orthop Res 35:2051-2058.

106. Steppacher SD, Tannast M, Werlen S, et al. 2008. Femoral morphology differs between deficient and excessive acetabular coverage. Clin Orthop Relat Res 466:782-790.

107. Sankar WN, Neubuerger CO, Moseley CF. 2010. Femoral head sphericity in untreated developmental dislocation of the hip. J Pediatr Orthop 30:558-561.

108. Cooper RJ, Williams S, Mengoni M, et al. 2018. Patient-specific parameterised cam geometry in finite element models of femoroacetabular impingement of the hip. Clin Biomech (Bristol, Avon) 54:62-70.

109. Chegini S, Beck M, Ferguson SJ. 2009. The effects of impingement and dysplasia on stress distributions in the hip joint during sitting and walking: A finite element analysis. J Orthop Res 27:195-201.

110. Hellwig FL, Tong J, Hussell JG. 2016. Hip joint degeneration due to cam impingement: A finite element analysis. Comput Methods Biomech Biomed Engin 19:41-48.

111. Liechti EF, Ferguson SJ, Tannast M. 2015. Protrusio acetabuli: Joint loading with severe pincer impingement and its theoretical implications for surgical therapy. J Orthop Res 33:106-113.

112. Arbabi E, Chegini S, Boulic R, et al. 2010. Penetration depth method--novel real-time strategy for evaluating femoroacetabular impingement. J Orthop Res 28:880-886.

113. Lenaerts G, De Groote F, Demeulenaere B, et al. 2008. Subject-specific hip geometry affects predicted hip joint contact forces during gait. J Biomech 41:1243-1252.

114. Lenaerts G, Bartels W, Gelaude F, et al. 2009. Subject-specific hip geometry and hip joint centre location affects calculated contact forces at the hip during gait. J Biomech 42:1246-1251.

115. Roling MA, Visser MI, Oei EH, et al. 2015. A quantitative non-invasive assessment of femoroacetabular impingement with CT-based dynamic simulation--cadaveric validation study. BMC Musculoskelet Disord 16:50.

116. Hamada H, Takao M, Nakahara I, et al. 2016. Hip range-of-motion (ROM) is less than normal after rotational acetabular osteotomy for developmental dysplasia of the hip: A simulated ROM analysis. J Orthop Res 34:217-223.

117. Kapron AL, Aoki SK, Peters CL, et al. 2015. In-vivo hip arthrokinematics during supine clinical exams: Application to the study of femoroacetabular impingement. J Biomech 48:2879-2886.

118. Czerny C, Hofmann S, Neuhold A, et al. 1996. Lesions of the acetabular labrum: Accuracy of MR imaging and MR arthrography in detection and staging. Radiology 200:225-230.

119. Bedi A, Dolan M, Magennis E, et al. 2012. Computer-assisted modeling of osseous impingement and resection in femoroacetabular impingement. Arthroscopy 28:204-210.

120. Liu L, Ecker T, Schumann S, et al. 2014. Computer assisted planning and navigation of periacetabular osteotomy with range of motion optimization. Med Image Comput Comput Assist Interv 17:643-650.

121. Safran MR, Giordano G, Lindsey DP, et al. 2011. Strains across the acetabular labrum during hip motion: A cadaveric model. Am J Sports Med 39 Suppl:92s-102s.

122. Smith MV, Costic RS, Allaire R, et al. 2014. A biomechanical analysis of the soft tissue and osseous constraints of the hip joint. Knee Surg Sports Traumatol Arthrosc 22:946-952.

123. van Arkel RJ, Amis AA, Jeffers JR. 2015. The envelope of passive motion allowed by the capsular ligaments of the hip. J Biomech 48:3803-3809.

124. Beaule PE, Zaragoza E, Motamedi K, et al. 2005. Three-dimensional computed tomography of the hip in the assessment of femoroacetabular impingement. J Orthop Res 23:1286-1292.

125. Clohisy JC, Carlisle JC, Beaule PE, et al. 2008. A systematic approach to the plain radiographic evaluation of the young adult hip. J Bone Joint Surg Am 90 Suppl 4:47-66.

126. Fadul DA, Carrino JA. 2009. Imaging of femoroacetabular impingement. J Bone Joint Surg Am 91 Suppl 1:138-143.

127. Ayeni OR, Chan K, Whelan DB, et al. 2014. Diagnosing femoroacetabular impingement from plain radiographs: Do radiologists and orthopaedic surgeons differ? Orthop J Sports Med 2:2325967114541414.

128. Eijer H, Leunig M, Mahomed MN, et al. 2001. Cross-table lateral radiographs for screening of anterior femoral head-neck offset in patients with femoro-acetabular impingement. Hip Int 11:37-41.

129. Meyer DC, Beck M, Ellis T, et al. 2006. Comparison of six radiographic projections to assess femoral head/neck asphericity. Clin Orthop Relat Res 445:181-185.

130. Siebelt M, Agricola R, Weinans H, et al. 2014. The role of imaging in early hip OA. Osteoarthritis Cartilage 22:1470-1480.

131. Bittersohl B, Steppacher S, Haamberg T, et al. 2009. Cartilage damage in femoroacetabular impingement (FAI): Preliminary results on comparison of standard diagnostic vs delayed gadolinium-enhanced magnetic resonance imaging of cartilage (dGEMRIC). Osteoarthritis Cartilage 17:1297-1306.

132. Matzat SJ, van Tiel J, Gold GE, et al. 2013. Quantitative MRI techniques of cartilage composition. Quant Imaging Med Surg 3:162-174.

133. Wheaton AJ, Casey FL, Gougoutas AJ, et al. 2004. Correlation of T1rho with fixed charge density in cartilage. J Magn Reson Imaging 20:519-525.

134. Watanabe A, Boesch C, Siebenrock K, et al. 2007. T2 mapping of hip articular cartilage in healthy volunteers at 3T: A study of topographic variation. J Magn Reson Imaging 26:165-171.

135. Du J, Bydder GM. 2013. Qualitative and quantitative ultrashort-TE MRI of cortical bone. NMR Biomed 26:489-506.

136. Wadhwa V, Malhotra V, Xi Y, et al. 2016. Bone and joint modeling from 3D knee MRI: Feasibility and comparison with radiographs and 2D MRI. Clin Imaging 40:765-768.

137. Nepple JJ, Martel JM, Kim YJ, et al. 2012. Do plain radiographs correlate with CT for imaging of cam-type femoroacetabular impingement? Clin Orthop Relat Res 470:3313-3320.

138. Domayer SE, Ziebarth K, Chan J, et al. 2011. Femoroacetabular cam-type impingement: Diagnostic sensitivity and specificity of radiographic views compared to radial MRI. Eur J Radiol 80:805-810.

139. Ross JR, Bedi A, Stone RM, et al. 2014. Intraoperative fluoroscopic imaging to treat cam deformities: Correlation with 3-dimensional computed tomography. Am J Sports Med 42:1370-1376.

140. Rakhra KS, Sheikh AM, Allen D, et al. 2009. Comparison of MRI alpha angle measurement planes in femoroacetabular impingement. Clin Orthop Relat Res 467:660-665.

141. Smith KM, Gerrie BJ, McCulloch PC, et al. 2017. Comparison of MRI, CT, Dunn 45 degrees and Dunn 90 degrees alpha angle measurements in femoroacetabular impingement. Hip Int:0.

142. Subburaj K, Valentinitsch A, Dillon AB, et al. 2013. Regional variations in MR relaxation of hip joint cartilage in subjects with and without femoralacetabular impingement. Magn Reson Imaging 31:1129-1136.

143. Sutter R, Dietrich TJ, Zingg PO, et al. 2012. How useful is the alpha angle for discriminating between symptomatic patients with cam-type femoroacetabular impingement and asymptomatic volunteers? Radiology 264:514-521.

144. Abraham CL, Bangerter NK, McGavin LS, et al. 2015. Accuracy of 3D dual echo steady state (DESS) MR arthrography to quantify acetabular cartilage thickness. J Magn Reson Imaging 42:1329-1338.

145. Henak CR, Abraham CL, Peters CL, et al. 2014. Computed tomography arthrography with traction in the human hip for three-dimensional reconstruction of cartilage and the acetabular labrum. Clin Radiol 69:e381-391.

146. Schmaranzer F, Klauser A, Kogler M, et al. 2014. Improving visualization of the central compartment of the hip with direct MR arthrography under axial leg traction: A feasibility study. Acad Radiol 21:1240-1247.

147. Suter A, Dietrich TJ, Maier M, et al. 2015. MR findings associated with positive distraction of the hip joint achieved by axial traction. Skeletal Radiol 44:787-795.

148. Larkin B, van Holsbeeck M, Koueiter D, et al. 2015. What is the impingement-free range of motion of the asymptomatic hip in young adult males? Clin Orthop Relat Res 473:1284-1288.

149. Kolo FC, Charbonnier C, Pfirrmann CW, et al. 2013. Extreme hip motion in professional ballet dancers: Dynamic and morphological evaluation based on magnetic resonance imaging. Skeletal Radiol 42:689-698.

150. Wassilew GI, Janz V, Heller MO, et al. 2013. Real time visualization of femoroacetabular impingement and subluxation using 320-slice computed tomography. J Orthop Res 31:275-281.

151. Kapron AL, Aoki SK, Peters CL, et al. 2014. Accuracy and feasibility of dual fluoroscopy and model-based tracking to quantify in vivo hip kinematics during clinical exams. J Appl Biomech 30:461-470.

152. Mozingo JD, Akbari Shandiz M, Marquez FM, et al. 2018. Validation of imaging-based quantification of glenohumeral joint kinematics using an unmodified clinical biplane fluoroscopy system. J Biomech 71:306-312.

153. Sharma GB, Kuntze G, Kukulski D, et al. 2015. Validating dual fluoroscopy system capabilities for determining in-vivo knee joint soft tissue deformation: A strategy for registration error management. J Biomech 48:2181-2185.

154. Wang B, Roach KE, Kapron AL, et al. 2015. Accuracy and feasibility of high-speed dual fluoroscopy and model-based tracking to measure in vivo ankle arthrokinematics. Gait Posture 41:888-893.

155. Bey MJ, Zauel R, Brock SK, et al. 2006. Validation of a new model-based tracking technique for measuring three-dimensional, in vivo glenohumeral joint kinematics. J Biomech Eng 128:604-609.

156. Kapron AL, Aoki SK, Peters CL, et al. 2014. Subject-specific patterns of femur-labrum contact are complex and vary in asymptomatic hips and hips with femoroacetabular impingement. Clin Orthop Relat Res 472:3912-3922.

157. Atkins PR, Fiorentino NM, Aoki SK, et al. 2017. In vivo measurements of the ischiofemoral space in recreationally active participants during dynamic activities: A high-speed dual fluoroscopy study. Am J Sports Med:363546517712990.

158. Uemura K, Atkins PR, Fiorentino NM, et al. 2018. Hip rotation during standing and dynamic activities and the compensatory effect of femoral anteversion: An in-vivo analysis of asymptomatic young adults using three-dimensional computed tomography models and dual fluoroscopy. Gait Posture 61:276-281.

159. Anderson AE, Ellis BJ, Maas SA, et al. 2008. Validation of finite element predictions of cartilage contact pressure in the human hip joint. J Biomech Eng 130:051008.

160. Harris MD, Anderson AE, Henak CR, et al. 2012. Finite element prediction of cartilage contact stresses in normal human hips. J Orthop Res 30:1133-1139.

161. Henak CR, Ateshian GA, Weiss JA. 2014. Finite element prediction of transchondral stress and strain in the human hip. J Biomech Eng 136:021021.

162. Henak CR, Ellis BJ, Harris MD, et al. 2011. Role of the acetabular labrum in load support across the hip joint. J Biomech 44:2201-2206.

163. Maas SA, Ellis BJ, Rawlins DS, et al. 2016. Finite element simulation of articular contact mechanics with quadratic tetrahedral elements. J Biomech 49:659-667.

164. Ng KC, Mantovani G, Lamontagne M, et al. 2016. Increased hip stresses resulting from a cam deformity and decreased femoral neck-shaft angle during level walking. Clin Orthop Relat Res. 475:998-1008.

165. Todd JN, Maak TG, Ateshian GA, et al. 2018. Hip chondrolabral mechanics during activities of daily living: Role of the labrum and interstitial fluid pressurization. J Biomech 69:113-120.

166. Henak CR, Carruth ED, Anderson AE, et al. 2013. Finite element predictions of cartilage contact mechanics in hips with retroverted acetabula. Osteoarthritis Cartilage 21:1522-1529.

167. Henak CR, Abraham CL, Anderson AE, et al. 2014. Patient-specific analysis of cartilage and labrum mechanics in human hips with acetabular dysplasia. Osteoarthritis Cartilage 22:210-217.

168. Rhyu KH, Kim YH, Park WM, et al. 2011. Application of finite element analysis in pre-operative planning for deformity correction of abnormal hip joints--a case series. Proc Inst Mech Eng H 225:929-936.

169. Henninger HB, Reese SP, Anderson AE, et al. 2010. Validation of computational models in biomechanics. Proc Inst Mech Eng H 224:801-812.

170. Anderson AE, Peters CL, Tuttle BD, et al. 2005. Subject-specific finite element model of the pelvis: Development, validation and sensitivity studies. J Biomech Eng 127:364-373.

171. Anderson AE, Ellis BJ, Maas SA, et al. 2010. Effects of idealized joint geometry on finite element predictions of cartilage contact stresses in the hip. J Biomech 43:1351-1357.

172. Chen G, Wu FY, Liu ZC, et al. 2015. Comparisons of node-based and element-based approaches of assigning bone material properties onto subject-specific finite element models. Med Eng Phys 37:808-812.

173. Klennert BJ, Ellis BJ, Maak TG, et al. 2017. The mechanics of focal chondral defects in the hip. J Biomech 52:31-37.

174. Ferguson SJ, Bryant JT, Ito K. 2001. The material properties of the bovine acetabular labrum. J Orthop Res 19:887-896.

175. Quapp KM, Weiss JA. 1998. Material characterization of human medial collateral ligament. J Biomech Eng 120:757-763.

176. Bergmann G, Deuretzbacher G, Heller M, et al. 2001. Hip contact forces and gait patterns from routine activities. J Biomech 34:859-871.

177. Ng KC, Rouhi G, Lamontagne M, et al. 2012. Finite element analysis examining the effects of cam FAI on hip joint mechanical loading using subject-specific geometries during standing and maximum squat. HSS J 8:206-212.

178. Assassi L, Magnenat-Thalmann N. 2016. Assessment of cartilage contact pressure and loading in the hip joint during split posture. Int J Comput Assist Radiol Surg 11:745-756.

179. Notzli HP, Wyss TF, Stoecklin CH, et al. 2002. The contour of the femoral head-neck junction as a predictor for the risk of anterior impingement. J Bone Joint Surg Br 84:556-560.

180. Nepple JJ, Carlisle JC, Nunley RM, et al. 2011. Clinical and radiographic predictors of intra-articular hip disease in arthroscopy. Am J Sports Med 39:296-303.

181. Tannast M, Siebenrock KA, Anderson SE. 2007. Femoroacetabular impingement: Radiographic diagnosis--what the radiologist should know. AJR Am J Roentgenol 188:1540-1552.

182. Frank JM, Harris JD, Erickson BJ, et al. 2015. Prevalence of femoroacetabular impingement imaging findings in asymptomatic volunteers: A systematic review. Arthroscopy 31:1199-1204.

183. Agricola R, Waarsing JH, Thomas GE, et al. 2014. Cam impingement: Defining the presence of a cam deformity by the alpha angle: Data from the check cohort and chingford cohort. Osteoarthritis Cartilage 22:218-225.

184. Espie A, Chaput B, Murgier J, et al. 2014. 45 degrees -45 degrees -30 degrees frog-leg radiograph for diagnosing cam-type anterior femoroacetabular impingement: Reproducibility and thresholds. Orthop Traumatol Surg Res 100:843-848.

185. Clohisy JC, Nunley RM, Otto RJ, et al. 2007. The frog-leg lateral radiograph accurately visualized hip cam impingement abnormalities. Clin Orthop Relat Res 462:115-121.

186. Laborie LB, Lehmann TG, Engesaeter IO, et al. 2014. The alpha angle in cam-type femoroacetabular impingement: New reference intervals based on 2038 healthy young adults. Bone Joint J 96-b:449-454.

187. Yamamoto Y, Hiejima Y. 2014. Usefulness of cross-table lateral view radiograph for the diagnosis of cam-type femoroacetabular impingement. Eur J Orthop Surg Traumatol 24:365-369.

188. Clohisy JC, Carlisle JC, Trousdale R, et al. 2009. Radiographic evaluation of the hip has limited reliability. Clin Orthop Relat Res 467:666-675.

189. Barton C, Salineros MJ, Rakhra KS, et al. 2011. Validity of the alpha angle measurement on plain radiographs in the evaluation of cam-type femoroacetabular impingement. Clin Orthop Relat Res 469:464-469.

190. Philippon MJ, Ho CP, Briggs KK, et al. 2013. Prevalence of increased alpha angles as a measure of cam-type femoroacetabular impingement in youth ice hockey players. Am J Sports Med 41:1357-1362.

191. Gerhardt MB, Romero AA, Silvers HJ, et al. 2012. The prevalence of radiographic hip abnormalities in elite soccer players. Am J Sports Med 40:584-588.

192. Hack K, Di Primio G, Rakhra K, et al. 2010. Prevalence of cam-type femoroacetabular impingement morphology in asymptomatic volunteers. J Bone Joint Surg Am 92:2436-2444.

193. McGuffin WS, Melkus G, Rakhra KS, et al. 2015. Is the contralateral hip at risk in patients with unilateral symptomatic cam femoroacetabular impingement? A quantitative T1rho MRI study. Osteoarthritis Cartilage 23:1337-1342.

194. Reiman MP, Thorborg K. 2015. Femoroacetabular impingement surgery: Are we moving too fast and too far beyond the evidence? Br J Sports Med 49:782-784.

195. Gregory JS, Waarsing JH, Day J, et al. 2007. Early identification of radiographic osteoarthritis of the hip using an active shape model to quantify changes in bone morphometric features: Can hip shape tell us anything about the progression of osteoarthritis? Arthritis Rheum 56:3634-3643.

196. Lynch JA, Parimi N, Chaganti RK, et al. 2009. The association of proximal femoral shape and incident radiographic hip OA in elderly women. Osteoarthritis Cartilage 17:1313-1318.

197. Nelson AE, Liu F, Lynch JA, et al. 2014. Incident symptomatic hip osteoarthritis is associated with differences in hip shape by active shape modeling: The johnston county osteoarthritis project. Arthritis Care Res (Hoboken) 66:74-81.

198. An H, Marron JS, Schwartz TA, et al. 2016. Novel statistical methodology reveals that hip shape is associated with incident radiographic hip osteoarthritis among african american women. Osteoarthritis Cartilage 24:640-646.

199. Castano-Betancourt MC, Van Meurs JB, Bierma-Zeinstra S, et al. 2013. The contribution of hip geometry to the prediction of hip osteoarthritis. Osteoarthritis Cartilage 21:1530-1536.

200. Zhang J, Hislop-Jambrich J, Besier TF. 2016. Predictive statistical models of baseline variations in 3-D femoral cortex morphology. Med Eng Phys 38:450-457.

201. Khanduja V, Baelde N, Dobbelaere A, et al. 2016. Patient-specific assessment of dysmorphism of the femoral head-neck junction: A statistical shape model approach. Int J Med Robot 12:765-772.

202. Ross JR, Larson CM, Adeoyo O, et al. 2015. Residual deformity is the most common reason for revision hip arthroscopy: A three-dimensional CT study. Clin Orthop Relat Res 473:1388-1395.

203. Zingg PO, Buehler TC, Poutawera VR, et al. 2014. Femoral neck fractures after arthroscopic femoral neck osteochondroplasty for femoroacetabular impingement. Knee Surg Sports Traumatol Arthrosc 22:926-931.

204. Sardana V, Philippon MJ, de Sa D, et al. 2015. Revision hip arthroscopy indications and outcomes: A systematic review. Arthroscopy 31:2047-2055.

205. Mardones RM, Gonzalez C, Chen Q, et al. 2005. Surgical treatment of femoroacetabular impingement: Evaluation of the effect of the size of the resection. J Bone Joint Surg Am 87:273-279.

206. Rothenfluh E, Zingg P, Dora C, et al. 2012. Influence of resection geometry on fracture risk in the treatment of femoroacetabular impingement a finite element study. Am J Sports Med 40:2002-2008.

207. Alonso-Rasgado T, Jimenez-Cruz D, Bailey CG, et al. 2012. Changes in the stress in the femoral head neck junction after osteochondroplasty for hip impingement: A finite element study. J Orthop Res 30:1999-2006.

208. Wijdicks CA, Balldin BC, Jansson KS, et al. 2013. Cam lesion femoral osteoplasty: In vitro biomechanical evaluation of iatrogenic femoral cortical notching and risk of neck fracture. Arthroscopy 29:1608-1614.

209. Haider I, Speirs A, Alnabelseya A, et al. 2016. Femoral subchondral bone properties of patients with cam-type femoroacetabular impingement. Osteoarthritis Cartilage 24:1000-1006.

210. Speirs AD, Beaule PE, Rakhra KS, et al. 2013. Bone density is higher in cam-type femoroacetabular impingement deformities compared to normal subchondral bone. Osteoarthritis Cartilage 21:1068-1073.

211. Agency for Healthcare Research and Quality. 2013. National and regional estimates on hospital use for all patients from the HCUP National Inpatient Sample (NIS). National statistics-principle procedure only. ICD-9-CM 81.51. http://hcupnet.ahrq.gov/: HCUPnet.

212. Atkins PR, Elhabian SY, Agrawal P, et al. 2017. Quantitative comparison of cortical bone thickness using correspondence-based shape modeling in patients with cam femoroacetabular impingement. J Orthop Res 35:1743-1753.

213. Atkins PR, Aoki SK, Whitaker RT, et al. 2017. Does removal of subchondral cortical bone provide sufficient resection depth for treatment of cam femoroacetabular impingement? Clin Orthop Relat Res 475:1977-1986.

CHAPTER 2

ALTERED PELVIC AND HIP JOINT KINEMATICS IN PATIENTS WITH CAM FEMOROACETABULAR IMPINGEMENT: A DUAL FLUOROSCOPY STUDY

Abstract

Femoroacetabular impingement syndrome (FAIS) may disrupt hip kinematics, resulting in pain and tissue damage. Nearly all kinematic motion studies of FAIS have employed skin markers, which are prone to soft tissue artifact errors and inaccurate calculation of the hip joint center. This may explain why the evidence linking FAIS with deleterious kinematics is contradictory.

The purpose of this study was to employ dual fluoroscopy (DF) to quantify in-vivo kinematics of patients with cam FAIS relative to asymptomatic, morphologically normal control subjects during standing, weight-bearing activities of daily living, and functional range of motion activities.

Eleven asymptomatic, morphologically-normal controls and seven cam-type FAIS patients were imaged with DF during standing, level walking, inclined walking, internal pivot, external pivot and two unweighted activities, abduction and a functional star-arc pattern maneuver. Model-based tracking calculated the kinematic position of the hip by registering projections of three-dimensional computed tomography models with DF

images.

FAIS patients stood with their hip extended (mean [95% confidence interval], -2.2 [-7.4,3.1]°, flexion positive), whereas controls were flexed (5.3 [2.6,8.0]°; p = 0.014). During level-walking, patients had a maximum external rotation angle (6.0 [0.4,11.7]°, external positive) that was greater than controls (-0.7 [-3.7,2.4]°; p = 0.050). Relative to their standing position, cam FAIS patients had less posterior pelvic tilt than the control subjects during heel-strike of self-selected speed level-walking (-0.3 [-2.5,1.8] vs. -3.7 [-5.5,-1.8]; p = 0.050) and less peak posterior pelvic tilt during the standardized speed (1.3 m/s) level walk (-1.0 [-3.8,1.7] vs. -4.4 [-6.0,-2.8]; p = 0.050). Pelvic tilt and obliquity were significantly different between self-selected speed level-walking and standing for 0% and 24% of the gait cycle, respectively for the cam FAIS patients and 35% and 39% of the gait cycle, respectively for the control subjects. Conversely for incline gait, pelvic tilt of cam FAIS patients was significantly different than standing for 56% of gait, but not for any time point of gait for control subjects.

FAIS patients had less hip internal rotation compared to controls during some functional activities. Compared to standing, cam FAIS patients had altered motion in pelvic tilt and obliquity during walking.

Even during submaximal range of motion activities, such as incline walking, patients may alter pelvic motion to avoid positions that approximate the cam lesion and the acetabular labrum. Conversely, patients may have overall patterns of reduced pelvic motion during common activities, like level walking.

Introduction

Cam-type femoroacetabular impingement syndrome (FAIS) is often identified as an etiological factor in the development of hip osteoarthritis (OA) and represents a common cause of hip pain in young and otherwise healthy adults.[1] Cam FAIS morphology is described as a femoral head asphericity with reduced head-neck offset over the anterosuperior and anterolateral regions of the femoral head-neck junction.[2] In addition to this morphology, patients with cam FAIS often report pain and reduced range of hip motion.[3; 4] It is hypothesized that the cam lesion abuts abnormally with and begins to pivot about the acetabular rim and labrum after contact, resulting in increased translations within the joint, especially during high range of motion activities of flexion and internal rotation.[5; 6] This hypothesis is supported by damage patterns observed in patients with cam FAIS.[1]

Many studies have attempted to quantify the kinematics of cam FAIS to assess the relationship between cam morphology and limited range of hip joint and pelvic motion, but results have been relatively inconsistent. The investigation of kinematics during gait has identified a decreased range of motion in one or more planes of motion in patients with cam FAIS.[7-10] Similarly, limited peak ranges of motion have been reported for cam FAIS patients in all planes of motion,[11] but these conclusions have not been consistent across studies.[8; 12] In addition to reduced hip range of motion, several studies have also identified reduced pelvic range of motion in cam FAIS patients, primarily in the frontal plane.[9; 13] However, the relationship between altered hip joint and pelvic motion patterns in cam FAIS patients has yet to be well defined and the role morphology plays in hip function remains poorly understood.

To combat these issues, several studies have used computer simulations or cadaveric specimens to better understand motion restrictions in the setting of cam FAIS using subject-specific morphology of the femur and pelvis. Herein, high range of motion activities, such as the anterior impingement exam, can be recreated using a computer model in which direct impingement between the femur and pelvis serves as the cause of reduced range of motion.[14-16] However, these simulations do not incorporate pelvic motion and assume direct impingement between the femoral neck and acetabular bone which do not represent in-vivo motion patterns.[6]

Studying kinematic movement relative to the underlying three-dimensional anatomy (i.e., arthrokinematics) may be required to elucidate the pathomechanics of FAIS. To this end, we previously developed and validated a dual fluoroscopy (DF) system to quantify in-vivo hip arthrokinematics, and found it to be accurate within 0.5 mm and 0.6°.[17] DF has been used to measure arthrokinematics during clinical exams for patients with FAIS and during weight-bearing activities of daily living for control subjects.[5; 18] However, this technology has not been applied to compare hip arthrokinematics between cam FAIS patients and controls during weight-bearing activities.

The purpose of this study was to employ DF to quantify in-vivo kinematics of patients with cam FAIS relative to asymptomatic, morphologically normal control subjects during standing, weight-bearing activities of daily living, and unweighted functional activities. We hypothesized that cam FAIS patients would have reduced hip and pelvic peak joint angles and range of motion during dynamic activities.

Participants and Methods

Seven cam FAIS patients (mean (standard deviation); age, 29 (7) years; height, 179.1 (10.1) cm; mass, 78.9 (15.2) kg; body mass index (BMI), 24.5 (3.2) kg/m^2) were recruited from the clinic of an orthopaedic surgeon (SKA). Diagnosis of cam FAIS was determined based on patient reported symptoms, positive clinical examinations (i.e., anterior impingement exam), and confirmation of cam morphology on radiographic images in the anteroposterior, modified false profile, and frog-leg lateral positions. Eleven control subjects (age, 23 (2) years; height, 173.3 (10.4) cm; mass, 63.8 (10.9) kg; BMI, 21.1 (1.9) kg/m^2), used for comparison, had been recruited for previous studies evaluating hip joint kinematics during weight bearing activities of daily living.[18-21] All subjects had no previous history of lower limb surgery, a BMI less than 30 kg/m^2, a lateral center edge angle between 20° and 40°, and no radiographic evidence of OA or other anatomical abnormalities. Each subject provided informed consent for this Institutional Review Board approved study. Subjects were then imaged with computed tomography (CT) and DF to capture in-vivo hip kinematics.

The CT and DF imaging protocols have been previously described.[17; 21] Briefly, CT images of the pelvis and proximal femur were acquired with a SOMATOM Definition 128 CT scanner (Siemens AG, Munich, Germany). Images were acquired at 120 kVp, 1.0 mm slice thickness, and 200 to 400 mAs with variable fields of view due to subject size.[22] The proximal femur and pelvis were segmented and reconstructed from CT images (Amira, v5.6, FEI, Hillsboro, OR, USA).

Each subject performed activities of daily living, including standing, level walking at a standardized speed (1.3 m/s), level and incline walking at a self-selected speed, internal and external rotational pivots, a functional star-arc maneuver,[23] and abduction to approximately 45°. The DF system consists of two pairs of x-ray emitters and image intensifiers mounted on independent bases and arranged with an overlapping field of view. Each subject performed dynamic activities on an instrumented treadmill (Bertec Corporation, Columbus, OH, USA) with the hip of interest positioned in the combined field of view of the custom DF system (Radiological Imaging Services, Hamburg, PA, USA) (Fig. 2.1). Images were captured at 100 Hz while fluoroscopy settings ranged from 78-100 kVp and 1.9-3.2 mAs with camera exposures of 4.5-7.0 ms.

CT voxel intensities within each bone were used as input to model-based markerless tracking of the DF images.[24] Here, projections of each bone were manipulated

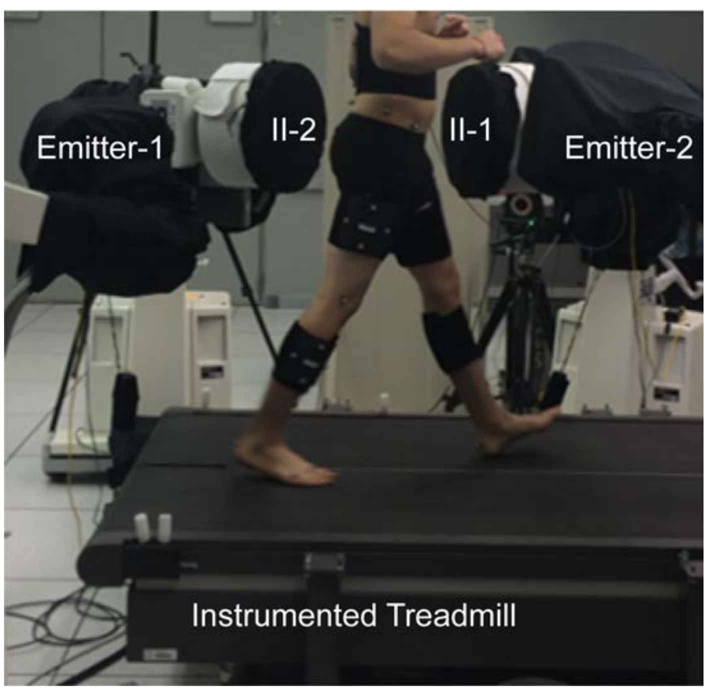

Figure 2.1. Dual fluoroscopy of the left hip of a representative male subject during level walking on an instrumented treadmill. Image intensifiers (II) are positioned on the far side of the subject, while the beam emitters are in the foreground.

in six degrees-of-freedom to simultaneously align with each frame from DF. The spatial position of each bone was tracked using bony landmarks over the length of each trial.[17] For each activity, two trials were captured when possible, but activity level, allotted DF time, and image quality limited the ability to capture and analyze activities from some subjects (Table 2.1).

For the walking trials at a self-selected speed, the same treadmill speed was used for level and incline walking trials based on the preferred walking speed of the subject.[18; 20] For all walking trials, a single gait cycle was evaluated herein. For rotational pivots and abduction, only the position of maximum range of motion was evaluated. For the functional star-arc activity, the five positions of the star (1, flexion; 2, flexion-abduction; 3, abduction; 4, extension-abduction; and 5, extension) and the range of motion during circumduction were evaluated while the subject balanced on the contralateral limb. Gait data and data from the functional star-arc activity were normalized across subjects for comparison. Kinematic data for the controls was previously published,[18; 20] while all activities for the cam FAIS patients were included herein for the first time.

Table 2.1 Participants for each activity, listed by sex.

Activity	Cam FAIS Patients	Control Subjects
Neutral Stance	5 M, 2 F	6 M, 5 F
Level Walk	5 M, 2 F	6 M, 5 F
Standardized Level Walk	4 M, 1 F	6 M, 5 F
Incline Walk	5 M, 2 F	6 M, 5 F
Rotation	5 M, 2 F	6 M, 5 F
FHJC	4 M, 2 F	5 M, 5 F
Abduction	4 M, 2 F	4 M, 5 F

For this study, kinematic joint angles were presented as raw joint angles between the local coordinate systems of the proximal femur and the pelvis and as angles relative to the standing position.[18] This approach provided data on both the in-vivo joint position and the relative relationship between static (i.e., standing) and dynamic motions. Joint translation data were evaluated in the local coordinate system of the pelvis, relative to the static neutral position, such that values represented the relative movement between the femoral head center and the acetabular center. The vertical axis of the lab was projected onto the sagittal and coronal planes of the local coordinate system of the pelvis to calculate pelvic tilt and obliquity, respectively. The lateral axis was projected onto the horizontal plane of the lab to measure pelvic rotation, all pelvic rotation angles were represented relative to the average pelvic rotation during the level walking activity at a self-selected speed. Joint angles, joint translations, and pelvic rotation angles were calculated using a custom script (MATLAB, v9.3.0, MathWorks, Natick, MA, USA).

Unless otherwise noted, all data were presented as mean [95% confidence interval]. Student's t-tests were used to evaluate mean differences between cam FAIS patients and control subjects. The Holm-Bonferroni method was used to correct for multiple comparisons, where corrections were applied across directions of motion. For time series data, the Benjamini and Hochberg method of false discovery rate was used to correct for nonindependence. Correlations were assessed between joint angles and pelvic rotation angles. All statistics were completed in MATLAB.

Results

Standing

FAIS patients stood with their hip extended (-2.2 [-7.4,3.1]°, flexion positive), whereas controls were flexed (5.3 [2.6,8.0]°, $p = 0.014$). All of the control subjects stood in a position of anterior pelvic tilt (9.7 [6.5,13.0]°, anterior tilt positive), while two males of the seven cam FAIS patients stood in a position of posterior pelvic tilt which brought the mean for the FAIS group into less anterior tilt (5.0 [-2.6,12.5]°), but group differences were not significant. For standing, there was a very strong correlation between flexion angle and pelvic tilt for cam FAIS patients ($r = 0.948$) and a strong correlation for control subjects ($r = 0.720$).

Gait Kinematics

No significant differences were observed in preferred walking speed or cadence during any of the gait activities. In particular, cam FAIS patients preferred a walking speed of 1.29 [1.13,1.45] m/s at 125 [118,132] steps/min for level walking and 120 [114,126] steps/min for incline walking; controls preferred a walking speed of 1.29 [1.22,1.37] m/s at 124 [118,131] steps/min for level walking and 122 [113,131] steps/min for incline walking.

During level walking, cam FAIS patients had greater overall external rotation ($p = 0.050$), but did not have less internal rotation ($p = 0.063$) (Fig. 2.2). While differences were not significant, cam FAIS patients appeared in more external rotation and extension with more posterior pelvic tilt and greater lateral translations when compared to controls throughout the gait cycle (Fig. 2.3).

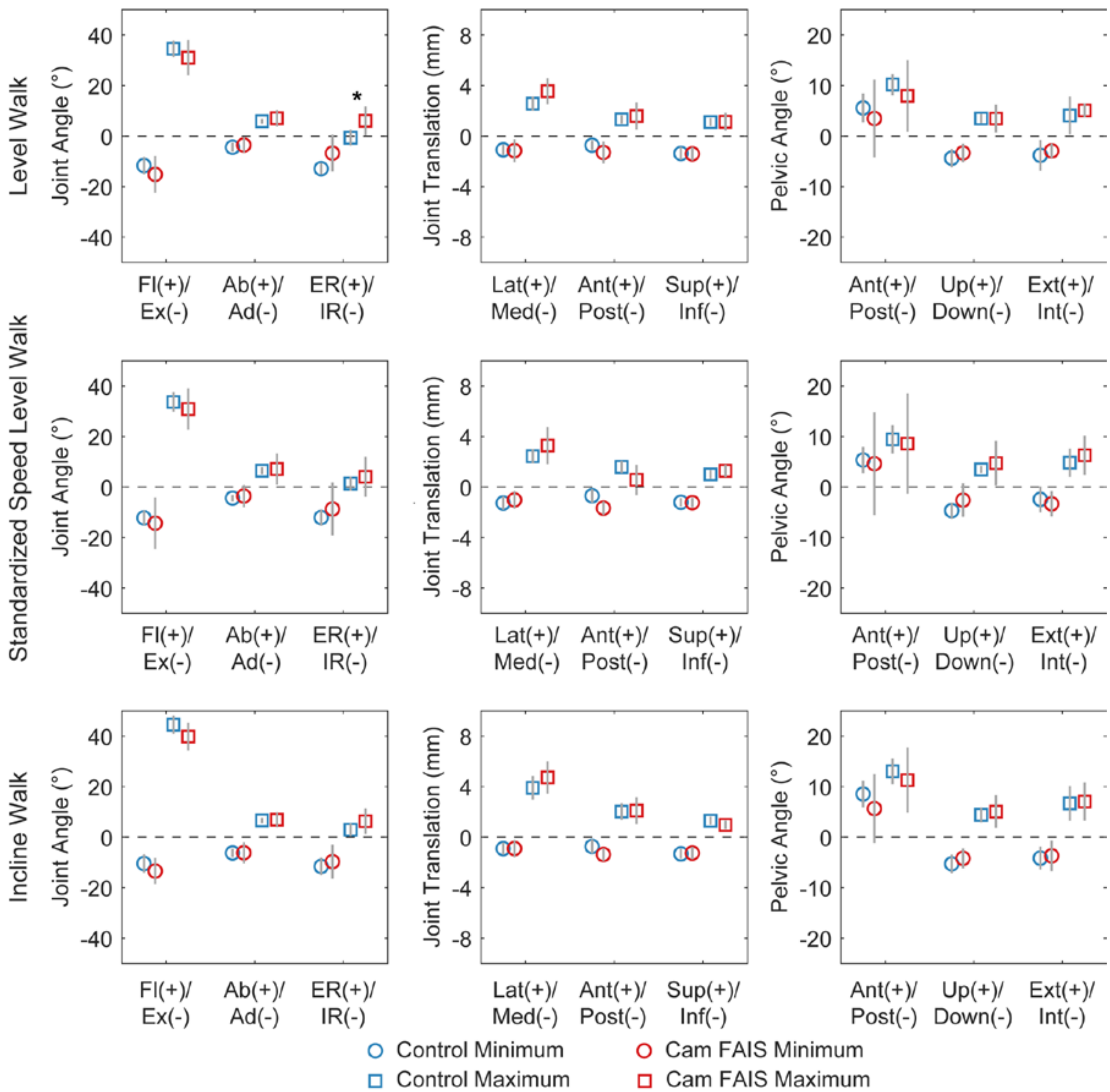

Figure 2.2. Peak joint angles, joint translations, and pelvic rotation angles during self-selected speed level walk (top), standardized speed level walk (middle), and self-selected speed incline walk (bottom). Significant differences between control subjects and cam FAIS patients are indicated with an asterisk (*).

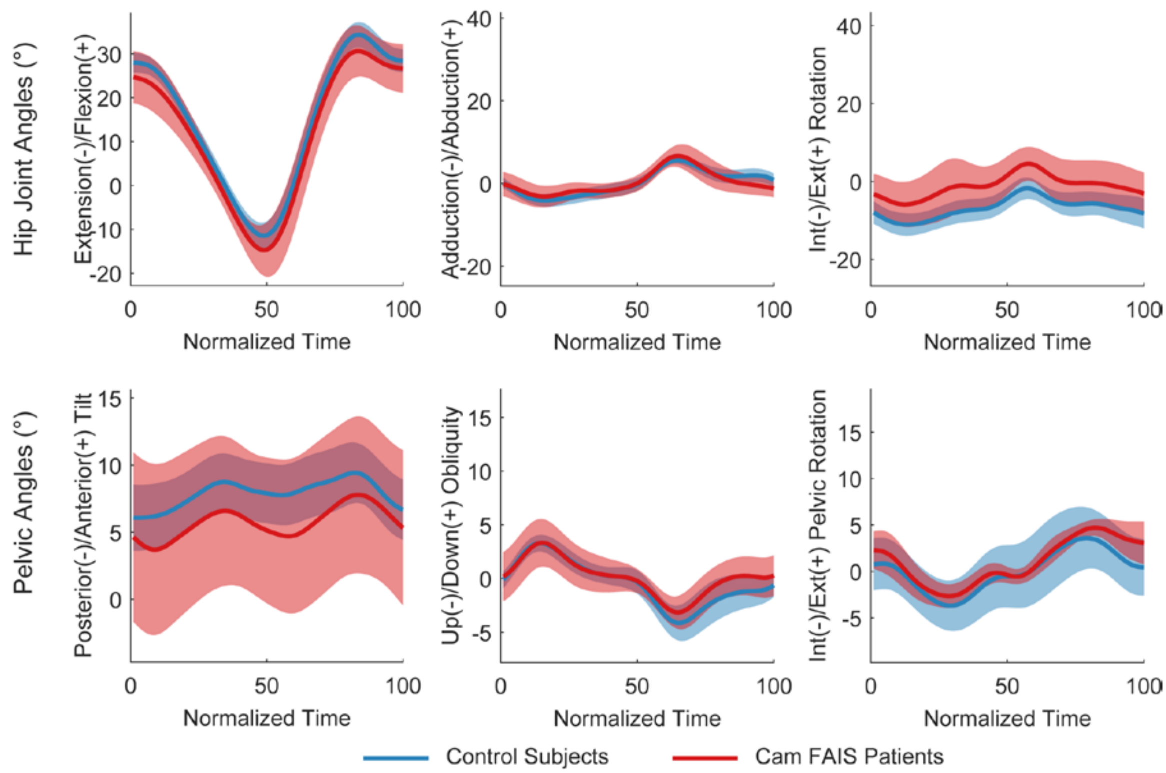

Figure 2.3. Hip joint angles and pelvic rotation angles for control subjects and cam FAIS patients during self-selected speed level walking. Solid line indicates mean, while the semi-transparent band represents the 95% confidence interval.

Abduction range of motion was strongly correlated to the range of pelvic obliquity during all gait activities, though not all correlations were significant (Table 2.2). Flexion angle was very strongly correlated to pelvic tilt during heel-strike and toe-off of both self-selected and standardized speeds of level gait for cam FAIS patients and during toe-off at self-selected speed for control subjects. At heel-strike, hip rotation angle and pelvic rotation angles were strongly correlated for cam patients for level gait and for control subjects for incline gait (Table 2.2). No differences were observed between cam FAIS

Table 2.2 Correlation between joint angle range of motion and pelvic rotation range of motion.

Activity	Correlation	Group	Flexion - Tilt	Abduction - Obliquity	Joint Rotation - Pelvic Rotation
Level Walk	Heel-Strike	Cam	0.932 *	-0.895 *	-0.868 *
		Control	0.526	-0.356	-0.206
	Toe-Off	Cam	0.976 *	-0.801	-0.480
		Control	0.796 *	-0.381	0.136
	Range of Motion	Cam	0.368	0.832 *	0.180
		Control	0.660 *	0.747 *	0.463
Standardized Level Walk	Heel-Strike	Cam	0.958 *	-0.871	-0.779
		Control	0.693	-0.647	-0.451
	Toe-Off	Cam	0.959 *	-0.687	0.678
		Control	0.656	-0.659	-0.506
	Range of Motion	Cam	0.477	0.871	0.268
		Control	0.457	0.735 *	0.573
Incline Walk	Heel-Strike	Cam	0.745	-0.801	-0.730
		Control	0.575	-0.650	-0.711 *
	Toe-Off	Cam	0.655	-0.500	-0.237
		Control	0.632	-0.710 *	-0.532
	Range of Motion	Cam	-0.739	0.734	0.825 *
		Control	0.117	0.867 *	0.376

*Correlations significant at the p<0.05 level.

patients and control subjects in joint angles or translations for range of motion (Fig. 2.2) or at the position of interest for the rotational pivots and functional activities (Table 2.3).

Hip Kinematics Relative to Standing

During heel-strike of level walking, patients had less posterior pelvic tilt relative to their position during standing than did control subjects (-0.3 [-2.5,1.8]° vs. -3.7 [-5.5,-1.8]°; $p = 0.050$). Overall, FAIS patients also had less relative posterior pelvic tilt during the standardized speed level walk compared to controls (-1.0 [-3.8,1.7]° vs. -4.4 [-6.0,-2.8]°; $p = 0.050$).

Relative to standing and compared to control subjects, cam FAIS patients were in

Table 2.3 Hip joint angles during standing and the maximum range of motion for the internal and external rotational pivot.

Activity	Joint Angle	Control (°)	Cam (°)	*p* val
Standing	Ex(-)/ Fl(+)	5.3 [2.6,8.0]	-2.2 [-7.4,3.1]	.014
	Ad(-)/ Ab(+)	3.1 [1.5,4.7]	0.8 [-3.1,4.7]	.325
	In(-)/ Ex(+) Rot	-10.3 [-14.7,-5.9]	-6.2 [-15.4,2.9]	.325
Internal Pivot	Ex(-)/ Fl(+)	25.5 [21.0,29.9]	19.2 [14.4,24.0]	.150
	Ad(-)/ Ab(+)	-4.2 [-7.2,-1.2]	-4.0 [-9.2,1.1]	.941
	In(-)/ Ex(+) Rot	-39.4 [-45.8,-33.1]	-31.8 [-38.7,-24.9]	.179
External Pivot	Ex(-)/ Fl(+)	2.0 [-2.9,6.9]	-1.4 [-7.6,4.9]	--
	Ad(-)/ Ab(+)	2.5 [-0.1,5.1]	2.1 [-3.0,7.1]	--
	In(-)/ Ex(+) Rot	25.9 [17.8,34.1]	25.8 [17.3,34.3]	--

--*p* value of 1.0 after correction for multiple comparisons.

more abduction (27.3 [22.5,32.1]° vs. 18.9 [14.3,23.6]°; $p = 0.046$), with more anterior pelvic tilt (6.6 [1.8,11.4]° vs. 1.7 [0.2,3.2]°; $p = 0.030$) and upward obliquity (13.1 [10.5,15.6]° vs. 10.2 [9.0,11.5]°; $p = 0.033$) during position 3 (abduction) of the functional star-arc activity. FAIS patients were also in less extension during position 5 (extension) when compared to controls (-2.1 [-8.0,3.7]° vs. -9.6 [-12.5,-6.7]°; $p = 0.024$).

Dynamic Pelvic Motion

During both standardized and self-selected speeds of level walking, dynamic pelvic tilt and obliquity were significantly different from pelvic tilt and obliquity of standing for less of the gait cycle for cam FAIS patients when compared to control subjects, who had significant differences during loading response, pre-swing, and terminal swing (Table 2.4). While pelvic obliquity had the same trends during incline gait, pelvic tilt in cam FAIS patients was significantly different than tilt during standing for more of the incline gait cycle, predominantly during the swing phase (Table 2.4). Differences between pelvic rotation during standing and gait were only found during incline gait (Table 2.4).

While no significant differences in pelvic tilt were observed during the functional star-arc activity, FAIS patients had consistent patterns of increasing followed by decreasing pelvic tilt, obliquity, and rotation during the arc (circumduction) portion of the activity (Fig. 2.4). Qualitatively, the control subjects had more variability in subject-specific patterns of pelvic motion during circumduction of the functional star-arc activity.

Table 2.4 Percent of gait cycle that the pelvic position was significantly different than during stance.

Activity	Pelvic Angle	Cam FAIS	Control
Level Walk	Tilt	0%	35% (1-20, 54-60, 93-100%)
	Obliquity	24% (55-78%)	39% (8-19, 54-80%)
	Pelvic Rotation	0%	0%
Standardized Level Walk	Tilt	0%	49% (1-21, 41-57, 90-100%)
	Obliquity	8% (64-71%)	59% (9-23, 54-98%)
	Pelvic Rotation	0%	0%
Incline Walk	Tilt	56% (30-41, 55-98%)	0%
	Obliquity	16% (57-71%)	69% (1-22, 44-81, 92-100%)
	Pelvic Rotation	23% (77-99%)	33% (1-6, 74-100%)

Values in parenthesis represent the specific periods of gait where the pelvic position was significantly different than pelvic position during stance.

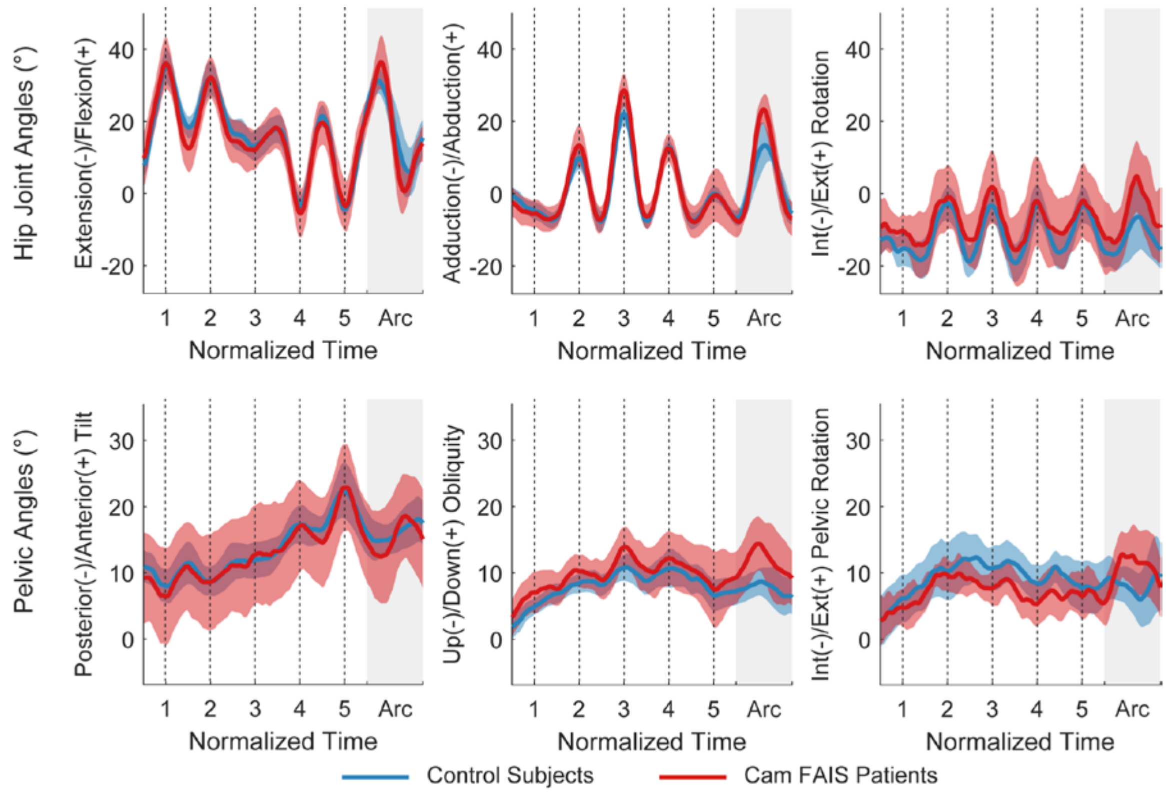

Figure 2.4. Hip joint angles and pelvic rotation angles for control subjects and cam FAIS patients during the functional star-arc activity. The five star positions are labeled numerically: 1, flexion; 2, flexion-abduction; 3, abduction; 4, extension-abduction; and 4, extension. The arc (circumduction) portion of the activity is indicated by a light gray vertical band. Solid line indicates mean, while the semi-transparent band represents the 95% confidence interval.

Discussion

We employed DF to quantify in-vivo kinematics of patients with cam FAIS relative to asymptomatic, morphologically normal control subjects during standing, weight-bearing activities of daily living, and unweighted functional activities. Cam FAIS patients stood with more extension and walked with more external rotation during self-selected speed level walking, but additional kinematic deviations were not found. While overall pelvic range of motion was not different between patients and controls, we observed reduced pelvic motion in cam FAIS patients during gait relative to their standing position when compared to control subjects. Thus, aside from peak external rotation during level walking, hip kinematics were not different in patients with cam FAIS. However, our results suggest that treatment strategies aimed at increasing dynamic pelvic motion during daily activities like level walking could benefit patients with cam FAIS.

This study was not without limitations. First, only a limited number of subjects were recruited and analyzed. While we were still able to detect significant differences in gait patterns and pelvic motion between the cam FAIS patients and control subjects, additional differences in external rotation and flexion would likely have been observed with a larger sample size. Thus, our results should be viewed in the context of a preliminary study. Second, only a single gait cycle or activity was analyzed for each subject. While multiple gait cycles and activities were captured and analyzed as allowed by subject activity level, allotted DF time, and image quality, the high accuracy and low bias of DF reduces the need to average results across gait cycles.[17] Third, along these lines, the use of DF and CT exposed subjects to ionizing radiation. The radiation exposure for the subjects, including CT and DF, was 10.72 mSv. This amounts to 21% of the annual exposure limit for a radiation worker, or nearly three years of background radiation in the Salt Lake City, Utah area.[25] The reader should also note that the annual dose limit for the general public from licensed operation is 1.0 mSv,[26] but this limit excludes background radiation and voluntary participation in medical research studies.

To our knowledge, this is the first study to evaluate in-vivo kinematics of patients with cam FAIS during weight-bearing activities of daily living. Consistent with previous studies evaluating kinematics and range of motion in cam FAIS patients, we observed no differences in cadence between cam FAIS patients and controls.[9] While previous studies have reported reduced peak internal rotation, we found instead that cam FAIS patients have greater external rotation during level walking.[7; 10; 11] The difference in measures of transverse plane kinematics is likely due to the effect of soft tissue artifact. In particular, soft tissue artifact can cause errors on the order of 20° when estimating kinematics in the transverse plane.[18] Previous studies have observed limited sagittal range of motion or reduced peak extension in FAIS patients during weight-bearing activities.[7; 9-13] However, we did not consistently observe differences in sagittal range of motion when using DF during the same activities. Without subject-specific bony anatomy of the pelvis, it is difficult to measure in-vivo pelvic tilt, therefore the altered sagittal pelvic tilt may have instead appeared as overall reduced hip range of motion in the sagittal plane with the use of skin marker motion analysis, as previously reported.[7; 9-13] While not significant, cam FAIS patients had trends of reduced peak downward obliquity which could manifest as reduced pelvic obliquity range of motion as has previously been observed during level gait.[9] Interestingly, we found no significant differences in range of motion even during the high range of motion rotational pivots. This finding may be the result of joint mobility limitations, as both subject cohorts had large intersubject variability indicating that bony morphology may not be the only factor responsible for changes in range of motion.

Previous reports of patients with FAIS, hip OA, and lower back pain have reported reduced pelvic range of motion.[9; 13; 27; 28] While we did not explicitly identify any reductions in pelvic range of motion, we did find that when compared to control subjects, cam FAIS patients had reduced pelvic tilt during level gait relative to their standing position. Interestingly, this was not true for incline gait, which may indicate that patients with FAIS move with reduced pelvic range of motion as a result of altered stability strategies during regular tasks. Conversely, for more challenging or irregular tasks, like incline walking or circumduction (Fig. 2.4), patients may compensate with increased pelvic motion to avoid positions that approximate the cam lesion and the acetabular labrum.

Our study findings are important, as they provide calculations of in-vivo pelvic and hip joint motion of FAIS patients during activities of daily living and functional range of motion activities relative to subject-specific morphology. Our results represent active motion patterns that are free from errors associated with soft tissue artifact. Further, we did not have to assume generic morphology or motion patterns when evaluating kinematics, as we directly measured in-vivo bone motion based on anatomical landmarks specific to each individual. Given the use of subject-specific morphology and in-vivo kinematics, we still did not find consistent reductions in peak joint angles or range of motion, indicating that it is likely that the effect of FAIS morphology on daily motion patterns is minimal. Nevertheless, reduced pelvic motion may play a role in this disease.

In conclusion, our findings agree with those previous studies that concluded that the kinematic effects of cam FAIS are minimal during weight-bearing activities and highlight the possible importance of reduced pelvic range of motion in patient populations with hip pain. Future studies should investigate altered pelvic relative to femur-labrum approximation to understand whether these differences are compensatory strategies to minimize pain.

Acknowledgments

We thank Michael Kutschke, Tyler Skinner, Michael Austin West, Trevor Hafer, Sara Fauver, and YoungJae Shin for their contributions towards image and data processing. We thank Dr. Kent Saunders for performing the CT arthrograms.

References

1. Ganz R, Leunig M, Leunig-Ganz K, et al. 2008. The etiology of osteoarthritis of the hip: An integrated mechanical concept. Clin Orthop Relat Res 466:264-272.

2. Ito K, Minka MA, 2nd, Leunig M, et al. 2001. Femoroacetabular impingement and the cam-effect. A MRI-based quantitative anatomical study of the femoral head-neck offset. J Bone Joint Surg Br 83:171-176.

3. Griffin DR, Dickenson EJ, O'Donnell J, et al. 2016. The Warwick Agreement on femoroacetabular impingement syndrome (FAI syndrome): An international consensus statement. Br J Sports Med 50:1169-1176.

4. Freke MD, Kemp J, Svege I, et al. 2016. Physical impairments in symptomatic femoroacetabular impingement: A systematic review of the evidence. Br J Sports Med 50:1180.

5. Kapron AL, Aoki SK, Peters CL, et al. 2015. In-vivo hip arthrokinematics during supine clinical exams: Application to the study of femoroacetabular impingement. J Biomech 48:2879-2886.

6. Kapron AL, Aoki SK, Peters CL, et al. 2014. Subject-specific patterns of femur-labrum contact are complex and vary in asymptomatic hips and hips with femoroacetabular impingement. Clin Orthop Relat Res 472:3912-3922.

7. Rylander J, Shu B, Favre J, et al. 2013. Functional testing provides unique insights into the pathomechanics of femoroacetabular impingement and an objective basis for evaluating treatment outcome. J Orthop Res 31:1461-1468.

8. Brisson N, Lamontagne M, Kennedy MJ, et al. 2013. The effects of cam femoroacetabular impingement corrective surgery on lower-extremity gait biomechanics. Gait Posture 37:258-263.

9. Kennedy MJ, Lamontagne M, Beaule PE. 2009. Femoroacetabular impingement alters hip and pelvic biomechanics during gait walking biomechanics of FAI. Gait Posture 30:41-44.

10. Diamond LE, Wrigley TV, Bennell KL, et al. 2016. Hip joint biomechanics during gait in people with and without symptomatic femoroacetabular impingement. Gait Posture 43:198-203.

11. Hunt MA, Guenther JR, Gilbart MK. 2013. Kinematic and kinetic differences during walking in patients with and without symptomatic femoroacetabular impingement. Clin Biomech (Bristol, Avon) 28:519-523.

12. Kumar D, Dillon A, Nardo L, et al. 2014. Differences in the association of hip cartilage lesions and cam-type femoroacetabular impingement with movement patterns: A preliminary study. PM R 6:681-689.

13. Lamontagne M, Kennedy MJ, Beaulé PE. 2009. The effect of cam FAI on hip and pelvic motion during maximum squat. Clinical Orthopaedics and Related Research 467:645-650.

14. Audenaert E, Van Houcke J, Maes B, et al. 2012. Range of motion in femoroacetabular impingement. Acta Orthop Belg 78:327-332.

15. Kubiak-Langer M, Tannast M, Murphy SB, et al. 2007. Range of motion in anterior femoroacetabular impingement. Clin Orthop Relat Res 458:117-124.

16. Tannast M, Kubiak-Langer M, Langlotz F, et al. 2007. Noninvasive three-dimensional assessment of femoroacetabular impingement. J Orthop Res 25:122-131.

17. Kapron AL, Aoki SK, Peters CL, et al. 2014. Accuracy and feasibility of dual fluoroscopy and model-based tracking to quantify in vivo hip kinematics during clinical exams. J Appl Biomech 30:461-470.

18. Fiorentino NM, Atkins PR, Kutschke MJ, et al. 2017. Soft tissue artifact causes significant errors in the calculation of joint angles and range of motion at the hip. Gait Posture 55:184-190.

19. Atkins PR, Fiorentino NM, Aoki SK, et al. 2017. In vivo measurements of the ischiofemoral space in recreationally active participants during dynamic activities: A high-speed dual fluoroscopy study. Am J Sports Med:363546517712990.

20. Fiorentino NM, Atkins PR, Kutschke MJ, et al. 2016. In-vivo quantification of dynamic hip joint center errors and soft tissue artifact. Gait Posture 50:246-251.

21. Fiorentino NM, Kutschke MJ, Atkins PR, et al. 2016. Accuracy of functional and predictive methods to calculate the hip joint center in young non-pathologic asymptomatic adults with dual fluoroscopy as a reference standard. Ann Biomed Eng 44:2168-2180.

22. Henak CR, Abraham CL, Peters CL, et al. 2014. Computed tomography arthrography with traction in the human hip for three-dimensional reconstruction of cartilage and the acetabular labrum. Clin Radiol 69:e381-391.

23. Camomilla V, Cereatti A, Vannozzi G, et al. 2006. An optimized protocol for hip joint centre determination using the functional method. J Biomech 39:1096-1106.

24. Bey MJ, Zauel R, Brock SK, et al. 2006. Validation of a new model-based tracking technique for measuring three-dimensional, in vivo glenohumeral joint kinematics. J Biomech Eng 128:604-609.

25. Committee TRS. 1996. Radiation safety policy manual. University of Utah.

26. Commission USNR. 2017. Subpart d--radiation dose limits for individual members of the public.

27. Bolink SA, Brunton LR, van Laarhoven S, et al. 2015. Frontal plane pelvic motion during gait captures hip osteoarthritis related disability. Hip Int 25:413-419.

28. Taylor N, Goldie P, Evans O. 2004. Movements of the pelvis and lumbar spine during walking in people with acute low back pain. Physiother Res Int 9:74-84.

.

CHAPTER 3

HOW WELL CAN 2D RADIOGRAPHIC MEASUREMENTS OF CAM FEMOROACETABULAR IMPINGEMENT DESCRIBE THE 3D SHAPE OF THE PROXIMAL FEMUR?

Abstract

Many two-dimensional (2D) plain films are used in the diagnosis of cam femoroacetabular impingement (FAI), but there is little consensus as to which of these views best visualizes the pathomorphology of the femur. Previous studies have evaluated 2D radiographic measurements from plain films against measurements from computed tomography (CT) or magnetic resonance images (MRI) as a reference standard. However, these reference images have often utilized 2D image slices instead of 3D surface data, which may not accurately describe the magnitude and extent of the cam lesion and associated asphericity of the femoral head.

The purpose of this study was to use digitally reconstructed radiographs (DRRs) and statistical shape modeling (SSM) to determine how well 2D radiographic measurements of cam FAI predict 3D metrics of proximal femoral shape and identify the combination of radiographic projections that best describe 3D shape of the proximal femur.

Femur surface reconstructions from 37 cam FAI patients (34 males) and 59 controls (36 males) were generated from CT images. Surfaces were input to SSM, which

objectively calculated a 3D shape score for the entire proximal femur and for a region representing only the cam lesion. DRRs for eight views were generated from CT data and measurements of the alpha angle and head-neck offset were acquired from each projection. Relationships between radiographic measurements from each DRR projection and the 3D shape scores (for the entire proximal femur and for the region specific to cam lesion) were assessed with linear correlation. Additionally, partial least squares (PLS) regression determined which combination of projections and measurements best-predicted 3D shape scores.

Correlations between radiographic measurements and 3D shape scores were strongest for alpha angle measurements on the cross-table view for the entire proximal femur (r = -0.568, $p < 0.001$) and on the Meyer lateral view for the region of the cam lesion (r = -0.669, $p < 0.001$). PLS demonstrated that DRR measurements from the Meyer lateral and 90° Dunn radiographs produced the optimized regression model for predicting shape scores for the proximal femur (R^2 = 0.394) and the region of the cam lesion (R^2 = 0.496). Interestingly, views with larger differences in alpha angle and head-beck offset between control and cam FAI groups did not did not have the strongest correlations with 3D shape.

Considered together, radiographic measurements from the Meyer lateral and 90° Dunn views provided the most effective predictions of 3D shape as determined using SSM. However, the alpha angle and head-neck offset measurements from these views described less than half of the overall variation in 3D anatomy of either the entire proximal femur or the region of the cam lesion. Furthermore, the magnitude of these radiographic measurements was not necessarily a strong predictor of the severity of the cam lesion.

Clinicians should consider that 2D radiographic measurements alone may be inadequate to fully-appreciate the shape of the cam lesion. Additionally, radiographic projections that result in greater differences in alpha angle and head-neck offset measurements between cam FAI patients and control subjects may not necessarily provide better visualization of the cam lesion.

Introduction

Cam-type femoroacetabular impingement (FAI) is now recognized as a major etiological factor in the development of hip osteoarthritis (OA) and represents a common cause of hip pain.[1] Morphologically, cam FAI presents as femoral head asphericity with reduced head-neck offset. The region of asphericity is often referred to as the cam lesion and is generally located in the anterosuperior and anterolateral regions of the proximal femur. Surgical treatment of cam FAI aims to resect the lesion and alleviate symptoms. As such, an accurate assessment of the severity of the deformity (i.e., magnitude and location of the cam lesion) is important for preoperative planning.[2-4] A multitude of two-dimensional (2D) plain films have been described for this purpose, but there lacks consensus as to which views are best for evaluating the cam lesion.[5-8]

Previous research has attempted to identify which plain film views best describe the three-dimensional (3D) anatomy of hips with and without cam FAI. Specifically, 2D plain film measurements were compared to those from the reference standard, which included either computed tomography (CT) or magnetic resonance images (MRI).[3; 7-12] Most measurements of CT and MRI were obtained from single image slices, acquired in either standard (axial, coronal, or sagittal) or radially reformatted planes.[3; 7-12] However, there is no guarantee that these 2D image slices capture the cam lesion such that the apex is aligned with the imaging plane.

Volumetric CT and MRI data can be reconstructed into 3D surface models of the hip, but in practice, it is difficult to extract quantitative measurements of these reconstructions using standard clinical metrics, and thus most are only qualitatively analyzed in a clinical setting. Statistical shape modeling (SSM) objectively quantifies 3D anatomic shape using reconstructions from CT or MRI and provides a technique to investigate clinical treatment strategies.[13; 14] We recently published an SSM study that described a method to assign a 3D shape score to each individual subject relative to the shape variation between the control and cam FAI groups.[14] Regressions between measurements of the alpha angle and head-neck offset from plain film views and 3D shape scores calculated objectively by SSM could identify which radiographic views and associated measurements best describe the true shape of proximal femur.

The purpose of this study was to use digitally reconstructed radiographs (DRRs) and SSM to determine how well 2D radiographic measurements of cam FAI predict 3D metrics of proximal femoral shape and identify the combination of radiographic projections that best describe 3D shape of the proximal femur. Anecdotally, we have observed considerable variation in the magnitude and location of the cam lesion across patients at the time of surgery. Thus, we hypothesized that 2D radiographic measurements from each plain film would not be strongly correlated to the 3D shape score, but that the use of multiple plain film views and associated measurements would improve the prediction of 3D shape scores calculated by SSM.

Participants and Methods

A total of 59 control subjects, including both living subjects and cadaveric specimens (36 males; age, mean: 29, range: 15-55) were included. Living subjects provided informed consent and were prospectively recruited between April 2008 and September 2014 with IRB approval.[13-16] Fourteen of 43 living control subjects and 29 of 59 cadaveric specimens were excluded for having anatomy of FAI or acetabular dysplasia, as evaluated using an anteroposterior radiograph for live subjects and a DRR in the frog-leg position for cadaveric specimens, leaving 59 controls in total. Thirty-seven nonconsecutive patients with cam FAI (34 males; age, mean: 27, range: 16-47), were recruited for convenience on the basis of radiographic findings of cam FAI and positive clinical examinations, as assessed by an orthopaedic surgeon with more than 10 years of experience treating FAI.

We leveraged previously-published participants for the current study. In particular, 28 out of the 37 patients and 45 out of the 59 controls were scanned with CT for SSM studies aimed at quantifying the distribution of cortical bone thickness in the proximal femur[14] and the ability of virtual resections to restore femoral shape.[13] Furthermore, 14 control subjects were previously scanned with CT for unrelated dual fluoroscopy motion analysis studies.[15; 16] The remaining 9 cam FAI patients were scanned for the purpose of completing the present study.

Computed tomography images of the proximal femur of all subjects were acquired using a previously described protocol[17] with a SOMATOM Definition1 128 CT scanner (Siemens AG, Munich, Germany) (29 control subjects, 24 patients with cam FAI), HiSpeed1 CTi Single Slice Helical CT scanner (GE Healthcare, Chicago, IL, USA) (30 control cadaver femurs), or LightSpeed1 VCT1 scanner (GE Healthcare) (13 patients with cam FAI). Images were acquired at 100 to 120 kVp, 512 x 512 acquisition matrix, 0.625 to 1.0 mm slice thickness, 0.9 to 1.0 pitch, and 100 to 200 mAs with variable fields of view.

The proximal femur was segmented from upsampled CT images (Amira, v5.6, FEI, Hillsboro, OR). DRRs were generated by projecting the CT image data of the femur (Fig. 3.1) to create eight plain film views described in the literature (Fig. 3.2).[5; 6; 18-22] A series of rotation angles was applied to each femur to generate consistent femur positioning for each DRR (Table 3.1). From each radiographic view, measurements of alpha angle and head-neck offset (Fig. 3.1)[22; 23] were obtained by two orthopaedic researchers with one to four years of experience with medical imaging using a custom code written in Matlab (v. 7.10, Natick, MA, USA). Researchers were blinded as to whether the images were from a control subject or an FAI patient.

Segmentations of 3D CT images were used to reconstruct surfaces of the proximal femur (Fig. 3.1). Femur surfaces were preprocessed for the SSM pipeline using the ShapeWorks command line tools (University of Utah, Salt Lake City, UT).[14] Correspondence points were automatically placed and optimized to be evenly spaced and located in the same relative anatomic position across subjects. The mean control and mean cam FAI femur correspondence point locations were used to define the spectrum of shape variability.[14] Subject correspondence point locations were then mapped onto this spectrum to determine the individual shape scores.[14] The assignment of shape scores was repeated for the subset of correspondence points that represented the region of the cam lesion, as defined by a difference in mean shapes greater than 1 mm.[14] Computer-generated femur surfaces were reconstructed for the mean cam FAI patient, the mean control subject, and to represent integer shape scores of the population between -4 and +4. The shape distance

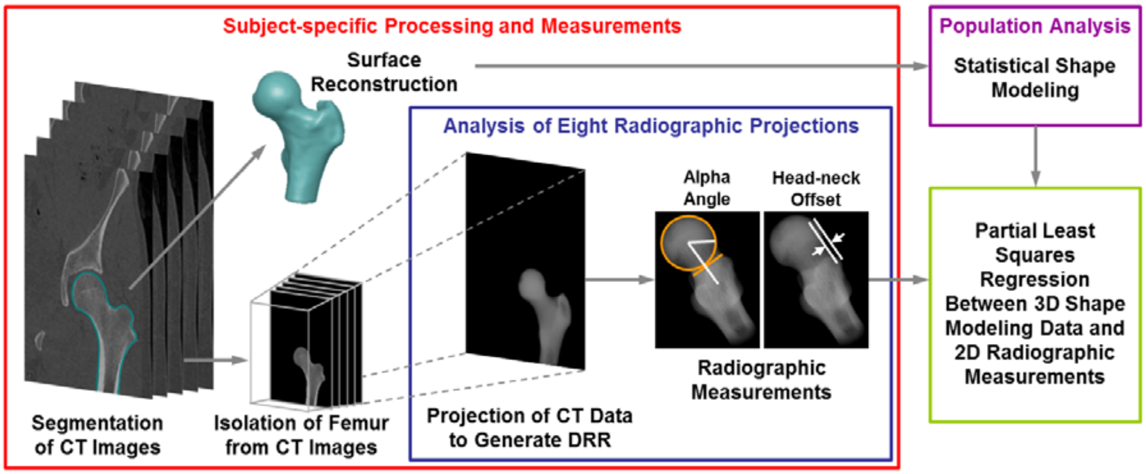

Figure 3.1. Flowchart of the methodological pipeline that included statistical shape modeling (SSM) and analysis of radiographic measurements used in the diagnosis of cam femoroacetabular impingement (FAI). Both cam FAI and control subjects were considered. For each subject analyzed, images from computed tomography (CT) were segmented to isolate the proximal femur. Reconstructed surfaces were input to SSM. Digitally reconstructed radiographs (DRRs) were then generated to represent eight plain film views commonly obtained in patients with suspected cam FAI. The DRRs were generated by projecting the CT image stack, including only the pixel intensities within the proximal femur, at fixed rotation angles (Table 3.1). Alpha angle and head-neck offset measurements were obtained on each DRR. Partial least squares regression was performed between the radiographic measurements and shape score to determine which radiographic view(s) and associated alpha angle and head-neck offset measurements best described the three-dimensional shape score calculated by SSM.

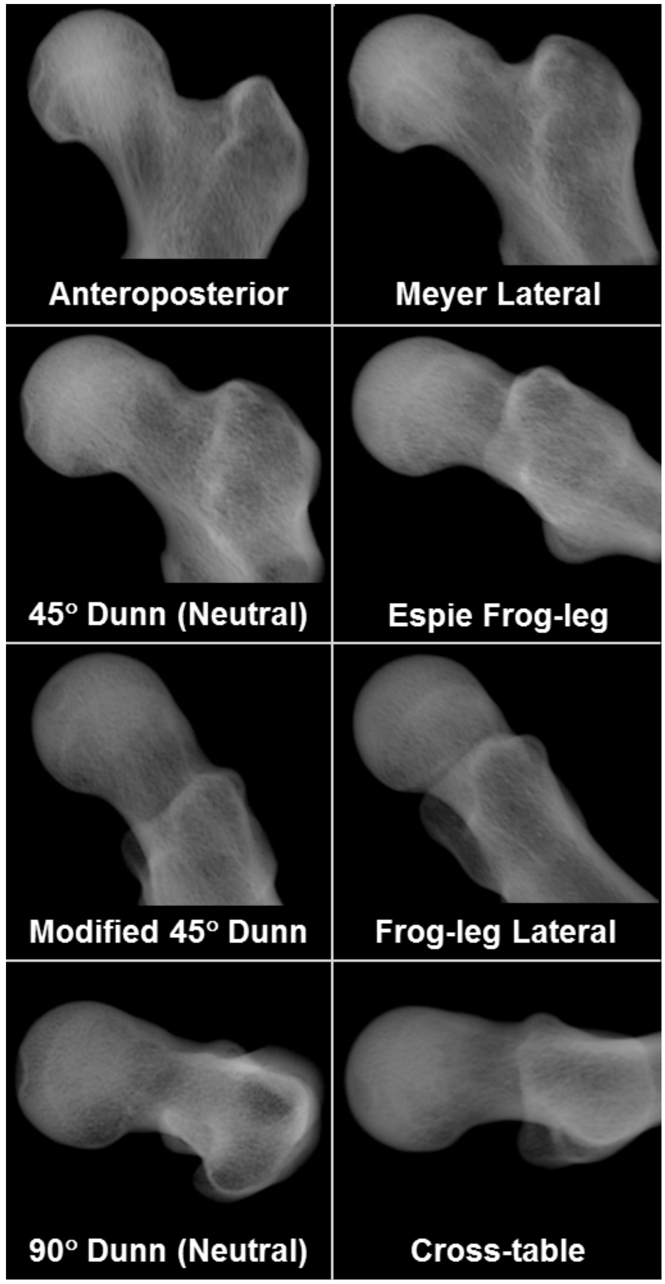

Figure 3.2. Digitally reconstructed radiographs (DRRs) of the eight views analyzed. The DRRs shown are from a representative cam femoroacetabular impingement patient (26 year old male).

Table 3.1 Femur positioning for the digitally reconstructed radiographs representing eight plain film views.

Radiographic View	Flexion	Abduction	External Rotation	Reference
Antero-posterior	0°	0°	-15°	[18]
Meyer Lateral	25°	20°	0°	[5]
45° Dunn (Neutral)	45°	20°	0°	[19]
Espié Frog-leg	45°	45°	30°	[20]
Modified 45° Dunn	45°	20°	40°	[6]
Frog-leg Lateral	45°	0°	60°*	[21]
90° Dunn	90°	20°	0°	[19]
Cross-table	0°	0°	-15°**	[22]

* External rotation angle was applied about the inferior superior axis of the body, not the femur.
** Inferomedial projection used for this view.

between the mean shapes was mapped onto the mean cam FAI femur to provide visualization of shape variation relative to the anatomy. The rotations used for the DRR projections were applied to this mapped surface to visualize how cam FAI anatomy was captured on each radiographic view.

The assumption that data were normally distributed was tested using the Shapiro-Wilk test. Those data that were normally distributed were represented as mean ± standard deviation, while non-normally distributed data were represented as median (interquartile range). The repeatability of alpha angle and head-neck offset measurements was determined using a two-way consistency calculation of intra-class correlation coefficient (ICC).[24; 25] Measurements were averaged between the two observers for all other statistical analyses. An unpaired Student's T test was used to compare measurements between groups. Spearman's rank-order correlation coefficient was used to evaluate the relationship between each individual radiographic measurement and the shape score. The Holm-

Bonferroni adjustment method corrected for multiple comparisons. Corrected *p* values less than 0.05 were used to identify significance. All statistical analyses were completed in R (v3.4.1).[26]

Partial least squares regression (PLS) was used to determine the set of radiographic views and associated measurements that best represented the shape scores of the proximal femur and the shape scores of the region of the cam lesion as quantified using SSM.[27] Leave-one-out cross-validation was used to calculate the predictive power of the model; components with goodness of prediction values (Q^2) greater than 0.0975 were kept in the model and the number of factors was determined to maximize the coefficient of determination (R^2) and minimize the number of radiographic views.[27] The variable influence on projection (VIP) was used to evaluate the relevance of each measurement in the explanation of the shape scores.

Results

The DRR-based radiographic measurements of the two groups were significantly different for all eight alpha angle measurements and seven of the head-neck offset measurements; the standard frog-leg lateral view head-neck offset measurement was not significantly different between groups (Table 3.2). The largest difference in measurements between groups was observed on the Meyer lateral for alpha angle and the 90° Dunn for head-neck offset (Table 3.2). Excellent inter-rater reliability was observed on all alpha angle measurements (ICC range: 0.80–0.94) and three head-neck offset measurements (anteroposterior, Espié frog-leg, and modified 45° Dunn; ICC range: 0.78–0.80), good

Table 3.2 Alpha angle and head-neck offset measurements of control subjects and cam femoroacetabular impingement (FAI) patients, as measured from digitally reconstructed radiographs (DRRs) representing eight plain film views.

	Alpha Angle (°)				Head-neck Offset (mm)			
DRR View	Control Group	Cam FAI Group	Diff, Range	*p* Value	Control Group	Cam FAI Group	Diff, Range	*p* Value
Antero-posterior	42.7 (8.4)	61.3 (32.2)	18.6, 58.6	<.0001	7.3±1.6	5.9±1.6	1.4, 7.4	.0006
Meyer Lateral	56.3 (14.2)	86.2 (16.0)	29.9, 69.4	<.0001	4.8±1.4	3.5±1.4	1.3, 6.2	.0002
45° Dunn (Neutral)	57.7 (12.5)	82.5 (23.0)	24.8, 63.9	<.0001	5.1±1.2	3.7±1.4	1.4, 6.8	<.0001
Espié Frog-leg	49.0 (10.2)	75.3 (25.7)	26.3, 68.8	<.0001	7.1±1.6	5.6±2.2	1.5, 8.2	.003
Modified 45° Dunn	45.1 (11.5)	67.4 (22.2)	22.3, 64.5	<.0001	8.5±1.6	6.7±2.2	1.8, 8.4	.0006
Frog-leg Lateral	42.2 (9.8)	60.5 (22.9)	18.3, 55.7	<.0001	8.5±1.8	7.8±2.0	0.7, 10.5	.13
90° Dunn	44.6 (9.7)	63.7 (21.9)	19.1, 61.0	<.0001	9.3±1.7	8.0±2.5	1.3, 11.8	.02
Cross-table	42.6 (8.1)	62.4 (19.9)	19.8, 59.8	<.0001	9.8±1.3	8.4±2.0	1.4, 7.9	.002

Note: Data presented as mean ± standard deviation for normally-distributed data, or median (interquartile range) for non-normally distributed data. The difference represents the difference in mean or median values between groups and the range represents the overall range of measurements including all subjects. The *p* value shown has been corrected for multiple comparisons and represents the significance level when making statistical comparisons between cam FAI and control groups. Abbreviations: FAI, femoroacetabular impingement; DRR, digitally reconstructed radiograph.

agreement on four head-neck offset measurements (Meyer lateral, frog-leg lateral, 90° Dunn, cross-table; ICC range: 0.64–0.72), and fair agreement on one head-neck offset measurement (45° Dunn, ICC = 0.42).

The mapping of the surface distance between the mean cam FAI and the mean control femurs from SSM provided clear visualization of the average location and magnitude of the cam lesion (Fig. 3.3, with the darkest red indicating the region of largest deviation). For many of the views, the positioning of the femur did not allow for visualization of the maximum deviation of the cam lesion (Fig. 3.3). Specifically, some radiographic projections, such as the anteroposterior or cross-table views, appeared more likely to position the cam lesion out of plane with the plain film projection.

The shape scores were significantly different between groups (cam: -1.0 ± 1.8 vs. control: 1.0 ± 1.7; $p < .0001$). The range of shape scores from SSM was wider for the cam group than the control group indicating larger shape variability (cam, range: -4.4 to 3.4 compared to controls, range: -2.3 to 4.5). Computer-generated femur reconstructions for the integer shape scores showed variability in both the femoral head-neck junction and the posterosuperior greater trochanter (Fig. 3.4).

All correlations between shape scores and 2D radiographic measurements were either weak or moderate (Table 3.3). The cross-table alpha angle and modified 45° Dunn head-neck offset provided the strongest correlations with proximal femur shape, while the Meyer lateral alpha angle and neutral 45° Dunn head-neck offset provided the strongest correlations with the shape of the isolated cam lesion (Table 3.3).

Results from PLS regression indicated that combined radiographic measurements from the Meyer lateral and 90° Dunn radiographs most effectively described femur shape,

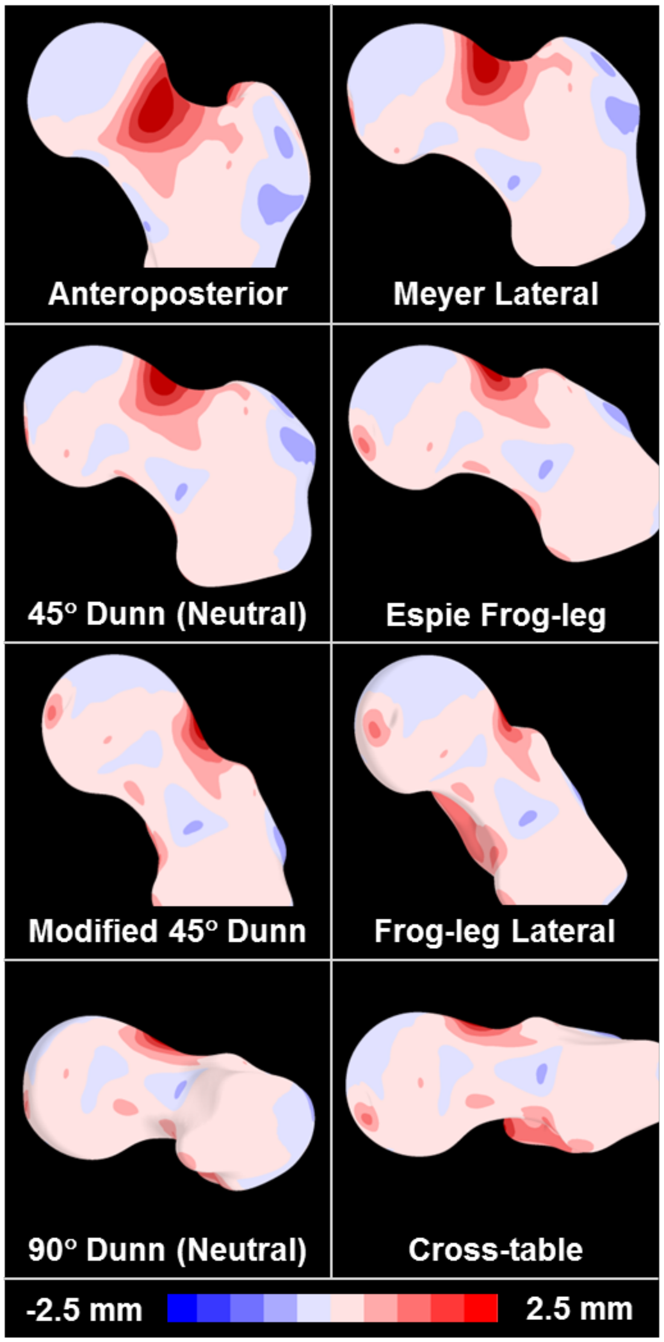

Figure 3.3. The mean cam femur from statistical shape modeling was aligned to the orientation of the eight digitally reconstructed radiographs to visualize the location and magnitude of the cam lesion relative to the imaging plane. The color map represents the spatial distance between the mean cam and mean control surface reconstructions.

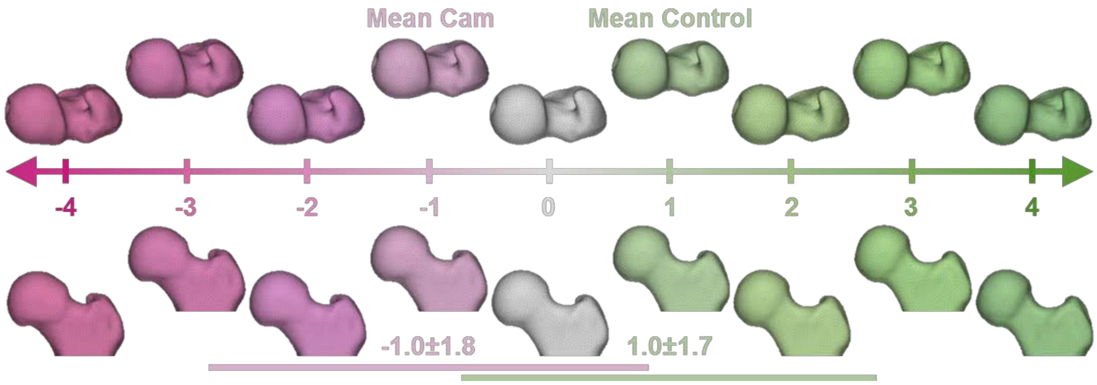

Figure 3.4. Computer-generated femur surface reconstructions representing the spectrum of variability in proximal femoral anatomy as calculated from statistical shape modeling. The correspondence points of each subject femur were mapped onto the spectrum of shape variation to generate a subject-specific shape score. Horizontal lines identify the standard deviation of shape scores for the femur shapes of the cam patients (magenta) and control subjects (green). Negative shape scores indicate shapes that resemble cam femurs, while positive shape scores indicate shapes that resemble control femurs. Along the spectrum, shape variation in the head-neck junction can be seen in both the superior view (top) and the anterior view (bottom), while variation of the greater trochanter is best seen in the superior view.

Table 3.3 Spearman correlation coefficients between the alpha angle or head-neck offset measurements of each radiographic view to three-dimensional shape scores from statistical shape modeling.

	Alpha Angle				Head-neck Offset			
	Femur		Lesion		Femur		Lesion	
Radiographic View	*r*	*p* Value	*r*	*p* Value	*r*	*p* Value	*r*	*p* Value
Antero-posterior	-0.358	.001	-0.509	<.0001	0.112	0.28	0.248	.03
Meyer Lateral	-0.536	<.0001	-0.669	<.0001	0.399	.0003	0.482	<.0001
45° Dunn (Neutral)	-0.484	<.0001	-0.613	<.0001	0.419	.0002	0.486	<.0001
Espié Frog-leg	-0.441	<.0001	-0.548	<.0001	0.403	.0003	0.419	.0001
Modified 45° Dunn	-0.547	<.0001	-0.620	<.0001	0.476	<.0001	0.481	<.0001
Frog-leg Lateral	-0.554	<.0001	-0.589	<.0001	0.257	0.02	0.172	.09
90° Dunn	-0.538	<.0001	-0.600	<.0001	0.364	0.001	0.333	.003
Cross-table	-0.568	<.0001	-0.630	<.0001	0.455	<.0001	0.413	.0001

Note: The *p* value shown has been corrected for multiple comparisons, and represents the significance when calculating the correlation coefficient.

including both the shape of the overall proximal femur and of the isolated cam lesion (Q^2 = 0.446) (Table 3.4). In this combined model, the relative shape of the isolated cam lesion was better predicted from radiographic measurements (R^2 = 0.497, Q^2 = 0.507) than the overall shape of the proximal femur (R^2 = 0.372, Q^2 = 0.384). Substitution of the cross-table for the 90° Dunn provided similar predictability, with variations in $R^2 < 0.01$. The combined regression model was improved slightly with the addition of the cross-table (Q^2 = 0.456) and diminished with the inclusion of the anteroposterior view (Q^2 = 0.386).

Discussion

We quantified the ability of various radiographic projections and associated 2D measurements of femoral head asphericity to describe the 3D shape score of the proximal femur, as determined from SSM. The best predictive model included the alpha angle and head-neck offset measurements from the Meyer lateral and 90° Dunn radiographs, thus confirming our hypothesis that 2D radiographic measurements from more than one view would be necessary to predict 3D shape. The predictability of the model was improved with the addition of the cross-table view; however, to minimize the number of radiographs and avoid concerns of poor image quality due to projection angle,[6] the cross-table view was not included in the final regression model.

This study was not without limitations. First, we used radiographic measurements to screen control subjects, yet morphologic features found in symptomatic cam FAI patients are prevalent among asymptomatic individuals.[28] Thus, our results should be interpreted with caution, as shape score values would change if asymptomatic controls with FAI morphology were included. Many previous studies evaluating the relevance of

Table 3.4 Partial least squares regression model coefficients and variable influence on projection values for the optimized model predicting the shape score from statistical shape modeling relative to the entire proximal femur and the region specific to the cam lesion.

	Alpha Angle			Head-neck Offset		
	PLS Coefficient			PLS Coefficient		
DRR View	Proximal Femur	Cam Lesion	VIP	Proximal Femur	Cam Lesion	VIP
Meyer Lateral	-0.229	-0.261	1.14	0.162	0.185	0.81
90° Dunn	-0.235	-0.268	1.18	0.161	0.184	0.81

PLS, partial least squares; DRR, digitally reconstructed radiograph; VIP, variable influence on projection

radiographic measurements did not include control subjects [8-12]. We included controls herein to evaluate regressions over a wide range of radiographic measurements. A majority of our recruited cam FAI patients were males which may affect the distribution of shape scores. However, cam FAI occurs more frequently in males, and therefore our results represent the population of interest.[29] A potential second limitation was that we used DRRs in-lieu of standard plain films; DRRs do not visualize soft-tissue bulk surrounding the hip, making them appear different than standard plain films. Nevertheless, DRRs have been shown to be a valid surrogate for plain films,[7] and are advantageous in that they can be generated consistently, thereby eliminating variability associated with positioning of the patient and/or radiographic equipment. Importantly, the ICC values for the measurement of alpha angle and head-neck offset on the DRRs were as good or better than those previously reported when measuring standard plain films.[21; 30; 31]

To our knowledge, this is the first study to use regression analysis to identify which radiographic views and associated 2D measurements provided the best predictors of 3D femur shape as quantified using SSM. A previous study by Harris et al. evaluated the relationship between alpha angles and head-neck offset measurements obtained on the frog-leg lateral view to results from principal component analysis of SSM data from cam FAI and control hips using linear correlation.[32] Harris et al. found moderate to weak correlations between 2D radiographic measurements of femoral shape and the first three principal component loading values from SSM,[32] which aligns with the moderate correlations we found between radiographic measurements and shape scores. Other studies have evaluated measurements from plain films and 2D slices from standard or radial reconstructions of CT or MRI in an attempt to identify the optimal plain film views.[3; 7-12] For example, Nepple et al. evaluated the sensitivity and specificity of cam FAI diagnosis based on the anteroposterior, 45° Dunn, frog-leg lateral, and cross-table views relative to measurements from radial CT images.[11] Based on their analysis, Nepple et al. recommended a set of three plain films, including the anteroposterior, 45° Dunn, and frog-leg lateral, be used in clinical decision-making. In contrast, none of the three views identified by Nepple et al. were used to predict 3D shape in our PLS regression model, and the one view they excluded, the cross-table, slightly improved predictability when added to our two radiograph model. These discrepancies are likely due to the fact that Nepple et al. used 2D measurements of radial images as the reference standard, whereas we used 3D shape scores quantified with SSM.

Importantly, measurements from radial imaging are often used as a reference standard, yet these measurements are still based on a single, 2D image slice, which likely does not capture the true 3D shape of the cam lesion. For example, 30° radial slices on a femoral head with a radius of 20 mm would be separated by 10.5 mm on the femoral surface. When correlating alpha angle measurements from plain films and radial CT images to measurements of 3D femoral head asphericity (i.e., deviation from best-fit sphere), Harris et al. found the modified 45° Dunn and cross-table views to be more strongly correlated to 3D asphericity measurements than any of the radial reconstructions.[7] Thus, in contrast to previous reports,[8-10] radial imaging may not serve as a good reference standard with which to evaluate the shape of the proximal femur.

Clinicians often obtain multiple radiographs of the hip to provide evaluations of hip pathologies, acetabular coverage, and degree of degeneration. One of the most commonly used radiographs is the anteroposterior radiograph. For this reason, measurements from the anteroposterior radiograph were incorporated into the regression model with the Meyer lateral and 90° Dunn radiographs. However, the inclusion of measurements from this third view actually reduced the predictability of the model from $Q^2 = 0.446$ to $Q^2 = 0.386$. As such, the use of measurements from this and other views should focus on the overall assessment of the hip joint and not on the assessment of cam FAI.

Our study findings are important, as they question the assumption that radiographic projections that result in higher alpha angle measurements and greater differences in measurements between patients with cam FAI and control subjects are better projections for visualizing the cam lesion. Specifically, as we showed herein, some of the radiographic projections that best represented the 3D shape score had some of the smallest alpha angle or largest head-neck offset measurements (e.g., 90° Dunn). Similarly, large differences in measurements were observed between the cam and control groups on the Espie frog-leg and modified 45° Dunn radiograph, yet these views were not identified through PLS regression as being predictive of 3D shape scores of the proximal femur.

In conclusion, the combined alpha angle and head-neck offset measurements from the Meyer lateral and 90° Dunn radiographic views provided the most effective predictions of 3D shape of the proximal femur. Therefore, we recommend that clinicians use these views when evaluating patients with clinical symptoms consistent with a diagnosis of cam FAI. However, these views were still only able to describe less than half of the actual anatomic variation observed for the proximal femur. Thus, 3D reconstructions generated from CT or MRI data may better visualize femoral morphology. However, to our knowledge, clinical tools that extract measurements of 3D hip shape are not readily available. As such, future work should focus on refining the SSM software such that it can be used to objectively quantify deformity severity on a patient-specific basis.

Acknowledgments

We thank Trevor Hafer, Tyler Skinner, Samuel Colby, and Lindsay Schuring for their contributions towards image processing.

References

1. Ganz R, Leunig M, Leunig-Ganz K, et al. 2008. The etiology of osteoarthritis of the hip: An integrated mechanical concept. Clin Orthop Relat Res 466:264-272.

2. Griffin DR, Dickenson EJ, O'Donnell J, et al. 2016. The Warwick Agreement on femoroacetabular impingement syndrome (FAI syndrome): An international consensus statement. Br J Sports Med 50:1169-1176.

3. Sutter R, Dietrich TJ, Zingg PO, et al. 2012. How useful is the alpha angle for discriminating between symptomatic patients with cam-type femoroacetabular impingement and asymptomatic volunteers? Radiology 264:514-521.

4. Tannast M, Siebenrock KA, Anderson SE. 2007. Femoroacetabular impingement: Radiographic diagnosis--what the radiologist should know. AJR Am J Roentgenol 188:1540-1552.

5. Meyer DC, Beck M, Ellis T, et al. 2006. Comparison of six radiographic projections to assess femoral head/neck asphericity. Clin Orthop Relat Res 445:181-185.

6. Clohisy JC, Carlisle JC, Beaule PE, et al. 2008. A systematic approach to the plain radiographic evaluation of the young adult hip. J Bone Joint Surg Am 90 Suppl 4:47-66.

7. Harris MD, Kapron AL, Peters CL, et al. 2014. Correlations between the alpha angle and femoral head asphericity: Implications and recommendations for the diagnosis of cam femoroacetabular impingement. Eur J Radiol 83:788-796.

8. Domayer SE, Ziebarth K, Chan J, et al. 2011. Femoroacetabular cam-type impingement: Diagnostic sensitivity and specificity of radiographic views compared to radial MRI. Eur J Radiol 80:805-810.

9. Barton C, Salineros MJ, Rakhra KS, et al. 2011. Validity of the alpha angle measurement on plain radiographs in the evaluation of cam-type femoroacetabular impingement. Clin Orthop Relat Res 469:464-469.

10. Dudda M, Albers C, Mamisch TC, et al. 2009. Do normal radiographs exclude asphericity of the femoral head-neck junction? Clin Orthop Relat Res 467:651-659.

11. Nepple JJ, Martel JM, Kim YJ, et al. 2012. Do plain radiographs correlate with CT for imaging of cam-type femoroacetabular impingement? Clin Orthop Relat Res 470:3313-3320.

12. Konan S, Rayan F, Haddad FS. 2010. Is the frog lateral plain radiograph a reliable predictor of the alpha angle in femoroacetabular impingement? J Bone Joint Surg Br 92:47-50.

13. Atkins PR, Aoki SK, Whitaker RT, et al. 2017. Does removal of subchondral cortical bone provide sufficient resection depth for treatment of cam femoroacetabular impingement? Clin Orthop Relat Res 475:1977-1986.

14. Atkins PR, Elhabian SY, Agrawal P, et al. 2017. Quantitative comparison of cortical bone thickness using correspondence-based shape modeling in patients with cam femoroacetabular impingement. J Orthop Res 35:1743-1753.

15. Kapron AL, Aoki SK, Peters CL, et al. 2015. In-vivo hip arthrokinematics during supine clinical exams: Application to the study of femoroacetabular impingement. J Biomech 48:2879-2886.

16. Fiorentino NM, Kutschke MJ, Atkins PR, et al. 2016. Accuracy of functional and predictive methods to calculate the hip joint center in young non-pathologic asymptomatic adults with dual fluoroscopy as a reference standard. Ann Biomed Eng 44:2168-2180.

17. Henak CR, Abraham CL, Peters CL, et al. 2014. Computed tomography arthrography with traction in the human hip for three-dimensional reconstruction of cartilage and the acetabular labrum. Clin Radiol 69:e381-391.

18. Troelsen A, Jacobsen S, Rømer L, et al. 2008. Weightbearing anteroposterior pelvic radiographs are recommended in DDH assessment. Clin Orthop Relat Res 466:813-819.

19. Dunn DM. 1952. Anteversion of the neck of the femur; a method of measurement. J Bone Joint Surg Br 34-b:181-186.

20. Espie A, Chaput B, Murgier J, et al. 2014. 45 degrees -45 degrees -30 degrees frog-leg radiograph for diagnosing cam-type anterior femoroacetabular impingement: Reproducibility and thresholds. Orthop Traumatol Surg Res 100:843-848.

21. Clohisy JC, Nunley RM, Otto RJ, et al. 2007. The frog-leg lateral radiograph accurately visualized hip cam impingement abnormalities. Clin Orthop Relat Res 462:115-121.

22. Eijer H, Leunig M, Mahomed MN, et al. 2001. Cross-table lateral radiographs for screening of anterior femoral head-neck offset in patients with femoro-acetabular impingement. Hip Int 11:37-41.

23. Notzli HP, Wyss TF, Stoecklin CH, et al. 2002. The contour of the femoral head-neck junction as a predictor for the risk of anterior impingement. J Bone Joint Surg Br 84:556-560.

24. Gamer M, Lemon J, Fellows I, et al. 2012. Irr: Various coefficients of interrater reliability and agreement. CRAN.

25. Cicchetti DV, Sparrow SA. 1981. Developing criteria for establishing interrater reliability of specific items: Applications to assessment of adaptive behavior. Am J Ment Defic 86:127-137.

26. RCoreTeam. 2014. R: A language and environment for statistical computing. 3.1.2 ed. Vienna, Austria: R Foundation for Statistical Computing.

27. Le Cao K, Gonzalez I, Dejean S. 2015. Mixomics: Omics data integration project. 5.2.0 ed: CRAN.

28. Frank JM, Harris JD, Erickson BJ, et al. 2015. Prevalence of femoroacetabular impingement imaging findings in asymptomatic volunteers: A systematic review. Arthroscopy 31:1199-1204.

29. Halim A, Badrinath R, Carter CW. 2015. The importance of sex of patient in the management of femoroacetabular impingement. Am J Orthop (Belle Mead NJ) 44:172-175.

30. Nepple JJ, Martell JM, Kim YJ, et al. 2014. Interobserver and intraobserver reliability of the radiographic analysis of femoroacetabular impingement and dysplasia using computer-assisted measurements. Am J Sports Med 42:2393-2401.

31. Carlisle JC, Zebala LP, Shia DS, et al. 2011. Reliability of various observers in determining common radiographic parameters of adult hip structural anatomy. Iowa Orthop J 31:52-58.

32. Harris MD, Datar M, Whitaker RT, et al. 2013. Statistical shape modeling of cam femoroacetabular impingement. J Orthop Res 31:1620-1626.

CHAPTER 4

QUANTITATIVE COMPARISON OF CORTICAL BONE THICKNESS USING CORRESPONDENCE-BASED SHAPE MODELING IN PATIENTS WITH CAM FEMOROACETABULAR IMPINGEMENT

Reprinted with permission from Atkins PR, Elhabian SY, Agrawal P, Harris MD, Whitaker RT, Weiss JA, Peters CL, Anderson AE. *J Orthop Res*. 2017; 35(8):1743-1753.

Quantitative Comparison of Cortical Bone Thickness Using Correspondence-Based Shape Modeling in Patients With Cam Femoroacetabular Impingement

Penny R. Atkins,[1,2] Shireen Y. Elhabian,[3,4] Praful Agrawal,[3,4] Michael D. Harris,[5,6] Ross T. Whitaker,[1,3,4] Jeffrey A. Weiss,[1,2,3,4] Christopher L. Peters,[1,2] Andrew E. Anderson[1,2,3,7]

[1]Department of Bioengineering, University of Utah, Salt Lake City, Utah 84112, [2]Department of Orthopaedics, University of Utah, 590 Wakara Way Rm A100, Salt Lake City, Utah 84108, [3]Scientific Computing and Imaging Institute, Salt Lake City, Utah 84112, [4]School of Computing, University of Utah, Salt Lake City, Utah 84112, [5]Program of Physical Therapy, Washington University School of Medicine, Saint Louis, Missouri 63110, [6]Department of Orthopaedic Surgery, Washington University School of Medicine, Saint Louis, Missouri 63110, [7]Department of Physical Therapy, University of Utah, Salt Lake City, Utah 84108

Received 12 April 2016; accepted 23 October 2016
Published online 8 November 2016 in Wiley Online Library (wileyonlinelibrary.com). DOI 10.1002/jor.23468

ABSTRACT: The proximal femur is abnormally shaped in patients with cam-type femoroacetabular impingement (FAI). Impingement may elicit bone remodeling at the proximal femur, causing increases in cortical bone thickness. We used correspondence-based shape modeling to quantify and compare cortical thickness between cam patients and controls for the location of the cam lesion and the proximal femur. Computed tomography images were segmented for 45 controls and 28 cam-type FAI patients. The segmentations were input to a correspondence-based shape model to identify the region of the cam lesion. Median cortical thickness data over the region of the cam lesion and the proximal femur were compared between mixed-gender and gender-specific groups. Median [interquartile range] thickness was significantly greater in FAI patients than controls in the cam lesion (1.47 [0.64] vs. 1.13 [0.22] mm, respectively; $p < 0.001$) and proximal femur (1.28 [0.30] vs. 0.97 [0.22] mm, respectively; $p < 0.001$). Maximum thickness in the region of the cam lesion was more anterior and less lateral ($p < 0.001$) in FAI patients. Male FAI patients had increased thickness compared to male controls in the cam lesion (1.47 [0.72] vs. 1.10 [0.19] mm, respectively; $p < 0.001$) and proximal femur (1.25 [0.29] vs. 0.94 [0.17] mm, respectively; $p < 0.001$). Thickness was not significantly different between male and female controls. Clinical significance: Studies of non-pathologic cadavers have provided guidelines regarding safe surgical resection depth for FAI patients. However, our results suggest impingement induces cortical thickening in cam patients, which may strengthen the proximal femur. Thus, these previously established guidelines may be too conservative. © 2016 Orthopaedic Research Society. Published by Wiley Periodicals, Inc. J Orthop Res 35:1743–1753, 2017.

Keywords: disease process; FAI and morphology; bone; statistics

One in four people will develop hip osteoarthritis (OA) in their lifetime.[1] Within the last decade, femoroacetabular impingement (FAI) has been implicated as a primary cause of hip OA in young adults.[2–5] Two distinct presentations of FAI have been identified: pincer, defined as overcoverage of the femoral head, and cam, characterized by an aspherical femoral head and reduced head–neck offset. While many patients present with both cam and pincer FAI deformities, the morphological features of cam FAI tend to result in accelerated joint degeneration.[3] In particular, cam-type femoral morphology may shear the cartilage at the chondrolabral junction during flexion and internal rotation of the hip.[6–8]

Cam FAI is treated by resection of bone in the region of the femur believed to be abnormally shaped; the specific location of this region varies among patients but is generally located in the anterolateral or superolateral region of the femoral head–neck junction.[4] If the amount of resection is too conservative, the underlying impingement may not be fully addressed, which is a common reason for revision surgery.[9] However, too aggressive of a resection may lead to an iatrogenic femoral neck fracture.[10] In previous studies, non-pathologic cadaveric femurs,[11] or generalized femoral anatomy,[12,13] were used to evaluate the effects of resection depth and shape on femoral neck strength. However, use of non-pathologic cadavers and simplified anatomy may not accurately represent the biomechanics of the femur in cam FAI patients.

The density and shape of bone is modified by the mechanical environment.[14] In the case of cam-type FAI, repetitive impingement may induce hypertrophy of the bone, which may manifest as increased cortical thickness. The cortex contributes to the majority of load bearing within the hip.[15] Thus, it is important to establish a baseline understanding of cortical bone thickness in patients with cam-type FAI, especially over regions that may be resected during surgery. Theoretically, a thicker cortex in cam FAI patients could imply that resection limits based on analyses of non-pathologic cadavers and generalized anatomy are overly conservative.

True anatomical variation of biological tissues can be difficult to identify due to complex morphology. Radiographic or other image-based measurements serve as the foundation for diagnosing cam FAI.[16–18] However, there is a high prevalence of radiographic

Conflicts of interest: None of the authors report conflicts of interest associated with the design, execution, and publication of this study.
Grant sponsor: National Institutes of Health; Grant numbers: R01-EB016701, P41-GM103545-17, R01-GM083925, R21-AR063844.
Correspondence to: Andrew E. Anderson (T: +1 801 587 5208; F: +1 801 587 5482; E-mail: Andrew.Anderson@hsc.utah.edu)

signs of cam FAI among asymptomatic, healthy hips,[19,20] which calls into question the ability of radiographic projections and measurements to define anatomical variation specific to this disease. Equally important, assessing the severity of cam FAI using radiographs requires the assumption that a morphologically normal hip is perfectly spherical. Yet, even healthy hips are aspherical.[21,22] Finally, the projection of complex 3D anatomy to a 2D plane can fail to visualize the magnitude and location of the cam lesion.[23]

Correspondence-based computing methods, such as statistical shape modeling (SSM), are powerful tools used to quantify 3D anatomical variation and identify shape differences.[24–26] Correspondence-based methods are ideal because they do not determine, a-priori, the ideal shape that the structure should conform to. We previously used SSM to demonstrate that cam femora are significantly different in shape compared to controls, and established principal component analysis (PCA) modes that captured the variance in shape.[25] In our prior study, a hierarchical splitting strategy was used to automatically place correspondence particles onto the proximal femur. This entropy-based approach to distribute correspondence particles reduces subjectivity as it does not require manual landmark identification or the use of training shapes. From the correspondence model, scalar attributes that accompany shape, such as the thickness of the cortical bone, can be sampled at the same relative anatomic location across a population.

The objective of this study was to use this correspondence-based modeling approach to quantify and compare cortical thickness between cam patients and non-pathologic controls in the location of the cam lesion and throughout the proximal femur. We hypothesized that cam FAI patients would have increased cortical thickness in the region of the cam lesion.

METHODS

Subject Recruitment and Screening

Institutional Review Board (IRB) approval was obtained through the University of Utah (IRBs 11755 and 56086) and Intermountain Healthcare (IRB 1024270). Twenty-eight cam FAI patients (26 males) and 45 control subjects (29 males) of similar age, weight, and body mass index (BMI) were recruited for the study.

Volumetric computed tomography (CT) images of the proximal femur were acquired using a: Siemens SOMATOM 128 Definition CT Scanner (IRB 56086, 20 control subjects, 15 cam patients), GE High Speed CTI Single Slice Helical CT Scanner (IRB 11755, 59 control cadaver femurs), and GE LightSpeed VCT scanner (IRB 1024270, 13 cam patients).[25]

Patients were diagnosed with cam FAI based on clinical examination and radiographic measurements. Control subjects were selected based on the absence of bony abnormalities. For living control subjects, an anterior–posterior radiograph was read by members of the study team with 5–10 years of medical imaging experience to exclude morphologic abnormalities. For all control femurs, a digitally reconstructed radiograph (DRR) was generated from the CT images. The alpha angle, which defines the angle between the femoral neck axis and the point at which the femoral head bone deviates laterally from a circle templated onto the radiograph, was measured on the frog-leg lateral DRR. Alpha angles greater than 60° were used to exclude femurs with cam-like morphology.[27] A total of 34 out of 79 control femurs were omitted based on these criteria,[28] leaving 45 control subjects (15 live subjects and 30 cadaver femurs).

CT datasets were upsampled to axial slice thicknesses of 0.33 mm to improve resolution. Cortical and trabecular bone layers of each proximal femur were semi-automatically segmented and reconstructed from the CT image data using Amira (v5.6, FEI, Hillsboro, OR). Segmentation was completed using the methods of Anderson et al. which previously resulted in less than 10% error for cortical thicknesses greater than 0.7 mm.[29] Surfaces were smoothed and decimated in Amira, and then reformatted to visual toolkit (VTK) format.[30] Reconstructed surfaces of the two layers were used to determine the thickness of the cortical bone over the surface of the femoral head and proximal shaft using PreView.[31] Thickness values were calculated using a normal projection from the cortical surface to the trabecular surface and recorded for each node (Fig. 1, top).

Correspondence-Based Shape Modeling

Surfaces representing right femurs were reflected to appear as left femurs and all surfaces were aligned using the iterative closest point algorithm as part of preprocessing.[32] ShapeWorks[33] was used to quantify anatomical variation in the shape of the outer cortex, and provided the medium to calculate differences in cortical thickness between groups through modifications to the software framework described below.

ShapeWorks performs analysis on volumetric datasets, and thus requires input of a voxel-based representation of each 3D surface. To accurately represent surfaces using voxels, it is often necessary to reduce voxel size (i.e., increase resolution), which in turn increases the computational size of each volume. To circumvent this issue, a pipeline was developed to accurately generate volume-based representations without the need to reduce the size of each voxel. Here, a spatial partitioning algorithm was used to define a list of candidate surface mesh faces closest to each voxel of a volume. From the list of candidate faces, the nearest triangular face was identified and the physical distance encoded for each voxel of the distance transform (i.e., a volume which includes data of the distance to the nearest surface for each voxel). This technique ensured that the nearest face was chosen using the barycentric distance, which is based on the centers of mass, between each voxel and the surface vertices. The resultant isosurface (i.e., surface representation generated by connecting the zero-distance voxels) approximated the input surface mesh to an error that did not exceed 0.31 mm using an input voxel size of 0.5 mm.

The primary purpose of this study was to analyze differences in the thickness of the cortex at the proximal femur. To limit placement of correspondence particles to this region, a cutting plane was identified perpendicular to the femoral shaft just proximal to the lesser trochanter for a single template shape. An initial correspondence model, with 512 particles, was used to optimize the transformation of the template plane onto each femur (Fig. 1, middle). Transformed cutting planes were visually verified for

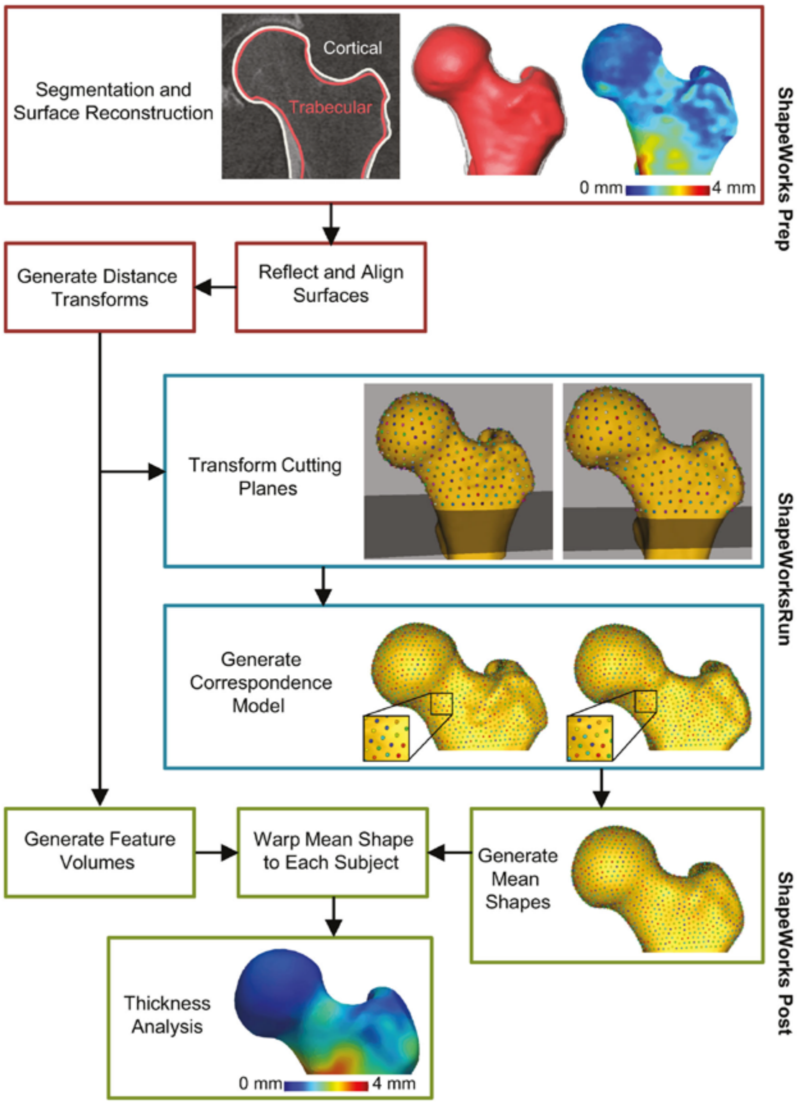

Figure 1. Flowchart for modeling pipeline. Subject specific shapes of the inner and outer boundaries of the cortex were segmented and reconstructed from computed tomography scans; cortical thickness was determined. Surfaces were aligned and rasterized in preparation for analysis. Cutting planes were transformed to each shape and used to limit locations of correspondence points. The correspondence model was generated by placement of particles on each rasterized surface. Mean shapes were calculated from average locations of the correspondence particles. Cortical thickness obtained from each subject was then mapped to the mean shapes of each group using the correspondence model to display variation.

consistency across the population. Correspondence particles ($n = 2{,}048$) were hierarchically placed above the cutting plane for all shapes using ShapeWorks.[25,33] The spatial positions of the particles were optimized based on correspondence across shapes and sampling over each surface (Fig. 1, middle).

The correspondence model and volumetric distance transforms for each subject were used to generate a mean distance transform for the whole population and for each group. The iso-surface generated from this mean distance transform was smoothed and decimated to roughly 50,000 vertices to create the mean surface.[34,35] Using the correspondence model, the population mean surface was warped to each subject and to the mean shapes of each group using compactly supported radial basis functions,[36] which resulted in dense surface meshes for each subject and group that were in correspondence. Using this approach facilitated vertex-to-vertex comparisons, which were necessary to directly compare thickness between shapes.

Volumes of the same dimensions and voxel size as the distance transforms, which represented the 3D femur surface, were generated to include scalar data for each subject, specifically, cortical thickness. This approach could be applied to any feature that accompanies shape. Accordingly, these volumes were referred to as feature volumes. Using the correspondence model, the feature volumes were warped to the mean shapes. Once warped, scalar cortical thickness data for each subject was directly sampled and mapped onto the mean surfaces. From the subject specific cortical thickness data, mean and median values were mapped onto the mean surfaces in Matlab (v7.10, The Mathworks, Inc., Natick, MA). Mean thickness for each group was used in the quantification of group differences, while maximum, median, and mean thicknesses were used for comparison of the subjects within each group. For visualization of cortical thickness variability within groups, thickness at each vertex was sorted to identify the median and 10th, 25th, 75th, and 90th percentile values. These values were mapped onto the surface of the mean cam and control femurs for visualization (Fig. 1, bottom).

The region of the cam lesion was identified to allow for analysis of cortical thickness at the location of surgical resection. The region was identified by first calculating the surface distance between the mean cam and control femur surfaces in PreView.[31] A region on the femoral head–neck junction, designated by distance greater than 1.5 mm between the mean shapes, was isolated as the region of the cam lesion. A distance of 1.5 mm between shapes isolated a large region of the head–neck junction, while minimizing inclusion of the saddle between the femoral head and the greater trochanter.

Within the region of the cam lesion, the location of maximum thickness was found on both the mean shapes and on each subject specific shape. This location was represented as a vector from the sphere-fit center of the femoral head to the location of maximum thickness and mapped onto each anatomical plane. The best-fit sphere was calculated by first isolating faces of the femoral head based on first principal curvature of the mean cam and control shapes in PostView.[31] These faces were identified for each subject based on the faces from each respective mean shape. The nodes corresponding to these faces were then fit to a sphere using a linear system of equations in Matlab.

Statistical Analysis

The Shapiro test was used to evaluate normality, and the Wilcoxon rank sum test or Student's T-test to evaluate group demographic differences between cam and control subjects in the R statistical software.[37] Since there was predominance for male patients, with only two female patients, statistical analysis was completed to compare not only between cam and control subject populations, but also within control and male populations separately. This resulted in comparisons of cortical bone thickness between female and male control subjects (16 and 29 subjects, respectively) and male cam and control subjects (26 and 29 subjects, respectively).

Principal component analysis (PCA) isolated the modes of variation from the correspondence particle locations. The PCA modes containing significant variation were determined using parallel analysis.[38] Within these significant modes, PCA loading values were compared between the two groups using a Student's T-test with Finner's adjustment for multiple comparisons.[39] Hotelling's T^2 test was utilized to determine whether a significant shape difference existed between the two groups.

The mean correspondence particle locations and thickness values for the mean cam and control femurs were used to generate a linear discrimination between the two shapes in high-dimensional shape space (i.e., high-dimensional vector). Specifically, the 2,048 scalar data points representing cortical thickness at each correspondence particle location were organized into a vector for each subject specific and mean shape. The linear discrimination between the two mean shapes in shape space was then defined as the difference of the two mean shape vectors. Each subject shape was then mapped to this shape space representation by taking the dot product between the subject specific and linear discrimination vectors, which resulted in a single scalar value representation of thickness of each subject shape. This analysis was repeated for the correspondence particle locations to provide a scalar representation of shape. These scalar values were evaluated against shape statistics using Spearman's correlation coefficient.

Maximum, median, and mean cortical thickness values and the angular components of the vector representing the location of maximum thickness were evaluated for normality using the Shapiro-Wilk test and then compared using a Wilcoxon rank sum test or Student's T-test with Finner's adjustment for multiple comparisons.

RESULTS

Age and BMI were not normally distributed across the population. Thus, for consistency, all demographics were analyzed using the Wilcoxon rank sum test. The weight of the female controls was significantly less than that of the males ($p = 0.006$); all other metrics between the cam and control populations, male cam and control subgroups, and the female and male control subgroups were not significantly different ($p > 0.05$) (Table 1).

Parallel analysis of the PCA loading values based on the correspondence particle locations on the outer bone cortex identified ten modes of significant variation, which included 85.8% of the total variation within the population, representing 33.5%, 20.4%, 8.3%, 6.4%, 4.7%, 3.9%, 2.6%, 2.4%, 2.1%, and 1.7% of the overall variation, respectively. Three of these modes (PCA modes 1, 5, and 7; Fig. 2) aligned with significant group differences based on analysis of PCA loading values (adj. $p = 0.019$, $p = 0.040$, and $p < 0.001$, respectively). Mode one described general variation in anterior–posterior widths. Modes 5 and 7 represented

Table 1. Demographics for Groups and Subgroups of the Population Represented as Median [Interquartile Range]

	Entire Cohort		Subject Subgroups			
	Controls	Patients	Female Controls	Male Controls	Female Patients*	Male Patients
Subjects, n	45	28	16	29	2	26
Age, years	28 [12]	23 [13]	30 [18]	27 [10]	21, 47	23 [13]
Weight, kg	81.0 [22.0]	81.0 [15.4]	62.8 [22.5]	81.0 [19.0]	68.5, 97.0	81.0 [14.7]
BMI, kg/m^2	24.2 [7.9]	25.0 [3.9]	22.0 [11.3]	25.6 [5.1]	25.9, 32.8	24.8 [4.0]

*Individual values are presented for the female patients due to sample size ($n = 2$).

variations in head–neck offset and femoral head circumference; mode 7 also described variations in the greater trochanter. Modes 2, 3, 4, and 6 represented variations in the curvature of the saddle between the femoral head and greater trochanter, lateral extent of the femoral head and greater trochanter, and shape of the proximal shaft. Hotelling's T^2 test showed the outer cortex of cam and control patient groups to be significantly different in shape ($p < 0.001$).

The scalar mapping of each subject femur onto the linear discrimination of variation in shape space between the cam and control shapes (Fig. 3) showed significant differences between the two groups in terms of both shape (using the three anatomical directions to describe the location of each particle) and thickness (using the scalar thickness value at each particle) ($p < 0.001$ for both). Mode one from PCA was strongly correlated to the shape mapping ($r = 0.94$, adj. $p < 0.001$); all other modes had no more than a weak correlation and were not significant after correction for multiple comparisons ($r < 0.15$, adj. $p > 0.684$). The thickness mapping values were weakly correlated with PCA modes 1, 2, 3, 6, 7, and 8, but were not significant after correction for multiple comparisons ($r < 0.29$; adj. $p > 0.118$ for all). The shape and thickness mappings were also weakly correlated ($r = 0.37$, $p = 0.001$).

Thickness data were not normally distributed. Thus, a Wilcoxon rank sum test was used for comparison of subject thickness metrics. Cam patients had increased cortical thickness compared to control subjects in terms of maximum, median, and mean thickness values within the region of the cam lesion, as identified by shape differences (Fig. 4, top right), and median thickness values over the proximal femur, whether gender effects were considered or not (Table 2). No difference in cortical thickness was evident between male and female control subjects.

When comparing thickness between mean shapes (one-to-one comparison, no p-values), qualitative inspection revealed increased cortical thickness in patients with cam FAI for the region of the cam lesion. The region of the cam lesion was also thicker on average than the entire proximal femur. Overall, the mean proximal cam femur was thicker than the mean control femur (Table 3). The maximum thickness of the cam lesion was greater for cam patients than controls (2.47 vs. 1.71 mm). The maximum difference in thickness between the two mean shapes was within the region of the cam lesion and 1.35 mm in magnitude (Fig. 4, bottom right). The mean cam shape had greater cortical thickness throughout the entire cam lesion.

The mean female control and male cam femurs were also thicker than the mean male control femur (Table 3). Among the mean male shapes, the maximum thickness within the region of the cam lesion was 2.53 and 1.65 mm for the cam and control subjects, respectively. The male cam shape had greater thickness throughout the entire region with a maximum difference in thickness of 1.47 mm. Among the controls, the maximum thickness for the female controls was greater than that of the male controls (1.91 vs. 1.65 mm, respectively). The female control shape was maximally 0.48 mm thicker and 0.19 mm thinner than the male control shape within the region identified as the cam lesion.

Median regional thickness, evaluated within the region of the cam lesion, for each subject was moder-

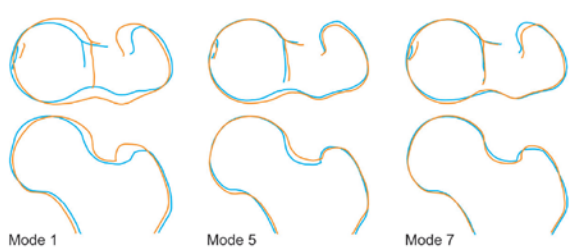

Figure 2. Contours representing the 2D projection of femur surfaces in the axial and coronal planes represent variation of plus (blue) and minus (orange) two standard deviations of each PCA mode that corresponded to a significant difference between the cam and control shapes. Modes represent variation in the curvature of the femoral head–neck junction and greater trochanter.

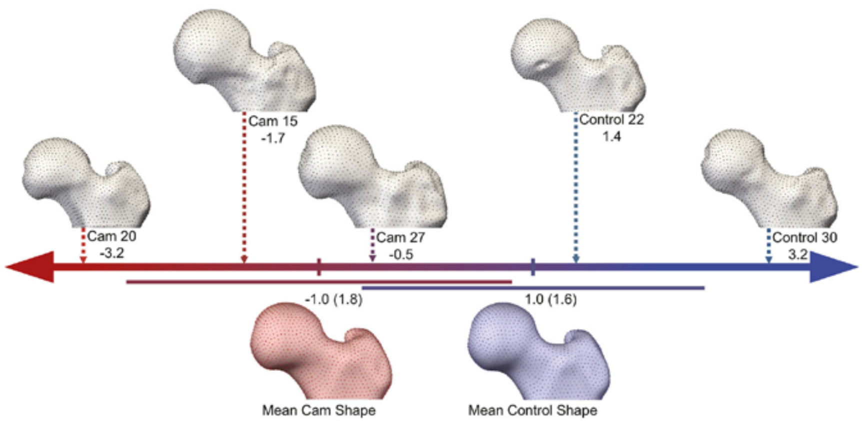

Figure 3. The correspondence model was used to determine a linear discrimination of the variation between the mean cam and mean control shapes in shape space (bottom row) which was normalized from −1 to +1. Standard deviations for each are shown in parentheses and mapped above the mean shapes. Each subject shape was then mapped to this linear representation of shape variabilities. Five subject specific shapes from three cam patients and two controls are shown with their mapping value at the appropriate location.

ately correlated with the thickness mapping ($r = 0.66$, $p < 0.001$). When comparing the PCA loading values for each significant mode of variation to the median thickness within the region of the cam lesion, a weak correlation with PCA mode 6 was identified ($r = 0.38$, adj. $p = 0.015$). No other correlations between thickness and shape statistics were found to be significant.

Median and percentile thickness values mapped onto the mean cam and control femurs showed a large region of variable thickness for the cam femur with minimal increase in thickness for the lower percentiles and clear increases in thickness for the higher percentiles (Fig. 5).

The vector between the femoral head center and the location of maximum thickness was directed more anterior and less inferior in patients compared to controls (median [interquartile range]; 46 [24]° vs. 30 [19]° anterior of lateral and 10 [25]° vs. 21 [26]° inferior of anterior; adj. $p = 0.016$, 0.039, respectively; Fig. 6). The coronal components of this vector were not significantly different between the two groups (9 [29]° vs. 11 [19]° inferior of lateral; adj. $p = 0.635$). When comparing the subgroups, similar results were seen for the male cam and control groups in the axial plane, with components of 46 (22)° versus 30 (21)° anterior of lateral (adj. $p = 0.009$). The location of maximum cortical thickness was less inferior in the sagittal plane (17 [26]° vs. 28 [17]°, adj. $p = 0.044$) in males than females in the control group. The vectors to maximum thickness for the mean cam and control shapes differed by 11° in the axial, 6° in the sagittal, and 0° in the coronal plane between the two groups, which agreed well with the differences identified based on the vectors identified on subject specific shapes.

DISCUSSION

Correspondence-based shape modeling was used to identify the region of the cam lesion based on shape variation between cam and control subjects. Cortical bone thickness in this region of the femur, as well as over the proximal surface, was significantly greater in patients with cam FAI than control subjects. The location of maximal cortical thickness was variable, but was more anterior and less inferior in patients. Cortical thickness magnitude was not significantly different between male and female control populations, but the location was less inferior in males. Similar to the population of cam and control subjects, the male cam and control groups showed significant differences in both maximum thickness and location of maximum cortical thickness in the axial plane.

The increase in thickness of cortical bone in the region of the cam lesion could be the result of hypertrophy due to a biological response to the repetitive impingement associated with deep flexion, internal rotation, and adduction.[3,14] This concept agrees with a previous study, which identified increased bone density of the subchondral bone in patients with cam FAI.[40] To understand the biomechanical and biological effect of impingement, additional focus should be placed on cortical bone thickness in the corresponding region of the acetabulum, as increased bone density has been identified in this region and hypothesized to a be a factor in osteoarthritis development.[41] Interestingly, we found that thickness of the entire proximal femur was greater in cam FAI patients. This could indicate generalized bone hypertrophy, possibly due to an adaptation of the entire femur due to altered loading at the primary impingement site.

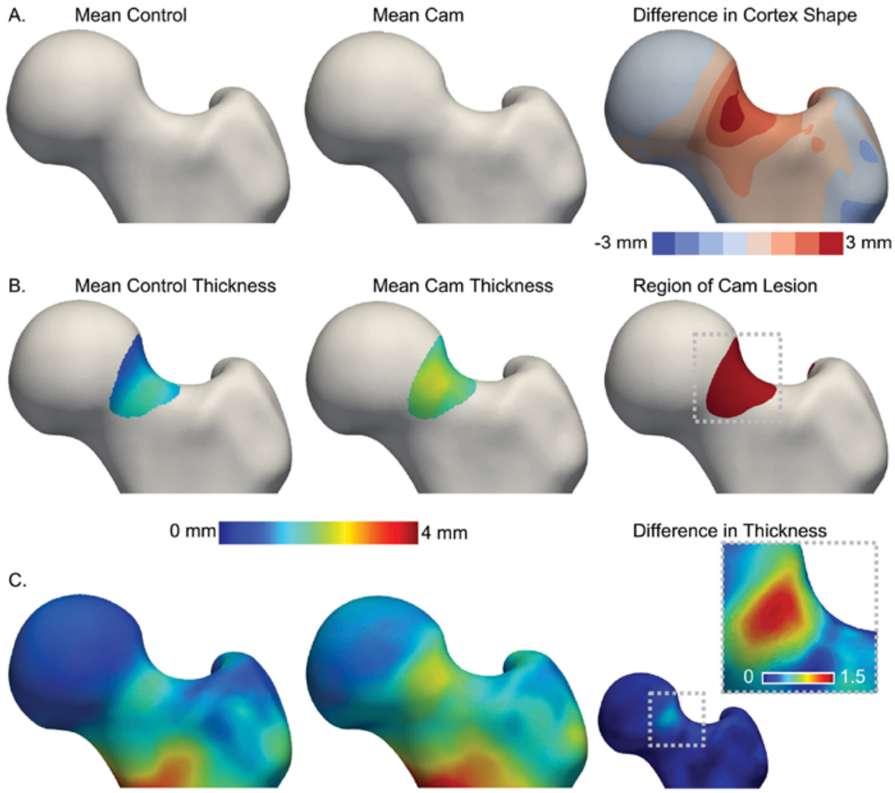

Figure 4. Anterior view of fringe plots showing differences in anatomy and mean cortical thickness for cam and control groups. (A) Mean shapes for the control (left) and cam (middle) groups shown with the shape difference mapped onto the mean control femur (right). (B) The region of the head–neck junction with greater than 1.5 mm of difference in the anatomy of the outer cortex was identified as the region of the cam lesion (right); thickness was evaluated for this region on the mean control (left) and cam (middle) shapes. (C) Mean cortical thickness of the control (left) and cam (middle) groups with the difference in mean thickness between groups (right). The greatest difference in thickness corresponded with the region of the cam lesion (right, inset). Note: The fringe plot in the inset has been re-scaled.

Results demonstrating the variability in thickness over the population could indicate that the proximal femur is stronger in cam FAI patients, due to increased cortical thickness. Specifically, for percentiles greater than the median, there was a clear increase in cortical thickness on the femoral neck near the region of the cam lesion and on the proximal medial femoral shaft. These increases in cortical thickness were much more obvious in the cam group than the control group. A small region of increased thickness could be seen on the mean control femur, although it was positioned more distally on the femoral neck than on the cam femur. This increase indicates some natural variability in cortical thickness over the femoral neck, even in the asymptomatic population. It will be important to confirm that cam femurs have increased strength due to elevated cortical thickness, as these mechanical data could help to refine guidelines pertaining to the optimal resection depth.

The general shape variations between cam FAI and control femurs agree with our prior research identifying shape variations at the head–neck junction and greater trochanter.[25] However, the content of each specific PCA mode varied. This difference in PCA modes is likely due to differences in alignment and cropping. Since the cutting planes were transformed onto each femur based on an initial optimized correspondence model, the plane location would have reduced the variability in vertical distance to the greater trochanter and any angular variations of the shaft. These variabilities may be important when evaluating shape variation of the proximal femur, but are likely not necessary in the evaluation of cortical

Table 2. Median and Interquartile Range (IQR) of Subject Specific Maximum, Median, and Mean Regional and Median Proximal Femur Thickness for All Groups and Subgroups

Entire Cohort			Subject Subgroups		
	Median [IQR]	adj. *p*		Median [IQR]	adj. *p*
Maximum regional thickness, mm					
Controls	2.30 [1.13]		Male controls	2.62 [1.20]	
			Female controls	2.24 [0.59]	0.897
Patients	3.47 [2.23]	<0.001	Male patients	3.47 [2.50]	0.002
			Female patients	2.88, 4.13	*
Mean regional thickness, mm					
Controls	1.18 [0.31]		Male controls	1.17 [0.29]	
			Female controls	1.21 [0.38]	0.866
Patients	1.71 [0.81]	<0.001	Male patients	1.71 [0.79]	<0.001
			Female patients	1.15, 1.92	*
Median regional thickness, mm					
Controls	1.13 [0.22]		Male controls	1.10 [0.19]	
			Female controls	1.13 [0.34]	0.568
Patients	1.47 [0.64]	<0.001	Male patients	1.47 [0.72]	<0.001
			Female patients	0.86, 1.63	*
Median proximal femur thickness, mm					
Controls	0.97 [0.22]		Male controls	0.94 [0.22]	
			Female controls	0.99 [0.17]	0.544
Patients	1.28 [0.30]	<0.001	Male patients	1.25 [0.29]	<0.001
			Female patients	1.77, 1.28	*

IQR indicates variation within each group. Regional thickness was evaluated within the region of the cam lesion. *p*-values shown are relative to control and male control groups for the entire cohort and subject subgroups, respectively. *No statistical comparisons were made with the female patient group due to sample size ($n = 2$).

thickness, especially for the region of the cam lesion. Further, reduced variability within the region of analysis may have helped to elucidate more subtle differences in this area.

For this study, we evaluated the cam lesion in the context of the entire proximal femur; this was done for several reasons. First and foremost, in addition to testing the hypothesis that cortical bone was thicker in the region of the cam lesion, we sought to determine if the entire proximal femur had increased cortical thickness. If we had isolated the analysis only to the region of the cam lesion, we would not have had the ability to evaluate differences over the proximal femur. Second, the region of the cam lesion represents only a small region of the femoral head and head–neck region, which is not normal anatomy. Without reference to nearby anatomy, it would be difficult to justify how any specific lesion or part of a lesion would relate to another lesion. The goal of this work was to evaluate the cam lesion and cortical thickness by virtue of their deviation from normal anatomy. Manually defining the lesions a-priori would not enable this objective quantification. In terms of technical issues, although our method to optimize the placement of

Table 3. Median and Interquartile Range (IQR) of Regional and Overall Thickness for Mean Shapes for All Groups and Subgroups

Entire Cohort	Median [IQR]	Subject Subgroups	Median [IQR]
Mean shape regional thickness, mm			
Controls	1.26 [0.48]	Male controls	1.23 [0.44]
		Female controls	1.28 [0.57]
Patients	1.91 [0.41]	Male patients	1.92 [0.44]
		Female patients	1.69 [0.95]
Mean shape overall thickness, mm			
Controls	1.02 [0.49]	Male controls	1.01 [0.49]
		Female controls	1.04 [0.49]
Patients	1.33 [0.52]	Male patients	1.32 [0.52]
		Female patients	1.52 [0.78]

IQR indicates the variation in mean thickness for each mean shape. Regional thickness was evaluated within the region of the cam lesion. *p*-values shown are relative to control and male control groups for the entire cohort and subject subgroups, respectively.

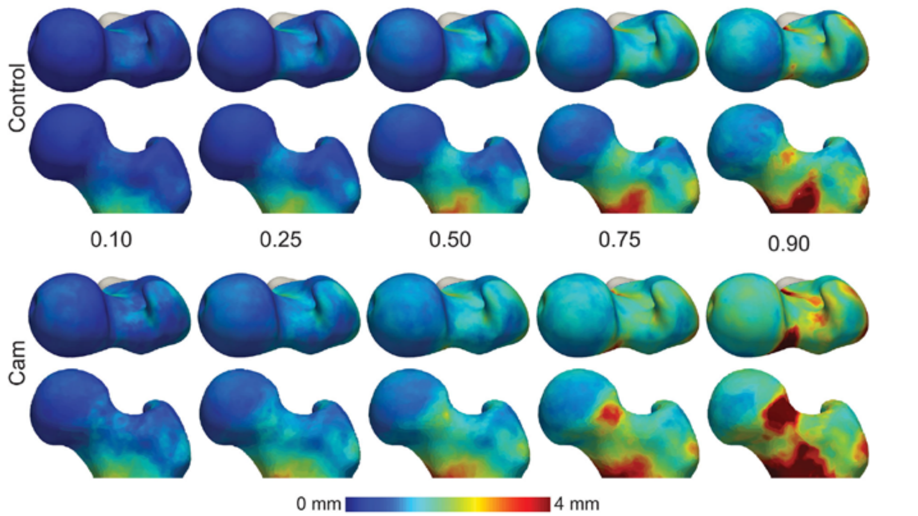

Figure 5. Percentile thickness representing the 10th, 25th, 50th, 75th, and 90th percentile of thickness for each of the vertices on the mean control (top) and cam (bottom) femur (median thickness is the 50th percentile). Increased cortical thickness was evident overall and in the region of the cam lesion on the mean cam femur.

correspondence particles is automatic, it does require unique anatomical features to ensure that correspondence particles are positioned across samples in the same relative anatomic position. Thus, it would be difficult to estimate correspondences on these isolated patches without the benefit of reference to nearby anatomy.

Each PCA mode is an objective measure that considers the entire shape space; it does not directly measure any single aspect of the anatomy that is clinically relevant, such as the shape of the head–neck junction. Since PCA was performed based on the entire proximal femur, it is important to note that each PCA mode described some aspect of shape variation of the proximal femur, but none were specific to the region of the cam lesion. Accordingly, it should not be surprising that PCA loading values were not strongly correlated with regional thickness metrics or the mapping of thickness between the mean cam and control shapes. While a strong correlation between thickness and a specific mode of variation would have identified shape variations, which could be used to identify increased cortical thickness clinically, a lack of correlation does not signify that shape and thickness are not related; cortical thickness in the region of the cam lesion was clearly increased in cam patients compared to controls.

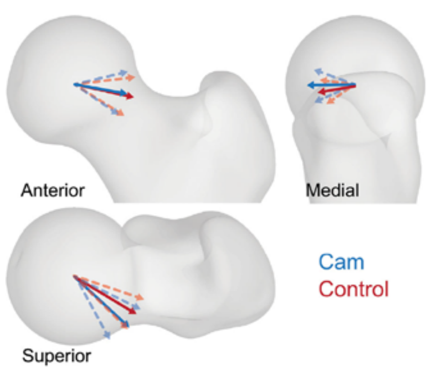

Figure 6. Vectorial representation of the location of maximum cortical bone thickness plotted relative to the mean shape of the control group. Solid vectors represent mean location for the cam (blue) and control (red) groups. Dashed vectors represent one standard deviation of angular variation in each view.

Previous studies have identified gender differences in the presentation of FAI including variations in radiographic measurements and intraoperative pathology,[42] which motivate analysis of cortical thickness specific to gender. The cam group only included two female subjects, and thus, statistically meaningful comparisons could not be made directly for female cam shapes. Our recruitment of control subjects was also imbalanced to include more males than females, with only 16 females compared to 29 males, since cam FAI is predominantly seen in males.[42] It is possible that with a larger number of female control subjects and better sampling of the population, differences in cortical thickness due to gender would be more evident. However, based on the data available, the gender differences in cortical thickness are of smaller magnitude than differences between the cam and control group. Thus, similar increases in cortical thickness could be expected in females with cam-type FAI.

The location of maximum thickness within the region of the cam lesion was variable across the populations. Most of the variation between groups could be captured in the axial plane with the location of maximum cortical thickness more anterior and less lateral in patients with cam FAI. A more anterior location of maximum cortical thickness could indicate bone hypertrophy caused by repetitive abutment during hip flexion and internal rotation.[4] Within the cam group the variation in each anatomic plane was high. This variability signifies the difficulty in generalizing the cam lesion across patients with cam FAI and justifies subject specific surgical planning.

Improved accuracy in the generation of volumetric distance transforms from surface data facilitates future biological and biomechanical studies where surface meshes are commonly used. The inclusion of reflection and alignment tools herein provided efficient and automated preprocessing to reduce manual time requirements in generation of the correspondence model. The automatic transformation of cutting planes could be extended to analysis of larger populations where a particular anatomical location is of primary interest. Advancements in warping techniques, which incorporate the correspondence model and original distance transforms, allow for direct vertex-to-vertex comparisons between both subject and mean shapes. Additionally, the incorporation of scalar attributes in shape analysis could be adapted to other applications. For this study, a scalar value was used to represent cortical bone thickness, but future studies could use this technique to evaluate other attributes that accompany shape, such as bone densities from CT data or stresses from finite element analysis.

While we did not find strong correlative relationships between shape and cortical bone thickness, it is clinically important to understand that cortical bone thickness is increased proximally and in the region of the cam lesion for patients with cam FAI. Previous studies evaluating resection depth have not taken into account possible variations in cortical thickness for patients with cam FAI.[11–13] Additional research is required to establish parameters of the resection to prevent both under-resection and iatrogenic femoral neck fractures that are specific to the anatomical characteristics in patients with cam FAI.[10]

AUTHORS' CONTRIBUTIONS

PRA processed data, conducted the study, and drafted the manuscript. SE and PA implemented the software to complete the study and reviewed the results for accuracy. MH collected and processed the original data and interpreted study results. RW, JW, and CP contributed to the design of the study, assisted with clinical interpretation, and reviewed the results for accuracy. AA designed the study, supervised the study, reviewed the results for accuracy, and assisted with clinical interpretation. All authors provided revisions and final approval of the manuscript.

ACKNOWLEDGMENTS

The research content herein is solely the responsibility of the authors and does not necessarily represent the official views of the National Institutes of Health. The authors also acknowledge Trevor Hafer and Tyler Skinner.

REFERENCES

1. Murphy LB, Helmick CG, Schwartz TA, et al. 2010. One in four people may develop symptomatic hip osteoarthritis in his or her lifetime. Osteoarthritis Cartilage 18:1372–1379.
2. Beck M, Kalhor M, Leunig M, et al. 2005. Hip morphology influences the pattern of damage to the acetabular cartilage femoroacetabular impingement as a cause of early osteoarthritis of the hip. J Bone Joint Surg Br 87:1012–1018.
3. Ganz R, Leunig M, Leunig-Ganz K, et al. 2008. The etiology of osteoarthritis of the hip. Clin Orthop Relat Res 466:264–272.
4. Ganz R, Parvizi J, Beck M, et al. 2003. Femoroacetabular impingement: a cause for osteoarthritis of the hip. Clin Orthop Relat Res 417:112–120.
5. Wagner S, Hofstetter W, Chiquet M, et al. 2003. Early osteoarthritic changes of human femoral head cartilage subsequent to femoro-acetabular impingement. Osteoarthritis Cartilage 11:508–518.
6. Kapron AL, Anderson AE, Peters CL, et al. 2012. Hip internal rotation is correlated to radiographic findings of cam femoroacetabular impingement in collegiate football players. Arthroscopy 28:1661–1670.
7. Kapron AL, Aoki SK, Peters CL, et al. 2014. Subject-specific patterns of femur-labrum contact are complex and vary in asymptomatic hips and hips with femoroacetabular impingement. Clin Orthop Relat Res 472:3912–3922.
8. Kapron AL, Aoki SK, Peters CL, et al. 2015. In-vivo hip arthrokinematics during supine clinical exams: application to the study of femoroacetabular impingement. J Biomech 48:2879–2886.
9. Philippon MJ, Schenker ML, Briggs KK, et al. 2007. Revision hip arthroscopy. Am J Sports Med 35:1918–1921.
10. Ayeni OR, Bedi A, Lorich DG, et al. 2011. Femoral neck fracture after arthroscopic management of femoroacetabular impingement: a case report. J Bone Joint Surg Am 93:e47.
11. Mardones RM, Gonzalez C, Chen Q, et al. 2005. Surgical treatment of femoroacetabular impingement: evaluation of the effect of the size of the resection. J Bone Joint Surg Am 87:273–279.
12. Rothenfluh E, Zingg P, Dora C, et al. 2012. Influence of resection geometry on fracture risk in the treatment of femoroacetabular impingement: a finite element study. Am J Sports Med 40:2002–2008.
13. Wijdicks CA, Balldin BC, Jansson KS, et al. 2013. Cam lesion femoral osteoplasty: in vitro biomechanical evaluation of iatrogenic femoral cortical notching and risk of neck fracture. Arthroscopy 29:1608–1614.
14. Robling AG, Castillo AB, Turner CH. 2006. Biomechanical and molecular regulation of bone remodeling. Annu Rev Biomed Eng 8:455–498.
15. Holzer G, von Skrbensky G, Holzer LA, et al. 2009. Hip fractures and the contribution of cortical versus trabecular bone to femoral neck strength. J Bone Miner Res 24:468–474.
16. Ito K, Minka-II M-A, Leunig M, et al. 2001. Femoroacetabular impingement and the cam-effect a MRI-based quantitative anatomical study of the femoral head-neck offset. J Bone Joint Surg Br 83:171–176.

17. Sutter R, Zanetti M, Pfirrmann CW. 2012. New developments in hip imaging. Radiology 264:651–667.
18. Tannast M, Siebenrock KA, Anderson SE. 2007. Femoroacetabular impingement: radiographic diagnosis—what the radiologist should know. Am J Roentgenol 188:1540–1552.
19. Hack K, Di Primio G, Rakhra K, et al. 2010. Prevalence of cam-type femoroacetabular impingement morphology in asymptomatic volunteers. J Bone Joint Surg Am 92:2436–2444.
20. Kapron AL, Anderson AE, Aoki SK, et al. 2011. Radiographic prevalence of femoroacetabular impingement in collegiate football players: aAOS exhibit selection. J Bone Joint Surg Am 93:e111.
21. Anderson AE, Ellis BJ, Maas SA, et al. 2010. Effects of idealized joint geometry on finite element predictions of cartilage contact stresses in the hip. J Biomech 43:1351–1357.
22. Menschik F. 1997. The hip joint as a conchoid shape. J Biomech 30:971–973.
23. Meyer DC, Beck M, Ellis T, et al. 2006. Comparison of six radiographic projections to assess femoral head/neck asphericity. Clin Orthop Relat Res 445:181–185.
24. Dudda M, Albers C, Mamisch TC, et al. 2009. Do normal radiographs exclude asphericity of the femoral head-neck junction? Clin Orthop Relat Res 467:651–659.
25. Harris MD, Datar M, Whitaker RT, et al. 2013. Statistical shape modeling of cam femoroacetabular impingement. J Orthop Res 31:1620–1626.
26. Harris MD, Kapron AL, Peters CL, et al. 2014. Correlations between the alpha angle and femoral head asphericity: implications and recommendations for the diagnosis of cam femoroacetabular impingement. Eur J Radiol 83:788–796.
27. Clohisy JC, Nunley RM, Otto RJ, et al. 2007. The frog-leg lateral radiograph accurately visualized hip cam impingement abnormalities. Clin Orthop Relat Res 462:115–121.
28. Sutter R, Dietrich TJ, Zingg PO, et al. 2012. How useful is the alpha angle for discriminating between symptomatic patients with cam-type femoroacetabular impingement and asymptomatic volunteers? Radiology 264:514–521.
29. Anderson AE, Peters CL, Tuttle BD, et al. 2005. Subject-specific finite element model of the pelvis: development, validation and sensitivity studies. J Biomech Eng 127:364–373.
30. Schroeder W, Martin K, Lorensen B, editors. 2006. The visualization toolkit, 4th ed. Cliford Park, NY, USA: Kitware.
31. Maas SA, Ellis BJ, Ateshian GA, et al. 2012. FEBio: finite elements for biomechanics. J Biomech Eng 134:011005.
32. Besl PJ, McKay HD. 1992. A method for registration of 3-D shapes. IEEE Trans Pattern Anal Mach Intell 14:239–256.
33. Cates J, Fletcher PT, Styner M, et al. 2007. Shape modeling and analysis with entropy-based particle systems. Inf Process Med Imaging 20:333–345.
34. Sorkine O, Cohen-Or D, Lipman Y, et al. 2004. Laplacian surface editing. Proceedings of the 2004 Eurographics/ACM SIGGRAPH symposium on geometry processing. Nice, France: ACM. p 175–184.
35. Valette S, Chassery JM, Prost R. 2008. Generic remeshing of 3D triangular meshes with metric-dependent discrete Voronoi diagrams. IEEE Trans Vis Comput Graph 14:369–381.
36. Zhu S-X. 2012. Compactly supported radial basis functions: how and why? Technical report. Oxford, England: The Mathematical Institute, University of Oxford.
37. RCoreTeam. 2014. R: a language and environment for statistical computing. Vienna, Austria: R Foundation for Statistical Computing.
38. Horn JL. A rationale and test for the number of factors in factor analysis. Psychometrika 30:179–185.
39. Finner H. 1993. On a monotonicity problem in step-down multiple test procedures. J Am Statist Assoc 88:920–923.
40. Speirs AD, Beaule PE, Rakhra KS, et al. 2013. Bone density is higher in cam-type femoroacetabular impingement deformities compared to normal subchondral bone. Osteoarthritis Cartilage 21:1068–1073.
41. Speirs A, Beaulé P, Rakhra K, et al. 2013. Increased acetabular subchondral bone density is associated with cam-type femoroacetabular impingement. Osteoarthritis Cartilage 21:551–558.
42. Nepple JJ, Riggs CN, Ross JR, et al. 2014. Clinical presentation and disease characteristics of femoroacetabular impingement are sex-dependent. J Bone Joint Surg Am 96:1683–1689.

CHAPTER 5

DOES REMOVAL OF SUBCHONDRAL CORTICAL BONE PROVIDE SUFFICIENT RESECTION DEPTH FOR TREATMENT OF CAM FEMOROACETABULAR IMPINGEMENT?

Reprinted with permission from Atkins PR, Aoki SK, Whitaker RT, Weiss JA, Peters CL, Anderson AE. *Clin Orthop Relat Res*. 2017; 475(8):1977-1986.

Clin Orthop Relat Res (2017) 475:1977–1986
DOI 10.1007/s11999-017-5326-5

Clinical Orthopaedics and Related Research®
A Publication of The Association of Bone and Joint Surgeons®

CrossMark

BASIC RESEARCH

Does Removal of Subchondral Cortical Bone Provide Sufficient Resection Depth for Treatment of Cam Femoroacetabular Impingement?

Penny R. Atkins BS, Stephen K. Aoki MD, Ross T. Whitaker PhD, Jeffrey A. Weiss PhD, Christopher L. Peters MD, Andrew E. Anderson PhD

Received: 25 October 2016 / Accepted: 16 March 2017 / Published online: 24 March 2017

Abstract

Background Residual impingement resulting from insufficient resection of bone during the index femoroplasty is the most-common reason for revision surgery in patients with cam-type femoroacetabular impingement (FAI). Development of surgical resection guidelines therefore could reduce the number of patients with persistent pain and reduced ROM after femoroplasty.

Questions/purposes We asked whether removal of subchondral cortical bone in the region of the lesion in patients with cam FAI could restore femoral anatomy to that of screened control subjects. To evaluate this, we analyzed shape models between: (1) native cam and screened control femurs to observe the location of the cam lesion and establish baseline shape differences between groups, and (2) cam femurs with simulated resections and screened

The institution of one or more of the authors (PRA, SKA, RTW, JAW, CLP, AEA) has received, during the study period, funding from the National Institutes of Health (R01-EB016701, P41-GM103545, R01-GM083925, R21-AR063844), and the LS-Peery Discovery Program in Musculoskeletal Research.
One of the authors certifies that he (SKA), or a member of his immediate family, has or may receive payments or benefits, during the study period, an amount of USD 10,000-USD 100,000, from Stryker Medical (Kalamazoo, MI, USA).
One of the authors certifies that he (CLP), or a member of his immediate family, has or may receive payments or benefits, during the study period, an amount of USD 100,001-USD 1,000,000, from Zimmer Biomet (Warsaw, IN, USA), and an amount of less than USD 10,000, from Conextions Medical (Salt Lake City, UT, USA).
All ICMJE Conflict of Interest Forms for authors and *Clinical Orthopaedics and Related Research*® editors and board members are on file with the publication and can be viewed on request.
Clinical Orthopaedics and Related Research® neither advocates nor endorses the use of any treatment, drug, or device. Readers are encouraged to always seek additional information, including FDA-approval status, of any drug or device prior to clinical use.
Each author certifies that his or her institution approved the human protocol for this investigation, that all investigations were conducted in conformity with ethical principles of research, and that informed consent for participation in the study was obtained.

P. R. Atkins, S. K. Aoki, J. A. Weiss, C. L. Peters,
A. E. Anderson (✉)
Department of Orthopaedics, University of Utah, 590 Wakara Way, Room A100, Salt Lake City, UT 84108, USA
e-mail: Andrew.Anderson@hsc.utah.edu

P. R. Atkins, R. T. Whitaker, J. A. Weiss, C. L. Peters,
A. E. Anderson
Department of Bioengineering, University of Utah, Salt Lake City, UT, USA

R. T. Whitaker, J. A. Weiss, A. E. Anderson
Scientific Computing and Imaging Institute, University of Utah, Salt Lake City, UT, USA

R. T. Whitaker, J. A. Weiss
School of Computing, University of Utah, Salt Lake City, UT, USA

A. E. Anderson
Department of Physical Therapy, University of Utah, Salt Lake City, UT, USA

control femurs to evaluate the sufficiency of subchondral cortical bone thickness to guide resection depth.

Methods Three-dimensional (3-D) reconstructions of the inner and outer cortical bone boundaries of the proximal femur were generated by segmenting CT images from 45 control subjects (29 males; 15 living subjects, 30 cadavers) with normal radiographic findings and 28 nonconsecutive patients (26 males) with a diagnosis of cam FAI based on radiographic measurements and clinical examinations. Correspondence particles were placed on each femur and statistical shape modeling (SSM) was used to create mean shapes for each cohort. The geometric difference between the mean shape of the patients with cam FAI and that of the screened controls was used to define a consistent region representing the cam lesion. Subchondral cortical bone in this region was removed from the 3-D reconstructions of each cam femur to create a simulated resection. SSM was repeated to determine if the resection produced femoral anatomy that better resembled that of control subjects. Correspondence particle locations were used to generate mean femur shapes and evaluate shape differences using principal component analysis.

Results In the region of the cam lesion, the median distance between the mean native cam and control femurs was 1.8 mm (range, 1.0–2.7 mm). This difference was reduced to 0.2 mm (range, −0.2 to 0.9 mm) after resection, with some areas of overresection anteriorly and underresection superiorly. In the region of resection for each subject, the distance from each correspondence particle to the mean control shape was greater for the cam femurs than the screened control femurs (1.8 mm, [range, 1.1–2.9 mm] and 0.0 mm [range, −0.2–0.1 mm], respectively; $p < 0.031$). After resection, the distance was not different between the resected cam and control femurs (0.3 mm; range, −0.2–1.0; $p > 0.473$).

Conclusions Removal of subchondral cortical bone in the region of resection reduced the deviation between the mean resected cam and control femurs to within a millimeter, which resulted in no difference in shape between patients with cam FAI and control subjects. Collectively, our results support the use of the subchondral cortical-cancellous bone margin as a visual intraoperative guide to limit resection depth in the correction of cam FAI.

Clinical Relevance Use of the subchondral cortical-cancellous bone boundary may provide a method to guide the depth of resection during arthroscopic surgery, which can be observed intraoperatively without advanced tooling, or imaging.

Introduction

One challenging aspect of hip arthroscopy is properly contouring the lesion in patients with cam femoroacetabular impingement (FAI) [25]. One of the most-common reasons for revision arthroscopy is underresection (68%–90% of revision arthroscopy procedures) [2, 23]. Although less common, overresection also has been noted as a cause of iatrogenic femoral neck fracture, loss of the normal joint suction seal, or loss of congruency (0.05%–1.9% of arthroscopies) [9, 10, 30]. Careful assessment of the resection during surgery may minimize complications. Intraoperatively, fluoroscopy attempts to recreate clinical radiographic views that show the area of the cam lesion before, during, and after resection [4, 16, 17, 27]. Arthroscopic views provide qualitative assessment, including confirmation that ROM is improved by the resection [21, 27]. However, there is no standard approach to evaluate arthroscopic images to determine the extent to which the resection has normalized femoral anatomy.

Experimental and computational techniques have been used to develop resection depth guidelines [18, 19, 24, 29]. For example, an experimental cadaver study showed that resections less than 30% of femoral head-neck diameter were safe in terms of avoiding fracture [19]. The primary limitation to that study and similar research in this area is that guidelines were based on results from cadaveric femurs from a normal population or generalized models of anatomy [24, 29]. A more-recent study used an ovine model of cam FAI and found that resections of up to 9 mm reduced the failure load by nearly 20%, but even the bones that underwent the largest resections failed at loads higher than those expected during daily activities [18]. Bone density and cortical thickness are elevated in the region of the cam lesion in patients with FAI, which suggests that the femoral neck in cam FAI femurs is stronger compared with that in control subjects [1, 26].

We have found that the margin between subchondral cortical bone and underlying cancellous bone, as observed radiographically and arthroscopically, provides a straightforward method to guide the depth of the resection during femoroplasty (Fig. 1). However, the extent to which a resection based on this boundary improves proximal femoral anatomy in patients with cam FAI has not been quantified. A major impediment to evaluation of the efficacy of this or any resection guideline is the difficulty in quantifying the baseline anatomic shape of the normal hip. Statistical shape modeling (SSM) offers the ability to objectively assess true, three-dimensional (3-D) anatomic variation across a population or between selected groups [3, 11]. By analyzing 3-D reconstructions generated from volumetric medical images, SSM reduces the bias and subjectivity that may occur when quantifying femoral anatomy using radiographs or single image slices of volumetric data.

Using 3-D CT reconstructions and SSM, we asked whether removal of subchondral cortical bone in the region

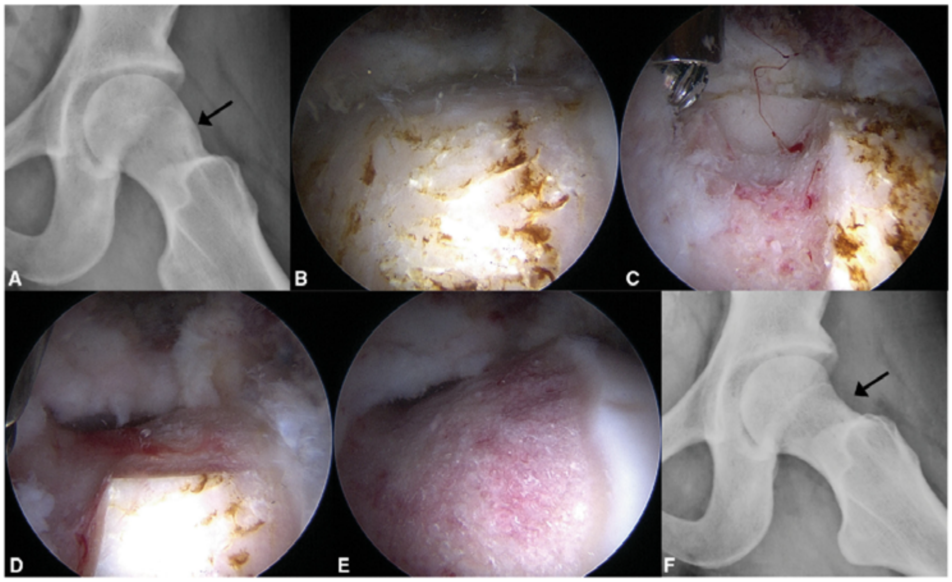

Fig. 1A–F A female patient with cam FAI was treated with femoroplasty using the sclerotic subchondral cortical bone thickness as a guide for resection depth. **(A)** Her preoperative frog-leg lateral radiograph shows the sclerotic region of the cam lesion (arrow). Intraoperative arthroscopic views from a 70° scope through the anterolateral portal show **(B)** the sclerotic region, **(C)** the initial resection trough where the depth was based on the sclerotic subchondral cortical bone thickness, **(D)** continuation of the resection based on trough depth and patient anatomy, and **(E)** the completed resection. **(F)** The patient's postoperative frog-leg lateral radiograph shows where the sclerotic region has been removed (arrow).

of the lesion in patients with cam FAI could restore femoral anatomy to that of screened control subjects. To evaluate this, we analyzed shape models for: (1) native cam and screened control femurs to observe the location of the cam lesion and establish baseline shape differences between groups, and (2) cam femurs with simulated resections and screened control femurs to evaluate the sufficiency of subchondral cortical bone thickness to guide resection depth. We hypothesized that resection of subchondral cortical bone in the region of the cam lesion would yield femoral anatomy that was not different from that of control femurs.

Patients and Methods

Two groups were defined for this study: screened controls and patients with symptomatic cam FAI. All subjects had been part of a previous SSM study [1] and were selected based on diagnosis and imaging availability from a cohort recruited for previous institutional review board-approved studies between 2005 and 2012; living subjects and cadavers were considered for the control cohort. Patients with cam FAI (n = 28) represented a convenience sample of nonconsecutive patients recruited solely for research purposes between February 2005 and January 2009 (n = 15) and January 2011 and January 2012 (n = 13). All patients had positive radiographic and clinical examination findings, including restricted ROM and pain elicited by the impingement examination, as assessed by an orthopaedic surgeon (CLP) with more than 15 years of experience treating FAI. Living subjects and cadavers were recruited for the control group to increase sample size. Living controls (n = 20) were recruited via word-of-mouth for a study conducted between April 2008 and July 2010; cadavers (n = 59) had undergone previous imaging for basic science studies. All potential controls (ie, living subjects and cadavers) were screened for radiographic evidence of cam FAI, using a digitally reconstructed radiograph of the frog-leg lateral position generated from CT images (see below) [12]. The α angle was measured by a member of the study team with 10 years of medical imaging experience (AEA).

Table 1. Summary of subject cohort demographics presented as median (range)

Cohort	Male/female	Age (years)	Weight (kg)	BMI (kg/m^2)
Patients with cam FAI (n = 28)	26/2	23 (16–47)	81 (52–107)	25 (19–33)
Screened controls (n = 45)	29/16	28 (15–55)	81 (49–117)	24 (16–39)
p Value		0.152	0.496	0.901

FAI femoroacetabular impingement.

Femurs with an α angle greater than 60° were excluded (n = 34) [5], leaving 45 screened controls (n = 15 living subjects, n = 30 cadavers). Demographics (ie, age, weight, and BMI) did not differ between patients with cam FAI and controls (Table 1).

CT images of the proximal femur of all subjects were acquired using a SOMATOM Definition® 128 CT scanner (Siemens AG, Munich, Germany) (15 control subjects, 15 patients with cam FAI), HiSpeed® CTi Single Slice Helical CT scanner (GE Healthcare, Chicago, IL, USA) (30 control cadaver femurs), or LightSpeed® VCT® scanner (GE Healthcare) (13 patients with cam FAI). Images were acquired at 100 to 120 kVp, 512 × 512 acquisition matrix, 0.625 to 1.0 mm slice thickness, 0.9 to 1.0 pitch, and 100 to 200 mAs with variable fields of view. Three-dimensional CT images were used to segment and reconstruct surfaces of the inner and outer cortex of the proximal femur (Fig. 2A) [1, 11].

The cam lesion was identified by first performing shape analysis between the native cam and control femurs (Fig. 2B), as described previously [1]. Correspondence particles, which serve as the basis to determine shape variation, were placed on the outer femoral cortex of the 28 cam FAI and 45 control femurs. Next, mean shapes were generated to represent the proximal femur of native cam and control subject populations. These mean shapes served as the basis for identification of the region of resection, specifically the distance between the mean surfaces was calculated to identify the difference in outer topology of the mean femurs between the native cam and control populations (Fig. 2C, left). The region of simulated resection then was defined as the region of the femoral head-neck junction where the outer topology of the mean native cam femur varied from that of the mean control femur by greater than 1 mm (Fig. 2C). Use of this 1-mm threshold on the mean cam shape provided a region that was thought to be an appropriate representation of the cam lesion, as assessed by a hip arthroscopist with 9 years of experience treating FAI (SKA). This region covered the femoral head-neck junction well, but limited the resection such that it did not extend past the junction between the neck and greater trochanter. To simulate a resection on each femur surface, the region identified on the mean cam shape was then mapped back onto each of the cam femur surfaces. In this region, the surface of the outer cortex was projected onto the surface of the inner cortex in MATLAB® Version 7.10 (MathWorks, Natick, MA, USA) (Fig. 2D, right). The simulated resections were smoothed locally to remove edge effects using 3-matic Version 10.0 (Materialise, Leuven, Belgium).

The extent (ie, areal coverage) of the resection was described using a set of angles from the center of the femoral head relative to each of the three anatomic axes. This was accomplished by mapping the areal coverage of the region of resection onto each of the three anatomic planes of the femur in MATLAB®. Resection volume and surface area then were quantified in 3-matic.

SSM for the analysis of shape variation after the simulated resection followed a similar protocol as that described previously for native femurs [1]. First, correspondence particles were placed for the entire population, including the native cam, resected cam, and control femurs (Fig. 2E), and used to generate mean shapes for each of these groups. From this analysis, the difference in shape between the mean native cam and resected cam shapes and the mean control shape was measured by calculating the distance between surfaces. Although SSM used input shapes from three separate groups, only two groups were evaluated simultaneously such that either native cam or resected cam populations were compared with the control population (Fig. 2F). To ensure the optimization of correspondence particles across shapes and consistent interpretation of shape variation, the native cam, resected cam, and screened control femurs were all included in this second analysis.

The spatial locations of correspondence particles can be used to describe the shape of each femur and the shape variation across a population, overall and specific to any region of interest. In the region of resection of each subject, the spatial location of each correspondence particle was compared with that of the same correspondence particle on the mean control shape. The distances were evaluated for each correspondence particle to identify shape variability over the region between cohorts.

Principal component analysis (PCA) was conducted on the correspondence particle locations from SSM to determine shape variation associated with cam FAI and to evaluate the sufficiency of resection. PCA provides a method to reduce high-dimensional data (ie,

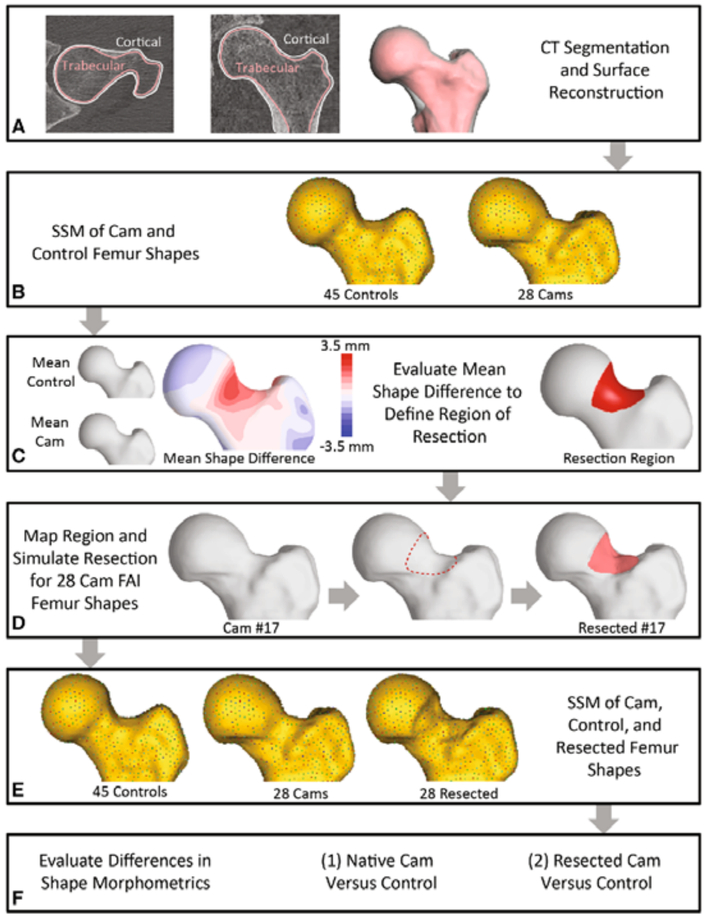

Fig. 2A–F The flowchart is shown for the computational protocol, which used statistical shape modeling (SSM) to objectively evaluate whether resection of the subchondral bone of the cam lesion restored anatomy to that of a screened control population. **(A)** Three-dimensional (3-D) models of the inner and outer cortex were created from CT images. **(B)** Correspondence particles were placed on the 3-D surfaces of each subject. **(C)** The morphologic difference in the mean cam and mean control shape was identified by SSM; this difference established the region where subchondral bone should be removed. **(D)** This region then was applied to 3-D models of each patient with cam femoroacetabular impingement (FAI) to generate a simulated resection. **(E)** SSM was again applied to control subject femurs, native cam femurs, and resected cam femurs. **(F)** Shape variation was determined through comparison of correspondence particles and mean shapes of the native cam and resected cam femurs with the control femurs.

correspondence particle locations) into fewer modes of variation, which best describe the variance in the data set. The results of PCA indicate modes of shape variation equal to the number of input shapes, with the first mode capturing the largest variance and each subsequent mode capturing less of the population variance than the previous mode. From PCA, each shape was represented by loading values for each of the modes describing shape variation (eg, similar to how a cylinder can be described using values of height and radius). Herein, PCA loading values were statistically evaluated to determine modes of variation which represented distinct shape variation between the native cam or resected cam and control groups.

Subject demographics, descriptive data regarding the resection (ie, depth and size), and distances between subject and mean correspondence particles in the region of resection were evaluated for normality using Shapiro's rank-sum test. Group differences of these metrics were evaluated using a Wilcoxon rank-sum test or Student's t-test based on the results of the normality evaluation. The nonspurious modes of variation from PCA were determined by analysis against random noise using a technique termed parallel analysis [8]. From these, overall group differences were evaluated using Hotelling's T-squared test [14], which is a multivariate generalization of Student's t-test that provides an overall analysis of group differences from the PCA loading values. Student's t-test then was used to determine the modes of variation that included distinct shape variations between groups. Significance was set at a probability less than 0.05 for all tests and Finner's method was used to control for multiple comparisons [7]. It was not possible to evaluate differences between mean shapes using statistical tests, as a single mean shape represents each cohort. Accordingly, the surface distance between the two mean shapes (ie, native cam to control, resected cam to control) was quantified and plotted using a color map. For consistency, all data were presented as median (range). All statistical analyses were completed using R© Version 3.1.2 (R Foundation for Statistical Computing, Vienna, Austria) [22].

Results

Morphometrics of Native Cam Femurs

Before resection, the mean group shape for the native cam femur was 1.8 (range, 1.0–2.7) mm larger (Fig. 3) in the region identified for simulated resection (Fig. 2C). This region extended from $-1°$ to 70° from lateral to anterolateral in the axial plane (Fig. 4A), 57° to 149° from superolateral to inferolateral in the coronal plane (Fig. 4B), and $-1°$ to 136° from superior to anteroinferior in the sagittal plane (Fig. 4C) on the mean cam shape. In addition to the shape variation over the head-neck junction, the shape difference between the mean native cam and mean control femurs showed variation over the entire proximal femur (Fig. 3). Qualitatively, the medial border of the femoral head did not extend as far medially in patients with cam FAI and the shape of the proximal greater trochanter had more curvature medially in the axial plane, which is consistent with a previous analysis [11].

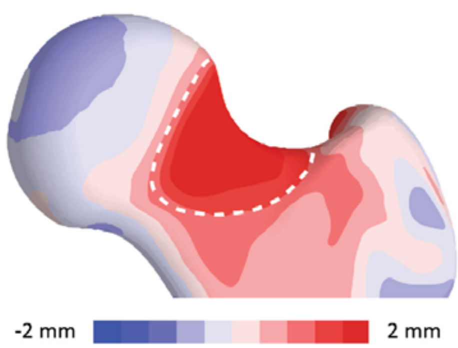

Fig. 3 An anterior view is shown of the quantitative comparison between the mean control shape and the mean native cam shape. The surface distance was mapped on the mean control shape. The shape variation over the surface to be resected, outlined with a dashed white line, had a maximum deviation between shapes of 2.7 mm.

The first 10 PCA modes included 87% of the overall shape variation and were found to be nonspurious from parallel analysis. Together, the loading values from these 10 modes identified differences in overall shape between the native cam and control populations as determined from Hotelling's T-squared test ($p < 0.001$). Of these 10 modes, four (Modes 1, 5, 6, and 8) described distinct shape differences between the two populations as identified by the results of the Student's t-test comparing loading values between groups ($p = 0.024$, 0.021, 0.023, and < 0.001, respectively) (Fig. 5). These modes accounted for 31.3%, 4.8%, 3.9%, and 2.4% of the overall shape variation, respectively. Qualitatively, Mode 1 described overall variation in AP and mediolateral widths, Modes 5 and 6 described variations in the anterosuperior head-neck junction and height and curvature changes of the greater trochanter, and Mode 8 described variations of the posterior greater trochanter and mediolateral width of the femoral head.

In the region of the identified cam lesion of each subject, the distance between each correspondence particle and the same mean control shape correspondence particle was greater for the cohort of native cam femurs than for the cohort of control femurs of the mean distance for each correspondence particle (median, 1.8 mm [range, 1.1–2.9

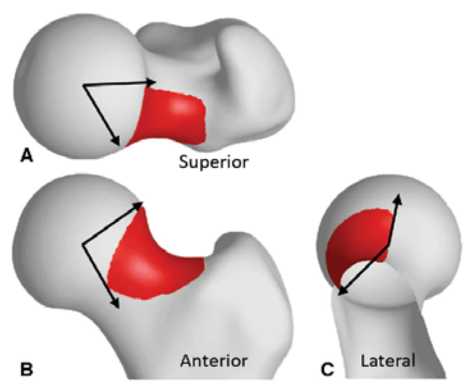

Fig. 4A–C The region of resection shown on the mean native cam shape was determined based on overall shape variation between patients with cam FAI and screened control subjects. The region was located primarily in the anterolateral head-neck junction, spanning 71°, 93°, and 138° in the **(A)** axial, **(B)** coronal, and **(C)** sagittal planes, respectively. The angle was measured clockwise from lateral in the superior view and from superior in the anterior and lateral views. The greater trochanter has been removed in the sagittal view to better observe the extent of the resection.

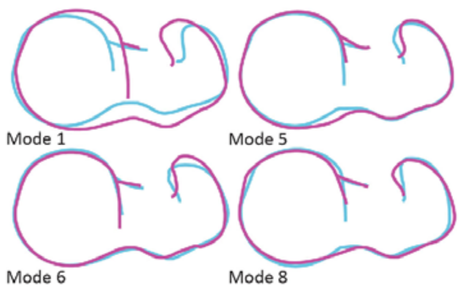

Fig. 5 Outlines of the two-dimensional projections of the femur surfaces from a superior view represent the variation associated with plus (magenta) and minus (blue) two SDs of the four principal component analysis modes which represent shape differences between the native cam and control populations.

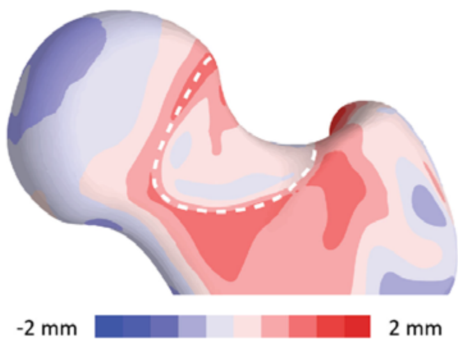

Fig. 6 An anterior view is shown of the quantitative comparison between the mean control shape and the resected cam shape. The surface distance was mapped on the mean control shape. The shape variation over the surface of resection, outlined with a dashed white line, showed 0.9 mm underresection superiorly and 0.2 mm overresection anteriorly.

mm] versus 0.0 mm [range, −0.2 to 0.1 mm], $p < 0.031$). Although, the difference in correspondence particle distances was expected, it provided statistical evidence that there was a lesion present in the hips with symptomatic cam FAI.

Morphometrics of Resected Cam Femurs

For the simulated resection on the cohort of cam femurs, removal of subchondral cortical bone in the region of the cam lesion resulted in maximum resection depths with a median of 3.5 mm (range, 1.8–7.7 mm), resected volumes of 1552 mm^3 (range, 881–3348 mm^3), and resected surface areas of 1034 mm^2 (range, 686–1246 mm^2). After resection, the difference between the mean resected cam shape and the mean control shape was reduced to 0.2 mm (range, −0.2–0.9 mm) in the region of resection. Analysis of the mean resected cam and control shapes indicated the maximum overresection occurred anteriorly and the maximum underresection superiorly (Fig. 6).

The first 10 PCA modes, which included 87% of the overall shape variation, were found to be nonspurious and together identified differences in overall shape between the resected cam and control populations ($p < 0.001$). Of these 10 modes, only one (Mode 8) described a distinct shape difference between the two populations ($p = 0.004$) and accounted for 2.3% of the overall shape variation. The variation captured in Mode 8 was similar to Mode 8 described between the native cam and control femurs (Fig. 5).

In the region of the resection, distances to the set of mean control correspondence particle locations were not different between the resected cam femurs and the control femurs (median, 0.3 mm [range, −0.2–1.0 mm] versus 0.0 mm [range, −0.2 to 0.1 mm], $p > 0.473$). This lack of difference indicated that resection of subchondral cortical bone resulted in anatomy similar to that of control subjects in the region of resection.

Discussion

In the treatment of cam FAI, overresection of a cam lesion may predispose the hip to femoral neck fracture or loss of the normal hip suction seal, while underresection is associated with persistent impingement-related symptoms. Assessment of proper resection depth intraoperatively can be challenging, especially for the inexperienced hip arthroscopist. We theorized that removal of subchondral cortical bone alone in the region of the cam lesion would yield femoral anatomy that was not different from control femurs. To evaluate this, we analyzed shape models between: (1) native cam and screened control femurs to observe the location of the cam lesion and establish baseline shape differences between groups, and (2) cam femurs with simulated resections and screened control femurs to evaluate the sufficiency of subchondral cortical bone thickness to guide resection depth. We found that removal of subchondral cortical bone reduced the deviation between resected cam and control femurs to less than a millimeter in the region of resection. In addition, the shape variation was eliminated over the region of the resection, as evidenced by the reduction in distance between the correspondence particles of the resected cam femurs and the mean control femur. Finally, PCA indicated that the number of modes representing distinct shape differences between groups was reduced from four to one after resection. Thus, collectively, our results support the use of the subchondral cortical-cancellous bone margin as a visual, intraoperative guide for resection depth in the correction of cam FAI. Fortunately, this boundary provides real-time feedback as it is clearly visible without additional operative tooling or imaging (Fig. 1). However, the cortical-cancellous boundary only provides a guide to limit resection depth; the surgeon still must identify the areal extent of the cam lesion based on his or her clinical knowledge and expertise.

Our study does have some limitations. First, our definition of the region of resection was based on a 1-mm threshold on the shape difference between mean shape of native cam and control femurs. We implemented this approach to aid in the automatic definition of a resection region for each patient with cam FAI, which reduced subjectivity and bias in this regard. However, the 1-mm threshold used to outline the simulated resection was based only on qualitative inspection of what was deemed to be an appropriate resection boundary on the mean cam femur shape. Use of this standardized region may have misidentified the anterosuperior location or over- or underestimated the true areal coverage of the cam lesion on a subject-specific basis, but it still represented the average region of the cam lesion for our population. Clinically, the discretion of the surgeon is required to identify the areal extent based on subject-specific morphologic features. Second, although we have been implementing this technique in our surgical practice, we have yet to quantify the accuracy of resection in terms of removing only cortical bone, and we have yet to determine how resections based on this guideline affect fracture strength, kinematic function, and patient-reported outcomes. Third, the study populations included subjects who were screened radiographically based on α angles. We chose to use the frog-leg view because it has been shown to capture lesions in patients with cam FAI [12], but we acknowledge that it is possible that control subjects could have had cam lesions visible on other views. Fourth, the cam population was predominantly male and therefore we advocate for caution when using the cortical-cancellous boundary as a resection guideline when treating female patients. However, our previous analysis of cortical thickness found no differences in cortical thickness between male and female control subjects, suggesting that this guideline may be applicable for both sexes [1]. Fifth, the clinical history of cadaver femurs used as controls was not available; it is possible these individuals had hip pain. However, we excluded all femurs with evidence of cam FAI. Finally, it is unclear if normalization of anatomy defines the ideal resection for patients with cam FAI; slight overcorrection may be preferred by surgeons to reduce the likelihood of impingement.

Previous studies have evaluated the shape of the cam lesion and cortical thickness in patients with cam FAI [1, 11, 13, 15]. Our results agree with previous shape analyses of the outer cortex. Specifically, a previous SSM study found maximum deviation between mean cam and control shapes to be 3.3 mm in the anterolateral head-neck junction, which is in good agreement with our data [11]. Another study mapped the femoral head-neck offset in reference to the radius of the femoral head for cam FAI and control subjects; results showed that the lateral and anterior quadrants were larger for the patients when compared with the control subjects, similar to our findings [15]. Although not quantitatively comparable as a result of normalization to the diameter of the femoral head, the group differences found herein are qualitatively comparable. Harris et al. [13] fit the femoral head of patients with cam FAI to idealized shapes (spheres and conchoids) and found maximum deviations from a sphere of (mean ± SD) 5.0 ± 0.4 mm for patients and 2.4 ± 0.3 mm for control subjects and from a conchoid of 4.1 ± 0.4 mm for patients and 1.8 ± 0.3 mm for control subjects. Our measurements of maximum deviation of the control subjects and patients with cam FAI from the mean shape were slightly less than data reported by Harris et al. [13]. We suspect this is because normal femora are not spherical, and thus, deviations to an idealized geometry would be expected to be higher.

Removal of the subchondral cortical bone tended to yield a 3-D shape that underresected the cam lesion superiorly and overresected anteriorly. These errors can be partially attributed to our definition of a single region of resection which was superimposed on each subject femur, as any errors in identifying the proper region of resection may result in under- or overresection. Superiorly, subchondral cortical bone may have diminutive thickness compared with the anterior region of the femoral head, and thus removal of cortical bone over a standardized region based on a 1-mm threshold may not normalize femoral head anatomy given the variability in location of the cam lesion [28]. Collectively, these regional results indicate that when using the cortical-cancellous bone boundary as a surgical guideline, it is important not only to evaluate the specific 3-D morphologic features using intraoperative techniques (ie, full ROM arthroscopic views and fluoroscopic recreations of radiographic views) [4, 16, 17, 27], but also to consider the effects of varied cortical thickness when resecting the cam lesion. Still, the amount of underresection superiorly and overresection anteriorly was on the submillimeter level, which may be an improvement on current methods given that computer navigation methods have an accuracy of ± 1.9 mm and have been shown to be more precise than freehand techniques [6, 20]. Additionally, observation of the cortical-cancellous boundary intraoperatively provides for real-time, subject-specific feedback on resection depth without requiring additional imaging or preoperative planning.

Overall, simulated resection of subchondral cortical bone provided an effective method to determine cam resection depth for the population of cam femurs evaluated herein. In particular, resection of subchondral cortical bone to cortical-cancellous boundary yielded mean femoral anatomy for patients with cam FAI that was within a millimeter of the mean shape of control subjects without FAI with no differences in anatomic shape over the region of resection, with the numbers available. Nevertheless, differences in overall shape (ie, sphericity of the femoral head and shape of the greater trochanter) were still present after resection, indicating that removal of subchondral cortical bone over the cam lesion in patients with cam FAI alone cannot restore the shape of the entire proximal femur. The primary advantage of the proposed guideline is that the resection depth can likely be verified by inspection of arthroscopic images intraoperatively and thus does not require advanced imaging or 3-D modeling to generate a surgical plan. Future studies should establish the accuracy of the surgeon's resection in following this guideline and should determine if normalization of anatomy through resection of subchondral cortical bone alone improves clinical outcomes after hip arthroscopy.

Acknowledgments We thank Shireen Elhabian PhD and Praful Agrawal MS (Scientific Computing and Imaging Institute, University of Utah) for assistance with software development, and Trevor Hafer BS and Tyler Skinner BS (Department of Bioengineering, University of Utah) for assistance with image segmentation.

References

1. Atkins PR, Elhabian SY, Agrawal P, Harris MD, Whitaker RT, Weiss JA, Peters CL, Anderson AE. Quantitative comparison of cortical bone thickness using correspondence-based shape modeling in patients with cam femoroacetabular impingement. *J Orthop Res.* 2016 Oct 27. [Epub ahead of print] doi:10.1002/jor.23468.
2. Bogunovic L, Gottlieb M, Pashos G, Baca G, Clohisy JC. Why do hip arthroscopy procedures fail? *Clin Orthop Relat Res.* 2013;471:2523–2529.
3. Chan EF, Farnsworth CL, Koziol JA, Hosalkar HS, Sah RL. Statistical shape modeling of proximal femoral shape deformities in Legg–Calvé–Perthes disease and slipped capital femoral epiphysis. *Osteoarthritis Cartilage.* 2013;21:443–449.
4. Chow RM, Kuzma SA, Krych AJ, Levy BA. Arthroscopic femoral neck osteoplasty in the treatment of femoroacetabular impingement. *Arthrosc Tech.* 2014;3:e21–e25.
5. Clohisy JC, Nunley RM, Otto RJ, Schoenecker PL. The frog-leg lateral radiograph accurately visualized hip cam impingement abnormalities. *Clin Orthop Relat Res.* 2007;462:115–121.
6. Ecker TM, Puls M, Steppacher SD, Bastian JD, Keel MJ, Siebenrock KA, Tannast M. Computer-assisted femoral head-neck osteochondroplasty using a surgical milling device an in vitro accuracy study. *J Arthroplasty.* 2012;27:310–316.
7. Finner H. On a monotonicity problem in step-down multiple test procedures. *J Am Stat Assoc.* 1993;88:920–923.
8. Franklin SB, Gibson DJ, Robertson PA, Pohlmann JT, Fralish JS. Parallel analysis: a method for determining significant principal components. *J Veg Sci.* 1995;6:99–106.
9. Guevara-Alvarez A, Lash N, Beck M. Femoral head-neck junction reconstruction, after iatrogenic bone resection. *J Hip Preserv Surg.* 2015;2:190–193.
10. Harris JD, McCormick FM, Abrams GD, Gupta AK, Ellis TJ, Bach BR Jr, Bush-Joseph CA, Nho SJ. Complications and reoperations during and after hip arthroscopy: a systematic review of 92 studies and more than 6,000 patients. *Arthroscopy.* 2013;29:589–595.
11. Harris MD, Datar M, Whitaker RT, Jurrus ER, Peters CL, Anderson AE. Statistical shape modeling of cam femoroacetabular impingement. *J Orthop Res.* 2013;31:1620–1626.
12. Harris MD, Kapron AL, Peters CL, Anderson AE. Correlations between the alpha angle and femoral head asphericity: implications and recommendations for the diagnosis of cam femoroacetabular impingement. *Eur J Radiol.* 2014;83:788–796.
13. Harris MD, Reese SP, Peters CL, Weiss JA, Anderson AE. Three-dimensional quantification of femoral head shape in controls and patients with cam-type femoroacetabular impingement. *Ann Biomed Eng.* 2013;41:1162–1171.
14. Hotelling H. The generalization of Student's ratio. In Kotz S, Johnson NL, eds. *Breakthroughs in Statistics:Foundations and Basic Theory.* New York, NY:Springer Science + Business Media; 1992:54–65.
15. Ito K, Minka MA 2nd, Leunig M, Werlen S, Ganz R. Femoroacetabular impingement and the cam-effect: a MRI-based quantitative anatomical study of the femoral head-neck offset. *J Bone Joint Surg Br.* 2001;83:171–176.
16. Jackson TJ, Stake CE, Trenga AP, Morgan J, Domb BG. Arthroscopic technique for treatment of femoroacetabular impingement. *Arthrosc Tech.* 2013;2:e55–e59.
17. Larson CM, Wulf CA. Intraoperative fluoroscopy for evaluation of bony resection during arthroscopic management of femoroacetabular impingement in the supine position. *Arthroscopy.* 2009;25:1183–1192.
18. Maquer G, Burki A, Nuss K, Zysset PK, Tannast M. Head-neck osteoplasty has minor effect on the strength of an ovine cam-FAI model: in vitro and finite element analyses. *Clin Orthop Relat Res.* 2016;474:2633–2640.
19. Mardones RM, Gonzalez C, Chen Q, Zobitz M, Kaufman KR, Trousdale RT. Surgical treatment of femoroacetabular impingement: evaluation of the effect of the size of the resection. *J Bone Joint Surg Am.* 2005;87:273–279.
20. Park CN, Nawabi DH, Christopher J, Conditt MA, Ranawat AS. Robotic-assisted femoral osteochondroplasty is more precise than a freehand technique in a Sawbone model. *J Hip Preserv Surg.* 2015;2:136–144.
21. Philippon MJ, Briggs KK, Yen Y-M, Kuppersmith DA. Outcomes following hip arthroscopy for femoroacetabular impingement with associated chondrolabral dysfunction: minimum two-year follow-up. *J Bone Joint Surg Br.* 2009;91:16–23.
22. R CoreTeam. R: A language and environment for statistical computing. *R Foundation for Statistical Computing.* Available at: https://cran.r-project.org/doc/manuals/r-release/fullrefman.pdf. Accessed March 9, 2017.
23. Ross JR, Larson CM, Adeoyo O, Kelly BT, Bedi A. Residual deformity is the most common reason for revision hip arthroscopy: a three-dimensional CT study. *Clin Orthop Relat Res.* 2015;473:1388–1395.
24. Rothenfluh E, Zingg P, Dora C, Snedeker JG, Favre P. Influence of resection geometry on fracture risk in the treatment of femoroacetabular impingement: a finite element study. *Am J Sports Med.* 2012;40:2002–2008.

25. Sardana V, Philippon MJ, de Sa D, Bedi A, Ye L, Simunovic N, Ayeni OR. Revision hip arthroscopy indications and outcomes: a systematic review. *Arthroscopy.* 2015;31:2047–2055.
26. Speirs AD, Beaule PE, Rakhra KS, Schweitzer ME, Frei H. Bone density is higher in cam-type femoroacetabular impingement deformities compared to normal subchondral bone. *Osteoarthritis Cartilage.* 2013;21:1068–073.
27. Stähelin L, Stähelin T, Jolles BM, Herzog RF. Arthroscopic offset restoration in femoroacetabular cam impingement: accuracy and early clinical outcome. *Arthroscopy.* 2008;24:51–57.e1.
28. Treece GM, Gee AH, Mayhew PM, Poole KE. High resolution cortical bone thickness measurement from clinical CT data. *Med Image Anal.* 2010;14:276–290.
29. Wijdicks CA, Balldin BC, Jansson KS, Stull JD, LaPrade RF, Philippon MJ. Cam lesion femoral osteoplasty: in vitro biomechanical evaluation of iatrogenic femoral cortical notching and risk of neck fracture. *Arthroscopy.* 2013;29:1608–1614.
30. Zingg PO, Buehler TC, Poutawera VR, Alireza A, Dora C. Femoral neck fractures after arthroscopic femoral neck osteochondroplasty for femoroacetabular impingement. *Knee Surg Sports Traumatol Arthrosc.* 2014;22:926–931.

CHAPTER 6

IMPACT, ONGOING RESEARCH, FUTURE DIRECTIONS

Impact

It is widely believed that cam femoroacetabular impingement syndrome (FAIS) is a major cause of hip osteoarthritis (OA).[1; 2] Despite numerous studies devoted to the topic, we continue to lack a comprehensive understanding of why some individuals with cam lesions rapidly develop hip OA, whereas others appear to live well into adulthood without ever developing symptoms or damage.[1-5] While this dissertation was unable to establish cause and effect relationships between shape, biomechanics, and OA in the setting of cam FAIS, the research did substantially advance our understanding of hip biomechanics and morphometrics using innovative techniques that spanned both experimental and computational paradigms.

Dual fluoroscopy (DF), which is devoid of errors caused by skin motion artifact, demonstrated that cam FAIS patients stood in more extension, and walked with greater external rotation on level terrain when compared to asymptomatic controls with normal hip morphology. Although other motion analysis studies have reported similar results,[6-8] our work is novel in that it captured in-vivo bone motion of the femur and pelvis. By tracking the spatial position of the bones directly, we were able to isolate the contributions of the femur and pelvis to overall joint motion and uncover subtle variations in pelvic motion that may have been overlooked in previous studies of hip joint range of motion. These data reveal that patients with FAIS may compensate for pain or reduced range of motion with altered patterns of pelvic motion, such that they have an overly stable pelvis during common activities, like level walking, but then may require additional pelvic motion, during more challenging activities where the femur more closely approximates the acetabular labrum, like incline walking or circumduction. It is possible that reduced pelvic motion during normal activities may lead to deleterious joint mechanics, and if corrected, could improve the function of patients with cam FAIS. Thus, the work herein may inform alternative treatment pathways for patients with cam FAIS.

Arthrokinematics of the hip provide unique insight on in-vivo bone motion, far beyond the kinematics that have been quantified to date. Importantly, our understanding of overall hip joint motion patterns, especially those of cam FAIS patients, can be improved with arthrokinematic data, as the six degree of freedom motion of the hip can be visualized and motion patterns can be analyzed relative to subject-specific anatomy.[9-12] While DF data provides a unique representation of hip function, the limited sample sizes, resultant of laborious data acquisition and processing pipelines, hinder the ability to find adequately powered differences when comparing groups, as observed in Chapter 2. Improvements to both the acquisition and processing of DF data have been proposed later in this chapter to enable larger sample sizes to be analyzed in the future.

The research detailed in Chapters 3, 4, and 5 employed statistical shape modeling (SSM) to evaluate clinical metrics of classifying cam morphology, quantifying cortical bone thickness in cam FAIS, and determining whether the resection of cortical bone restores morphology in these patients. Several technical advancements specific to SSM were made as a result of conducting these studies, including the development of improved pre- and post-processing tools and the identification of improvements to optimization strategies in the existing software, which have improved the usability of the pipeline. Importantly, these advancements to the SSM pipeline provided the ability to yield results with direct clinical relevance.

Radiographic measurements from plain films are utilized in the diagnosis of cam FAIS, yet there is still little agreement as to which views best describe the morphology of the femoral head-neck junction. Importantly, two-dimensional (2D) slice-based measurements of morphology are often used as the gold-standard for comparison of plain film measurements. To combat these inaccuracies, Chapter 3 presented three-dimensional (3D) shape statistics from SSM and regression models to identify the radiographic views that provided the best representation of femoral head morphology. Importantly, 2D radiographs only captured roughly half of the 3D morphology of the proximal femur, which may not adequately represent the morphology of cam FAIS. 3D imaging of the hip joint may provide crucial information during diagnosis and preoperative planning for cam FAIS patients.

In Chapter 4, the analysis of cortical thickness of the proximal femur in cam FAIS patients indicated that not only do patients have increased cortical thickness over the region of the cam lesion, as was hypothesized, but that patients also have generally increased cortical thickness over the entire proximal femur, even after removing sex as a factor.[13] In addition to having a generally thicker cortex over the proximal femur, the location of maximum cortical thickness was located more anterior and less lateral in cam FAIS patients. Importantly, this indicates that the previous use of generalized anatomy or asymptomatic cadaveric specimens to investigate the strength of the proximal femur may in fact lead to overly-conservative conclusions about the depth of resection considered to be safe. This is especially important, as the leading cause for revision arthroscopy is insufficient resection and residual impingement.[14; 15] The specific morphology and thickness of the cortex in cam FAIS patients indicates that the loading of the femur in cam FAIS may lead to altered stress distributions which would allow for surgical resection of the cam lesion without disruption of the overall strength of the femur.

The optimal depth of resection of the cam lesion is based on both ensuring that the mechanical strength of the proximal femur is not compromised and also ensuring the impingement has been alleviated. While many studies have aimed at evaluating the residual strength of the proximal femur, in Chapter 5 we used SSM to evaluate the sufficiency of a resection through the cortical bone layer for patients with cam FAIS. While it is difficult to test the hypothesis of whether a simulated resection is optimal for patient outcomes, the technique of resecting through the sclerotic cortex of the cam lesion has anecdotally been successful surgically.[16] Using SSM, the removal of sclerotic bone alone was determined to return cam FAIS morphology to within 1 mm of the anatomy of asymptomatic control subjects over the region of the cam lesion.[17] While experienced hip arthroscopists may not require intra-operative guides to determine the depth of surgical resection, many orthopaedic surgeons performing femoral osteochondroplasty arthroscopically are performing less than five operations per year, so the use of sclerotic cortical bone as an inherent guide for resection depth may improve patient outcomes.[18]

The use of SSM in orthopaedics provides a unique opportunity to objectively quantify morphology. However, the current implementation of SSM software has not been directed towards clinical use. In support of this dissertation, several advancements have been incorporated into ShapeWorks, an SSM implementation developed through the Scientific Computing and Imaging Institute (SCI) at the University of Utah, that provide more streamlined use for biomechanists and clinicians. In addition to improvements to the flexibility of the software to analyze more complex geometries, some of the most important improvements have been made towards improving the preprocessing of geometry for analysis. Towards this end, advanced methods of generating accurate volumetric distance transforms of surfaces have been implemented to improve the accuracy of input shapes, reflection and alignment tools have been incorporated into the SSM pipeline to avoid the need for external software packages, and the ability to incorporate scalar data into the analysis of shape have been added to the preprocessing functionality of ShapeWorks.[13] Additional postprocessing tools have been incorporated to allow linear discrimination of the shapes against overall population variation and tools are in-development to allow for analysis of scalar variability with reference to shape.[13] Importantly, the improvements to the ShapeWorks software package are in preparation for release to the general public in the near future, which is an important step towards being able to analyze 3D morphology as part of clinical diagnosis and treatment.

Ongoing Research – Finite Element and Musculoskeletal Models

The methodologies developed and refined as part of this dissertation have been instrumental in supporting several ongoing research projects specific to FAIS. For example, one of our major future goals is to employ finite element (FE) modeling to quantify chondrolabral mechanics in patients with FAIS. In doing so, we may be able to isolate specific bony protrusions that give rise to deleterious mechanics. These data can be used as part of preoperative planning to determine the region of bony resection which would normalize mechanics and prevent or delay hip OA.

Our lab has a long-standing history of using volumetric imaging methods, such as computed tomography (CT) arthrograms, to provide the images necessary to create faithful, 3D FE meshes of hip bone, cartilage, and labrum.[19-24] While we have demonstrated that accurate reconstructions of these structures are a necessary precursor to obtaining accurate predictions of hip contact mechanics,[20; 24] it is unclear if the same level of detail is required when assigning boundary and loading conditions to the FE model. More recently, subject-specific motion and loading patterns have been incorporated into models of cam FAIS,[25; 26] but without analysis of the sensitivity of the model to the boundary and loading conditions it is unclear whether this technique improves predictions of chondrolabral mechanics.

At present, we are executing a study that will compare FE predictions between models with varying levels of subject-specific boundary and loading conditions. More specifically, we are using ground reaction forces quantified by the instrumented treadmill along with kinematics measured directly by DF (see Chapter 2) and estimated by skin marker motion analysis as inputs to musculoskeletal models. These musculoskeletal models will predict the magnitude and direction of the hip joint reaction force (JRF). The kinematic positions measured by DF or estimated by skin markers will then be applied to the FE model with the corresponding JRF for each kinematic dataset. We will then compare FE predictions between models driven using DF-based data and those driven using skin marker data. In addition, we plan to compare FE predictions from the subject-specific boundary and loading condition models to FE models driven using data from the literature.[27] Specifically, Bergmann et al. used skin marker motion analysis and instrumented total hip replacement prosthetics to measure hip kinematics and JRFs in patients treated for end-stage hip OA with total hip arthroplasty.[27] These data have been used by numerous groups, including our lab and colleagues at the Musculoskeletal Research Laboratories, as the boundary and loading conditions for FE models aimed at estimating chondrolabral mechanics in asymptomatic controls, acetabular dysplasia patients, and acetabular retroversion patients, both before and after surgery.[20; 22; 24; 28-35] However, it is important to recognize that patients with FAIS may ambulate differently than total hip replacement patients. By comparing FE predictions between models with varying levels of subject-specificity in the assignment of boundary and loading conditions, we will establish the inputs required for FE modeling of FAIS moving forward. Beyond cam FAIS patients, these data will provide sensitivity data for FE predictions of hip chondrolabral mechanics to various boundary and loading conditions, which can be incorporated into other FE models of the hip.

Final results for the aforementioned FE boundary and loading condition study are still being processed. Nevertheless, it is worthwhile to discuss the musculoskeletal model in more detail to properly frame the research and the nuances of conducting such a study. Currently, we are using a publicly available, full-body musculoskeletal model developed in OpenSim (National Center for Simulation in Rehabilitation Research, www.opensim.standford.edu) to predict hip JRFs.[36] Within this model, anthropometric dimensions of the model are scaled to the dimensions of each subject during a static, standing trial using the Scale Tool in OpenSim. The degrees of freedom of the model are adjusted to minimize error between model and experimental marker locations using the Inverse Kinematics Tool. Joint moments are calculated from the inverse kinematics solutions and the ground reaction force measurements using the Inverse Dynamics Tool. From here, individual muscle activation levels and muscle-tendon unit forces are calculated Static Optimization Analysis.[37] and the JRFs in the reference frame of the pelvis are determined from the Analysis Tool's Joint Reaction Analysis.

While the process of calculating muscle forces and JRFs has been relatively well documented, the assumptions behind these models are numerous, and can be problematic. For example, as part of ongoing research, a former postdoctoral fellow, Dr. Niccolo Fiorentino, is providing an objective assessment of the effect of soft tissue artifact on kinematics and kinetics.

Importantly, some of the steps necessary to incorporate DF data into musculoskeletal models complicate the DF kinematic tracking of the hip joint. First, while true bony geometries are not usually available as part of standard gait analysis, our imaging protocol includes CT and DF which provide bone geometries and positions for model initialization and scaling. However, incorporation of subject-specific scaling parameters, which can include the position of the hip joint center, can produce additional errors, especially when these factors vary widely from what would be derived from skin marker locations. However, by using subject-specific scaling parameters from bone geometries, we hope to reduce aberrant movement of the hip joint center which would result in errors in the calculation of hip JRFs. Second, DF data is transformed into the motion capture lab coordinate system based on spatiotemporally synced images of a calibration cube. Due to the field of view of the DF system, the calibration cube is relatively small in size, such that even small errors in the calibration result in large errors in the transformation of virtual DF marker data from the DF system to the motion capture lab coordinate system. Once the markers are in the same coordinate system and the model is scaled, it is important to process the data sets as equivalently as possible. Due to the known issues with soft tissue artifact from skin marker motion capture,[38] markers can be preferentially weighted in OpenSim to use more reliable markers to track each segment.[39] Since the accuracy of the virtual DF markers is within 1° and 1 mm, it may be desirable to assign these markers higher weighting factors, but this would lead to inconsistencies between the skin marker and DF models. Similarly, it is usually advantageous to reduce residuals within the model to ensure that the forces within the model are reasonable, but kinematics are altered as part of the residual reduction analysis, which would eliminate the benefit of incorporating accurate DF kinematics. Further, it is difficult to apply the same residual reduction methods to two separate models. These aspects and others are currently being evaluated to provide an objective comparison of musculoskeletal modeling results between DF and skin marker kinematic inputs which will then be used to ascertain the sensitivity of FE predictions to changes in kinematics and kinetics.

Once we have obtained the JRFs from OpenSim models, we will assign them to subject-specific FE models generated from CT arthrography data. More specifically, subject-specific anatomy of the proximal femur, hemi-pelvis, femoral and acetabular cartilage layers, and the labrum will be segmented and reconstructed into triangular-meshed surfaces.[23] From these surfaces, subject-specific tetrahedral meshes of the bone cortex, cartilage, and labrum will be generated in Preview (FEBio software suite, www.febio.org) using a recently implemented automatic meshing pipeline.[40] The ability to semi-automatically generate volumetric tetrahedral meshes of complex geometries, such as the acetabular cartilage and labrum, is an important improvement to the FE modeling pipeline. Previously, we generated hexahedral meshes to represent cartilage and labrum from an unstructured block mesh (Fig. 6.1), but this approach was very time- and labor-intensive, which made it impractical to incorporate larger sample sizes within a single FE modeling study.

With the mesh created, we will then assign material properties to the various tissues. At least initially, the femur and pelvis will be modeled as isotropic elastic materials (Young's modulus E = 17 GPa, Poisson's ratio ν = 0.29).[41] The femoral and acetabular cartilage will be represented using an ellipsoidal fiber distribution (EFD) constitutive model with a Neo-Hookean ground matrix (shear modulus μ = 1.82 MPa, bulk modulus, K = 1860 MPa, fiber power coefficient β = 4, and initial modulus $\xi 1$ = 9.19 MPa).[42] The labrum will be modeled as an uncoupled transversely isotropic Mooney-Rivlan (μ = 2.8 MPa, K = 1000 MPa, exponential toe region coefficients C_3 = 0.05 MPa, C_4 = 36,

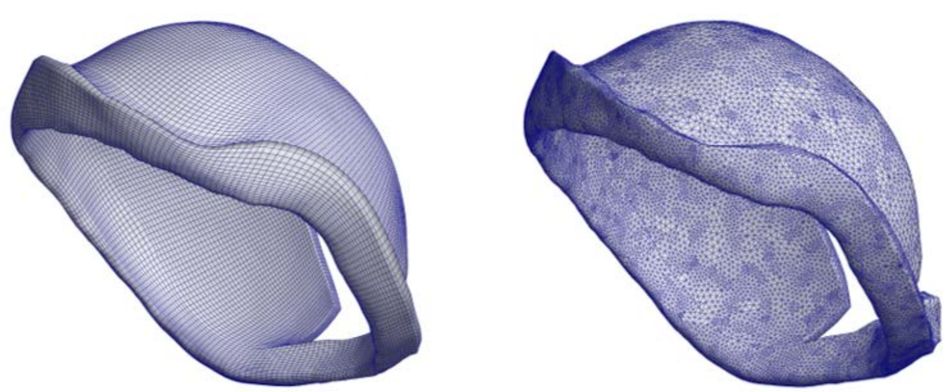

Figure 6.1. Volumetric mesh of the acetabular cartilage, labrum and transverse ligament generated with hexahedral elements from TrueGrid (left) and tetrahedral elements generated in Preview (right).

straightened fiber modulus C_5 = 66 MPa, and fiber stretch for straightened fibers λ = 1.103).[32; 43; 44]

As discussed above, boundary and loading conditions from three sources will be evaluated, including the generalized kinematics and joint reaction forces (JRFs) from the literature[27] and two subject-specific sources based on kinematic and load data from motion capture and musculoskeletal modeling. From these data sources, a total of five model combinations will be assessed to determine the sensitivity of FE predictions to the kinematics and loading from each data source (Table 6.1). Four of the models will be force driven, while the final model will be driven by the displacements obtained from the DF data without the use of force data. For each model, the impact and active peaks of gait, which correspond to the first and second peaks of the ground reaction force data, will be simulated. Subject-specific gait cycles will be temporally synched with the generalized gait cycle to allow for combination of and comparison between data sources. Rotations and displacements will be converted to rotation vectors from the generalized and subject-specific data for representation in PreView and FEBio. The subject-specific kinematics and displacements will be calculated relative to International Society of Biomechanics (ISB)

Table 6.1. Boundary and loading conditions used to assess the sensitivity of chondrolabral stress and strain to various input data.

Model	Boundary Condition Source	Loading Source
General	Bergmann Kinematics[27]	Bergmann JRF[27]
SM-Kinematic	SM motion capture	Bergmann JRF[27]
SM-Load	SM motion capture	OpenSim JRF (SM)
DF-Load	DF motion capture	OpenSim JRF (DF)
DF-Disp	DF motion capture	DF displacements

SM, skin marker; DF, dual fluoroscopy; JRF, joint reaction forces.

coordinate systems.[38; 45; 46] Importantly, the generalized data collected from instrumented hip prosthesis patients used a modified coordinate system based on the geometry of the hip prosthesis with alternative vertical and horizontal femoral axes.[27] For consistency between data sources and with other reports of kinematics, the generalized joint angles will be converted to ISB-based joint angles.

As discussed above, this is an ongoing study. Nevertheless, volumetric meshes have been generated for two cam FAIS patients and two control subjects. Here, estimates of contact area, contact stress, first principal Lagrange strain on the articular surface (E_1), and maximum shear stress at the osteochondral interface (τ_{max}) will be assessed, as these metrics are relevant to previous validation studies and appear to be the most relevant to hypothesized modes of injury in FAIS patients.[24; 34; 35] Preliminarily, a gait cycle model of a cam FAIS patient based on generalized kinematics and joint reaction forces from the literature[27] showed increased strain over both the anterosuperior and posterosuperior labrum during both the impact and active peaks of gait (Fig. 6.2). With the use of generalized kinematics, the abutment of the aspherical femoral head with the labrum caused increased strain over these two regions. The inclusion of subject-specific boundary and loading conditions will begin to answer the question of whether subject-specific kinematics provide alleviation from increased stress and strain due to aspherical anatomy or if they lead to patterns of higher stress and strain within the joint. While results are only preliminary, FE predictions appear to be at least moderately sensitive to the boundary and loading conditions applied. Future research will need to evaluate the extent to which boundary and loading conditions affect predictions for additional subjects.

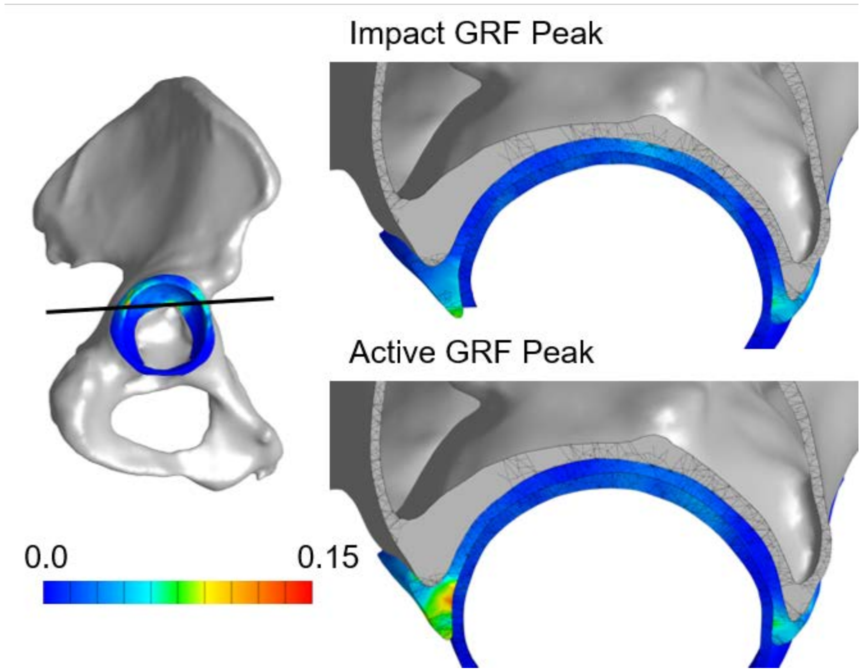

Figure 6.2. 1st Principal Lagrange strain through the thickness of the acetabular cartilage and labrum of a cam FAIS patient during the impact and active peaks of the gait cycle (14% and 46% gait). Line through pelvis indicates the cut plane, as viewed from the top.

Ongoing Research – Magnetic Resonance Imaging and Dual-Fluoroscopy

One major drawback of using DF and model-based markerless tracking is exposure to ionizing radiation from the fluoroscopes as well as the CT scanner. Importantly though, the majority of the radiation exposure is from the acquisition of CT images. Since both fluoroscopy and CT are radiation-based imaging modalities which represent tissue density similarly, the pixel intensities of the projections of bone generated from CT data are similar to those from the fluoroscopy images. Model-based markerless tracking exploits this notion during alignment of the digitally-reconstructed radiograph (DRR) with the fluoroscope images, suggesting that CT is indeed the best modality for DF tracking. Nevertheless, magnetic resonance (MR) images also provide images of bone which, when properly transformed, appear similar to CT-based image data for input to model-based markerless tracking. In doing so, radiation dose to the research subject would be reduced by 80% or more.

Recognizing the potential MR has, we acquired MR images of our subjects. In both CT and MR images, cortical and trabecular bone is differentiated, however in comparison to trabecular bone the cortex appears brighter in CT and darker in MR. Therefore, to generate DRRs from our T1-weighted, gradient echo MR images, voxel intensities from the MR scan were inverted and scaled based on histogram matching to approximate the CT voxel data for the femur and pelvis (Fig. 6.3). Kinematics tracked using the T1-weighted images were within 0.0 ± 0.5°, 0.1 ± 0.2°, -0.2 ± 0.5° of the data tracked by CT for flexion-extension, abduction-adduction, and internal-external rotation, respectively (mean ± 95%

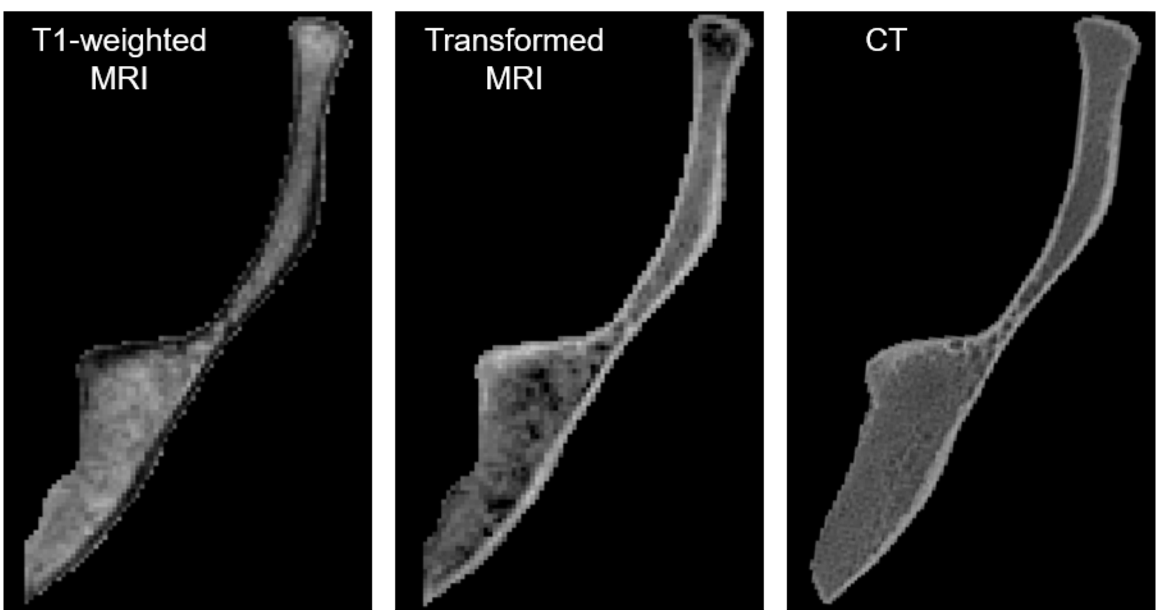

Figure 6.3. Pixels within the pelvis were isolated for a T1-weighted gradient echo image (left) and transformed to approximate voxel intensities of CT (center). Voxel intensities from a similar slice of a pelvis from CT are shown for reference (right).

confidence interval). Thus, assuming this level of accuracy is sufficient, as it is within the bounds of the original validation, future DF studies of the hip could be performed without the need for CT imaging.[38]

Ongoing Research – Statistical Shape Modeling

While the focus of this dissertation has been on capturing and defining the shape of the proximal femur in cam FAIS patients, we have made recent progress on quantifying the shape of the pelvis in control subjects and patients with acetabular dysplasia or retroversion. Due to the unique shape of the pelvis, including high curvature and thin regions of the iliac wing and acetabulum, SSM of the pelvis required improvements to the flexibility of ShapeWorks. Specifically, several assumptions were revisited and surface normal data was incorporated in the correspondence optimization scheme. From the model of the pelvis, we found the first ten modes of variation to be significant. Interestingly, significant differences were found in overall shape between the acetabular dysplasia and acetabular retroversion subjects ($p = 0.032$), but not between the control subjects and either the acetabular dysplasia or acetabular retroversion patients ($p = 0.482$ and $p = 0.060$, respectively). Two modes of variation seemed to be representative of these group-based differences (Fig. 6.4). Mode 0 was significant between the acetabular retroversion patients and both the acetabular dysplasia patients ($p = 0.003$) and the control subjects ($p = 0.024$). Mode 7 was significant between the control subjects and both the acetabular dysplasia ($p = 0.010$) and the acetabular retroversion patients ($p = 0.048$).

With the model of the pelvis, we are now able to begin building SSM models of the hip joint for the analysis of contact stress and strain from FE analysis across a population.

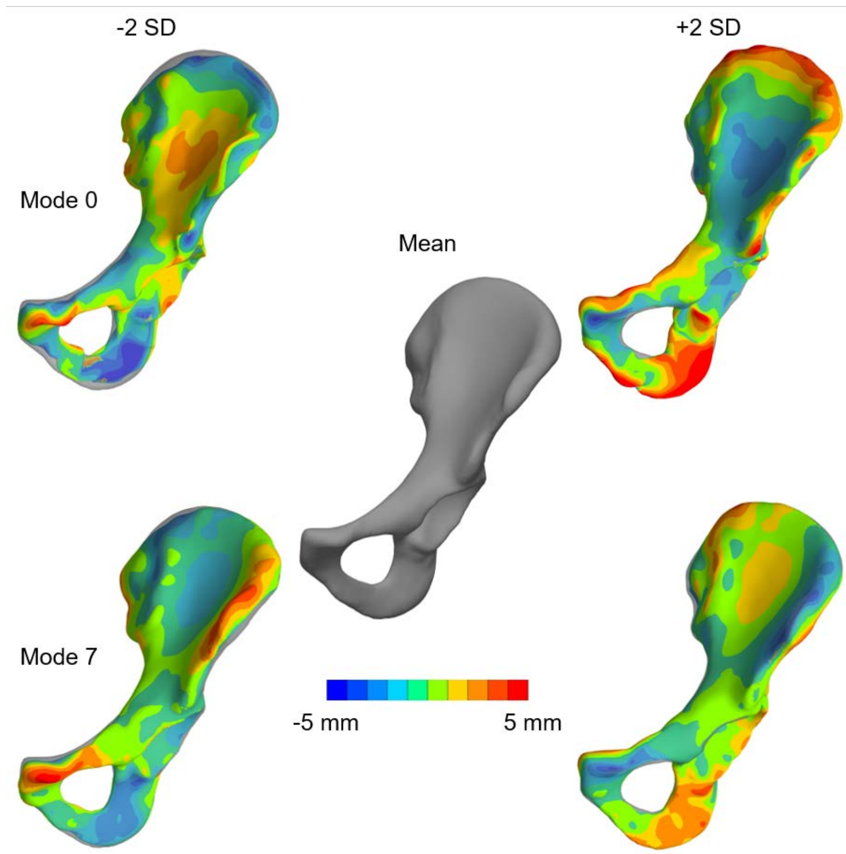

Figure 6.4. Principal component analysis modes of variation relevant to group differences between control subjects without pathology, patients with acetabular dysplasia, and patients with acetabular retroversion. The semitransparent mean hemi-pelvis shape is overlaid with each mode-based shape for reference.

Towards this end, an SSM model is being optimized to include the proximal femur, femoral cartilage, hemi-pelvis, and acetabular cartilage and labrum. Results from previous FE analyses will be incorporated as scalar values and used to validate the ability to predict mechanics relative to the shape of the joint (Fig. 6.5). As a secondary study, FE models will be generated using SSM-based geometries of different populations and disease severities to evaluate the use of population-based FE models in the assessment of damage patterns associated with disease.

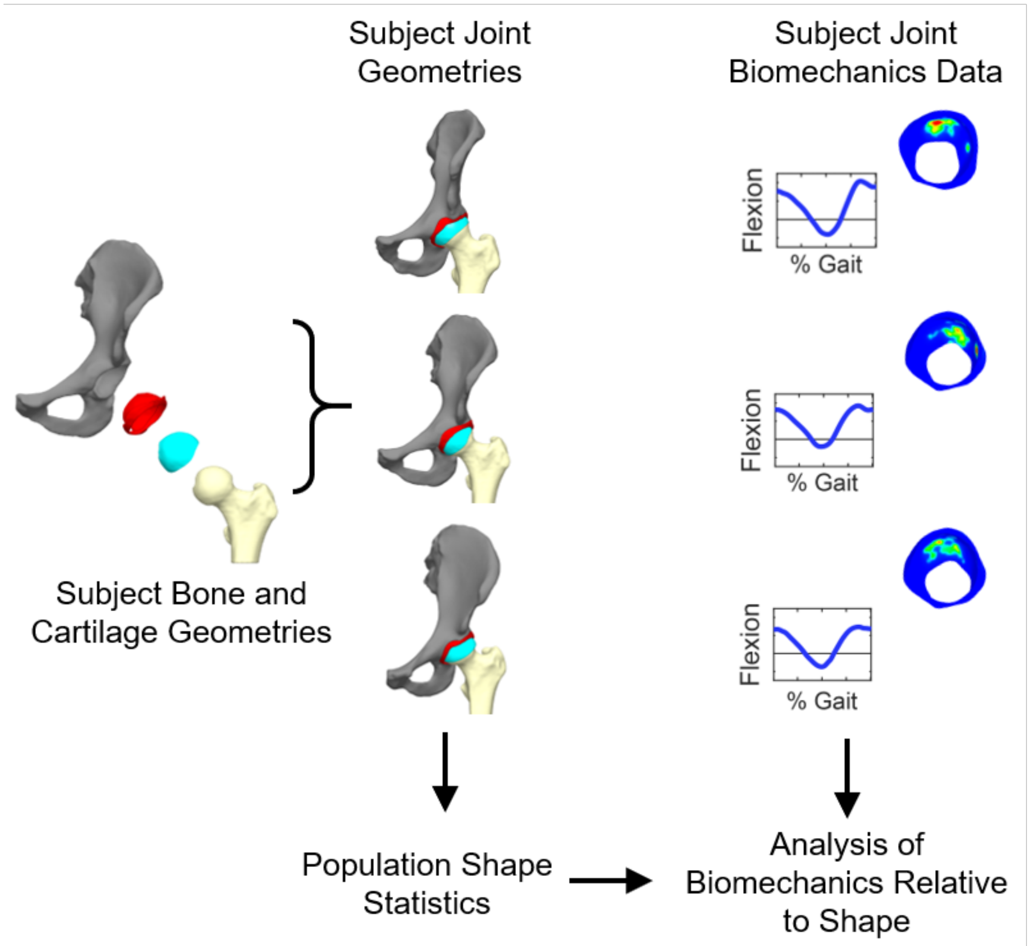

Figure 6.5. Pipeline for processing joint biomechanics through statistical shape modeling where subject geometries of the bone and cartilage will be combined with previous and ongoing biomechanical data to assess the relationship between shape and function.

Future Directions

While DF imaging provides an accurate method to capture in-vivo joint motion, it is extremely laborious to process the data, which perhaps precludes its use for studies where a large cohort is needed to test a hypothesis with sufficient statistical power. For this reason, there are several advancements to the DF processing pipeline that should be addressed in the future. Due to the poor signal-to-noise ratio of the DF images, model-based tracking of the hip is often completed with a large amount of manual intervention, which is both time intensive and prone to inaccuracies. We have preferentially recruited individuals with a body mass index less than 30 kg/m^2 to minimize radiation scatter and produce good quality images (i.e., high signal-to-noise ratio). However, another technique to improve image quality would be to use a pulsed fluoroscopy system instead of a continuous system, as these systems can provide high contrast images. Our DF system is a continuous system, which allows for capturing of data at a high imaging rate, however pulsed DF systems can capture up to 150 Hz, which is higher than what was used for our analysis of daily activities (100 Hz) and would therefore be a viable option for future DF system acquisitions.

In almost any kinematic study, the same series of activities is captured for each subject. While kinematics and bone positions would be expected to vary across the population, the general movement patterns should be very similar. Using machine learning techniques, movement patterns from one subject could possibly be used to initialize the tracking procedure for the next subject. Over a series of subjects, an average movement pattern with expected variations could be used to more efficiently track the movements of each new subject. Future studies evaluating in-vivo kinematics may be able to take advantage of several improvements to the data capturing and processing pipeline, which would allow for streamlined analysis of larger subject cohorts. With the use of MR images instead of CT, research subjects would be exposed to considerably less ionizing radiation for DF-related studies, which may allow for analysis at multiple time points, such as pre- and postoperatively.

We must recognize though that it may not be necessary to use DF when the research question can likely be answered using less invasive and time-consuming motion capture equipment. Once the musculoskeletal and biomechanical models have been processed, the specific advantages of using DF to capture kinematics of these patient cohorts will be clarified. With the data from these ongoing studies, the design of future studies can evaluate the potential benefits of incorporating DF or skin marker motion capture into the respective data collection and processing pipeline. It may be shown that the musculoskeletal and FE models are not sensitive to the differences between DF and skin marker data collection, such that future studies can use these data to make an educated decision on the appropriate level of detail of input data. Importantly, while our subject cohort was small, the trends of kinematic differences between DF and skin marker acquired data could be used to develop a correction factor, including an offset or scaling factor, to correct kinematics from skin markers for use in future studies.

Towards improving the analysis of shape, many advancements to the SSM pipeline were made in support of this dissertation. However, there are still many aspects of the pipeline that do not yet lend themselves well to clinical applications. Importantly, bone geometries must be segmented, reconstructed, and preprocessed prior to incorporation into SSM. The software developers at SCI are currently working on being able to use image data as direct input to the SSM pipeline. While this would likely still require 3D images to be obtained, eventually with a large enough dataset and the use of machine learning techniques, 3D SSM could be based directly off of radiographic images.

In addition to the need to expedite preprocessing steps, there is currently no method to incorporate shapes directly into a previously generated shape model. By projecting the mean correspondence points onto a new shape and performing optimization from this nearly optimized state, shape statistics quantifying disease severity could be provided in nearly real-time clinically. This functionality is important, since, at present, the generation of the correspondence model can take a week or more of computing time, which is not viable for a clinical setting with a constant influx of imaging data.

With the improvements to the FE modeling pipeline, larger cohorts of subjects can be analyzed in future studies. The resultant biomechanical data can be integrated into the SSM pipeline and analyzed relative to shape data to elucidate the relationship between bony morphology and mechanical function in cam FAIS. This relationship is important to defining the natural history of cam FAIS and preserving the native hip in these patients. With the help of an extensive team of collaborators, this research endeavor has provided the necessary foundation to integrate the analysis of hip shape and function towards understanding the role of morphology and mechanics in cam FAIS.

References

1. Ito K, Minka MA, 2nd, Leunig M, et al. 2001. Femoroacetabular impingement and the cam-effect. A MRI-based quantitative anatomical study of the femoral head-neck offset. J Bone Joint Surg Br 83:171-176.

2. Ganz R, Parvizi J, Beck M, et al. 2003. Femoroacetabular impingement: A cause for osteoarthritis of the hip. Clin Orthop Relat Res:112-120.

3. Sankar WN, Nevitt M, Parvizi J, et al. 2013. Femoroacetabular impingement: Defining the condition and its role in the pathophysiology of osteoarthritis. J Am Acad Orthop Surg 21 Suppl 1:S7-s15.

4. Kuhns BD, Weber AE, Levy DM, et al. 2015. The natural history of femoroacetabular impingement. Front Surg 2:58.

5. Beck M, Kalhor M, Leunig M, et al. 2005. Hip morphology influences the pattern of damage to the acetabular cartilage: Femoroacetabular impingement as a cause of early osteoarthritis of the hip. J Bone Joint Surg Br 87:1012-1018.

6. Diamond LE, Wrigley TV, Bennell KL, et al. 2016. Hip joint biomechanics during gait in people with and without symptomatic femoroacetabular impingement. Gait Posture 43:198-203.

7. Hunt MA, Guenther JR, Gilbart MK. 2013. Kinematic and kinetic differences during walking in patients with and without symptomatic femoroacetabular impingement. Clin Biomech (Bristol, Avon) 28:519-523.

8. Kennedy MJ, Lamontagne M, Beaule PE. 2009. Femoroacetabular impingement alters hip and pelvic biomechanics during gait walking biomechanics of FAI. Gait Posture 30:41-44.

9. Atkins PR, Fiorentino NM, Aoki SK, et al. 2017. In vivo measurements of the ischiofemoral space in recreationally active participants during dynamic activities: A high-speed dual fluoroscopy study. Am J Sports Med:363546517712990.

10. Uemura K, Atkins PR, Fiorentino NM, et al. 2018. Hip rotation during standing and dynamic activities and the compensatory effect of femoral anteversion: An in-vivo analysis of asymptomatic young adults using three-dimensional computed tomography models and dual fluoroscopy. Gait Posture 61:276-281.

11. Kapron AL, Aoki SK, Peters CL, et al. 2015. In-vivo hip arthrokinematics during supine clinical exams: Application to the study of femoroacetabular impingement. J Biomech 48:2879-2886.

12. Kapron AL, Aoki SK, Peters CL, et al. 2014. Subject-specific patterns of femur-labrum contact are complex and vary in asymptomatic hips and hips with femoroacetabular impingement. Clin Orthop Relat Res 472:3912-3922.

13. Atkins PR, Elhabian SY, Agrawal P, et al. 2017. Quantitative comparison of cortical bone thickness using correspondence-based shape modeling in patients with cam femoroacetabular impingement. J Orthop Res 35:1743-1753.

14. Ross JR, Larson CM, Adeoyo O, et al. 2015. Residual deformity is the most common reason for revision hip arthroscopy: A three-dimensional CT study. Clin Orthop Relat Res 473:1388-1395.

15. Sardana V, Philippon MJ, de Sa D, et al. 2015. Revision hip arthroscopy indications and outcomes: A systematic review. Arthroscopy 31:2047-2055.

16. Aoki SK, Beckmann JT, Wylie JD. 2016. Arthroscopic femoral osteochondroplasty for cam-type femoroacetabular impingement: The trough technique. Arthrosc Tech 5:e743-e749.

17. Atkins PR, Aoki SK, Whitaker RT, et al. 2017. Does removal of subchondral cortical bone provide sufficient resection depth for treatment of cam femoroacetabular impingement? Clin Orthop Relat Res 475:1977-1986.

18. Duchman KR, Westermann RW, Glass NA, et al. 2017. Who is performing hip arthroscopy?: An analysis of the American Board of Orthopaedic Surgery Part-II database. J Bone Joint Surg Am 99:2103-2109.

19. Abraham CL, Bangerter NK, McGavin LS, et al. 2015. Accuracy of 3D dual echo steady state (DESS) MR arthrography to quantify acetabular cartilage thickness. J Magn Reson Imaging 42:1329-1338.

20. Anderson AE, Ellis BJ, Maas SA, et al. 2010. Effects of idealized joint geometry on finite element predictions of cartilage contact stresses in the hip. J Biomech 43:1351-1357.

21. Anderson AE, Ellis BJ, Peters CL, et al. 2008. Cartilage thickness: Factors influencing multidetector CT measurements in a phantom study. Radiology 246:133-141.

22. Harris MD, Anderson AE, Henak CR, et al. 2012. Finite element prediction of cartilage contact stresses in normal human hips. J Orthop Res 30:1133-1139.

23. Henak CR, Abraham CL, Peters CL, et al. 2014. Computed tomography arthrography with traction in the human hip for three-dimensional reconstruction of cartilage and the acetabular labrum. Clin Radiol 69:e381-391.

24. Henak CR, Kapron AL, Anderson AE, et al. 2014. Specimen-specific predictions of contact stress under physiological loading in the human hip: Validation and sensitivity studies. Biomech Model Mechanobiol 13:387-400.

25. Ng KC, Mantovani G, Lamontagne M, et al. 2016. Increased hip stresses resulting from a cam deformity and decreased femoral neck-shaft angle during level walking. Clin Orthop Relat Res. 475:998-1008.

26. Ng KC, Rouhi G, Lamontagne M, et al. 2012. Finite element analysis examining the effects of cam FAI on hip joint mechanical loading using subject-specific geometries during standing and maximum squat. HSS J 8:206-212.

27. Bergmann G, Deuretzbacher G, Heller M, et al. 2001. Hip contact forces and gait patterns from routine activities. J Biomech 34:859-871.

28. Abraham CL, Knight SJ, Peters CL, et al. 2017. Patient-specific chondrolabral contact mechanics in patients with acetabular dysplasia following treatment with peri-acetabular osteotomy. Osteoarthritis Cartilage 25:676-684.

29. Anderson AE, Ellis BJ, Maas SA, et al. 2008. Validation of finite element predictions of cartilage contact pressure in the human hip joint. J Biomech Eng 130:051008.

30. Henak CR, Abraham CL, Anderson AE, et al. 2014. Patient-specific analysis of cartilage and labrum mechanics in human hips with acetabular dysplasia. Osteoarthritis Cartilage 22:210-217.

31. Henak CR, Carruth ED, Anderson AE, et al. 2013. Finite element predictions of cartilage contact mechanics in hips with retroverted acetabula. Osteoarthritis Cartilage 21:1522-1529.

32. Henak CR, Ellis BJ, Harris MD, et al. 2011. Role of the acetabular labrum in load support across the hip joint. J Biomech 44:2201-2206.

33. Knight SJ, Abraham CL, Peters CL, et al. 2017. Changes in chondrolabral mechanics, coverage, and congruency following peri-acetabular osteotomy for treatment of acetabular retroversion: A patient-specific finite element study. J Orthop Res 35:2567-2576.

34. Klennert BJ, Ellis BJ, Maak TG, et al. 2017. The mechanics of focal chondral defects in the hip. J Biomech 52:31-37.

35. Todd JN, Maak TG, Ateshian GA, et al. 2018. Hip chondrolabral mechanics during activities of daily living: Role of the labrum and interstitial fluid pressurization. J Biomech 69:113-120.

36. Rajagopal A, Dembia CL, DeMers MS, et al. 2016. Full-body musculoskeletal model for muscle-driven simulation of human gait. IEEE Trans Biomed Eng 63:2068-2079.

37. Steele KM, Demers MS, Schwartz MH, et al. 2012. Compressive tibiofemoral force during crouch gait. Gait Posture 35:556-560.

38. Kapron AL, Aoki SK, Peters CL, et al. 2014. Accuracy and feasibility of dual fluoroscopy and model-based tracking to quantify in vivo hip kinematics during clinical exams. J Appl Biomech 30:461-470.

39. Hicks JL, Uchida TK, Seth A, et al. 2015. Is my model good enough? Best practices for verification and validation of musculoskeletal models and simulations of movement. J Biomech Eng 137:020905.

40. Maas SA, Ellis BJ, Rawlins DS, et al. 2016. Finite element simulation of articular contact mechanics with quadratic tetrahedral elements. J Biomech 49:659-667.

41. Dalstra M, Huiskes R. 1995. Load transfer across the pelvic bone. Journal of Biomechanics 28:715-724.

42. Henak CR, Ateshian GA, Weiss JA. 2014. Finite element prediction of transchondral stress and strain in the human hip. J Biomech Eng 136:021021.

43. Ferguson SJ, Bryant JT, Ito K. 2001. The material properties of the bovine acetabular labrum. J Orthop Res 19:887-896.

44. Quapp KM, Weiss JA. 1998. Material characterization of human medial collateral ligament. J Biomech Eng 120:757-763.

45. Fiorentino NM, Atkins PR, Kutschke MJ, et al. 2017. Soft tissue artifact causes significant errors in the calculation of joint angles and range of motion at the hip. Gait Posture 55:184-190.

46. Wu G, Siegler S, Allard P, et al. 2002. ISB recommendation on definitions of joint coordinate system of various joints for the reporting of human joint motion—part I: Ankle, hip, and spine. J Biomech 35:543-548.